UNIVERSITÀ
DEGLI STUDI
FIRENZE

DOTTORATO DI RICERCA IN SCIENZE BIOMEDICHE

CICLO XXXIII

COORDINATORE Prof. Stefani Massimo

IDENTIFICATION OF MEMBRANE CA^{2+} CHANNELS ACTIVATED BY PROTEIN MISFOLDED OLIGOMERS AND THEIR ACTIVATION MECHANISM

Settore Scientifico Disciplinare BIO/10

Dottorando

Dott.ssa Fani Giulia

Tutore

Prof. Chiti Fabrizio

Coordinatore

Prof. Stefani Massimo

Anni 2017/2020

Index

Abstract

Alzheimer's disease is the most common form of dementia, characterized by the aggregation of the amyloid β peptide (Aβ) in the brain and by an impairment of calcium homeostasis caused by excessive activation of glutamatergic receptors, named excitotoxicity. Here, we studied the effects on calcium homeostasis caused by the formation of Aβ oligomeric assemblies, formed with $A\beta_{40}$ and $A\beta_{42}$ peptide, and by the model protein HypF-N. We found that these oligomers cause a rapid influx of calcium ions (Ca^{2+}) across the cell membrane by rapidly activating extrasynaptic N-methyl-D-aspartate receptors (NMDAr) and, to a lower extent, α-amino-3-hydroxy-5-methyl-4-isoxazolepropionic acid receptors (AMPAr), and also by causing a perforation of lipid bilayers. Instead, none of the Ca^{2+} channels, including those found in previous interactome studies to physically interact with the oligomers, were found to participate to the observed Ca^{2+} influx. We also observed, however, that misfolded oligomers do not interact directly with NMDAr and AMPAr. Further experiments with lysophosphatidylcholine and arachidonic acid, which cause membrane compression and stretch, respectively, indicated that these receptors are activated through a change in membrane tension induced by the oligomers and transmitted mechanically to the receptors via the lipid bilayer. Indeed, lysophosphatidylcholine is able to neutralise the oligomer-induced activation of the NMDAr, whereas arachidonic acid activates the receptors similarly to the oligomers with no additive effects. An increased rotational freedom observed for a fluorescent probe embedded within the membrane in the presence of the oligomers also indicates a membrane stretch. These results reveal a further mechanism of toxicity of Aβ oligomers in Alzheimer's disease through the perturbation of the mechanical properties of lipid membranes sensed by NMDAr and AMPAr, in addition to others based on the direct binding to membrane receptors and on permeabilization of lipid membranes.

1. Introduction

1.1. Protein misfolding and related diseases

1.1.1. Protein folding

Proteins are the most versatile macromolecules of living systems and play a fundamental role in practically all biological processes. There are many different types of proteins, which can play different roles, and each of these proteins has its characteristic structure and function. The folding is a key element for proteins, since most of them must correctly fold in specific three-dimensional structures to acquire their biological functionality, and it is determined by the aminoacidic chain itself (Hartl, 2017).

During the folding process from the primary structure, that is the linear chain of amino acids, the protein can take a secondary structure, that is generated by regions stabilized by hydrogen bonds between atoms in the polypeptide backbone, a tertiary structure, that is the three-dimensional shape of the protein determined by regions stabilized by interactions between the side chains, and a quaternary structure, resulting into the association between two or more polypeptides not present in every protein. Under physiological conditions, a polypeptide chain undergoes a series of conformational changes before adopting the most stable three-dimensional conformation which is generally attributed to the functional or native state of a protein. The number of all the possible conformations even a small polypeptide of ~100 amino acids can adopt is astronomically large ($\sim 10^{30}$) (Dobson *et al.*, 1998), incompatible with the times of cell synthesis in which the protein sequences fold in a single native state.

Two models used to describe the process of folding are the energy landscape and the folding funnels (Figure 1.1). According to them, newly synthesized proteins are in a state of maximum free energy, called the unfolded state, where the possible

conformations are as many as the protein molecules and the number of native contacts is very low. Proteins fold through some oriented processes increasing the number of native contacts and decreasing the free energy. The sequential formation of native contacts guides the formation of the next native contact until the formation of the native structure is attained. With the folding process the proteins can reach their three-dimensional conformation by ensuring the least amount of free energy: this is possible by optimizing the interaction forces (Dinner *et al.*, 2000; Dobson, 2003; Vendruscolo and Dobson, 2005). The lower energy structure would generally correspond to the native structure of the protein itself (Wolynes *et al.*, 1995; Karplus 1997).

In the energy landscape (Figure 1.1 A), the polypeptide chains in the unfolded states are on the top-back side of the cube characterized by high energy, and entropy. From this state the various molecules can take different paths of folding, increasing the number of native contacts leading to the functional three-dimensional structure of a protein in a native state characterized by many native contacts and a low level of free energy, represented in the front-bottom-left corner of the cube.

In the folding funnel (Fig. 1.1 B) the upper part is characterized by high energy levels and in this area, there is the unfolded state, with protein molecules with variable and random contacts. Along the surface of the funnel, the protein can pass through different paths that connect the upper part to the lower part. Despite the different paths, all proteins converge in the bottom of the funnel which corresponds exactly to the native state of the protein, which is unique, the most stable of all, therefore the lowest energy point (Wolynes *et al.*, 1995; Karplus, 1997).

During the folding, different conformational states can form, which constitute stable intermediates, different from unfolded or native states. Moreover, it is observed that energetically lower position than the native state is occupied by specific protein

aggregates, these are the amyloid fibrils, which are the species with the lowest total free energy, among all the possible conformations that a protein can acquire in its path.

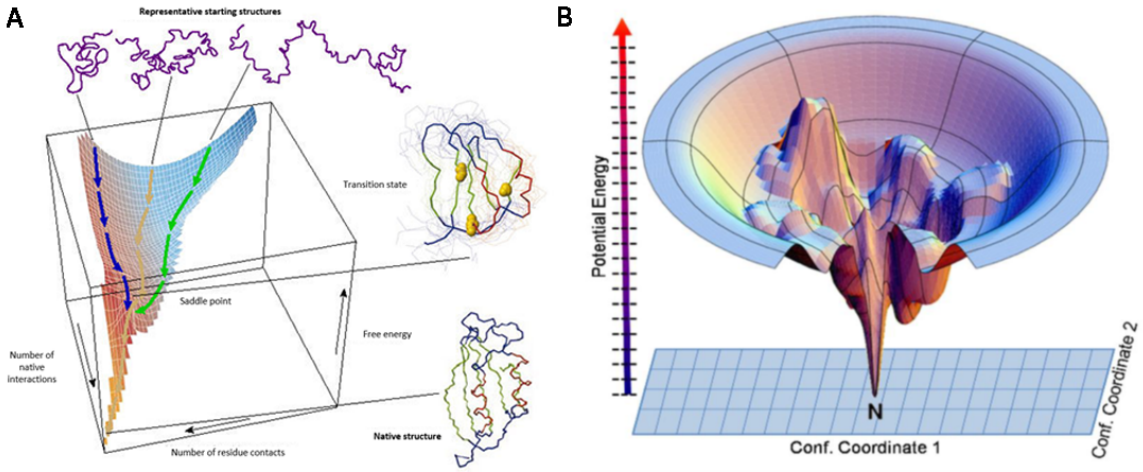

Figure 1.1. (**A**) A schematic representation of a free energy landscape. Newly synthesized proteins are in a state of maximum free energy called the unfolded state, on the top-back side of the cube. The sequential formation of native contacts guides the formation of the native structure, the front-bottom-left corner of the cube (Dobson, 2003). (**B**) Representation of the folding funnel: on the top the unfolded state. The protein can follow different trajectories which are illustrated by a series of depressions before the acquisition of the native structure, on the bottom (Dill and Chan, 1997).

In vivo, the correct folding requires the intervention of a large number of auxiliary proteins, which include protein folding catalysts, molecular chaperones and co-chaperones, whose main role is to protect the polypeptide chain from unwanted interactions, and cooperate with machineries of protein degradation in a large protein homeostasis (or proteostasis) network (Schiene and Fischer, 2000; Hartl and Hayer-Hartl, 2002; Hartl, 2017; Mannini and Chiti, 2017). Different classes of molecular chaperones have been described, which act at distinct moments of the folding process during which they interact, stabilize, or help a non-native protein to take possession of its native conformation but are not present in the final functional structure (Hartl and Hayer-Hartl, 2009; Hartl, 1996).

1.1.2. Protein misfolding and aggregation

Despite the presence of quality control systems, the folding process is error prone (Fig. 1.2) (Hartl, 2017), and the protein often tends to aggregate forming amorphous structures, which typically expose hydrophobic amino acid residues and unstructured regions of the polypeptide chain, characteristics absent in the native state (Vabulas *et al.*, 2010). This process, that often results in the conversion of a protein's native state to a different structure, frequently resulting in aggregation, is defined as protein misfolding (Chiti and Dobson, 2017). The early aggregates that form initially are clusters of a relatively small number of molecules, with weak intermolecular interaction involved, that make them rather instable. When the aggregation proceeds, there is an internal reorganization, with the formation of more stable species with β-sheet structures and with an increase in compactness and size. A further size increase of these β-structured oligomers, by self-association or addition of monomers, determine the formation of well-defined fibrils with cross-β structure and high level of structural orders. Alternatively, the disordered aggregates or native-like aggregates can grow without any major structural conversion and give rise to large amorphous deposits or native-like assemblies, respectively, retaining the structure characterizing the initial oligomers (Lee *et al.*, 2011; Cremades *et al.*, 2012; Plakoutsi *et al.*, 2005; Carulla *et al.*, 2009; Bleiholder *et al.*, 2011; Chiti and Dobson 2017).

The aggregation process of a protein leading to amyloid formation is divided in two different primary steps: the nucleation and the growth step (Galzitskaya *et al.*, 2018). This process has a kinetic profile with a sigmoid pattern, characterized by an initial lag-phase, an exponential or elongation phase, and an equilibrium or plateau phase. The amyloid formation process may differ depending on the conformational state of the starting peptide or protein and on the environment characteristics, such as pH or protein

concentration (Bader *et al.*, 2006; Gosal *et al.*, 2005). When a protein is partially unfolded and expose some aggregation-prone regions to the solvent, the nucleated polymerization can occur, with the conversion of completely or partially disordered monomers into nuclei, that are the smallest structures that can initiate fibril elongation, through a thermodynamically unfavourable process, and the consequent growth of fibrils from these nuclei through the addition of monomers (Morris *et al.*, 2009; Galzitskaya *et al.*, 2018). Another mechanism, named nucleated conformational conversion, occurs when monomers rapidly convert into misfolded aggregates, and then these aggregates undergo structural reorganization to generate nuclei (Serio *et al.*, 2000). When the starting protein is a fully folded globular protein, it must first convert into a partially unstructured state before the amyloid formation can proceed (Chiti and Dobson, 2009). However, a fully folded protein can also aggregate through interaction of native or native-like structures, in which aggregation-prone regions that are normally buried in the fully folded state, become exposed to the solvent. These native-like aggregates can grow without any major structural conversion and give rise to native-like deposits, retaining the structure characterizing the initial oligomers (Chiti and Dobson, 2017) (Fig. 1.2).

The primary pathways involved in the aggregation process, i.e. the primary nucleation and fibril elongation, are accompanied by a series of secondary processes, such as fragmentation and secondary nucleation reactions (Knowles *et al.*, 2009; Knowles *et al.*, 2014; Arosio *et al.*, 2015). Fragmentation events consist of the breaking of fibrillar aggregates in smaller pieces, determining the increase of the number of fibril ends. Since the growth of fibrils occurs from their ends, these events have an important impact on the kinetics of the aggregation process and on amyloid cytotoxicity (Arosio *et al.*, 2015; Xue *et al.*, 2010). Secondary nucleation consists on the formation of monomers that act as nuclei on the surface of an already existing fibrillar aggregate. The formation of new

nuclei determines an amplification of the self-assembly aggregation process (Linse, 2017; Cohen *et al.*, 2013; Padrick and Miranker, 2002; Meisl *et al.*, 2014).

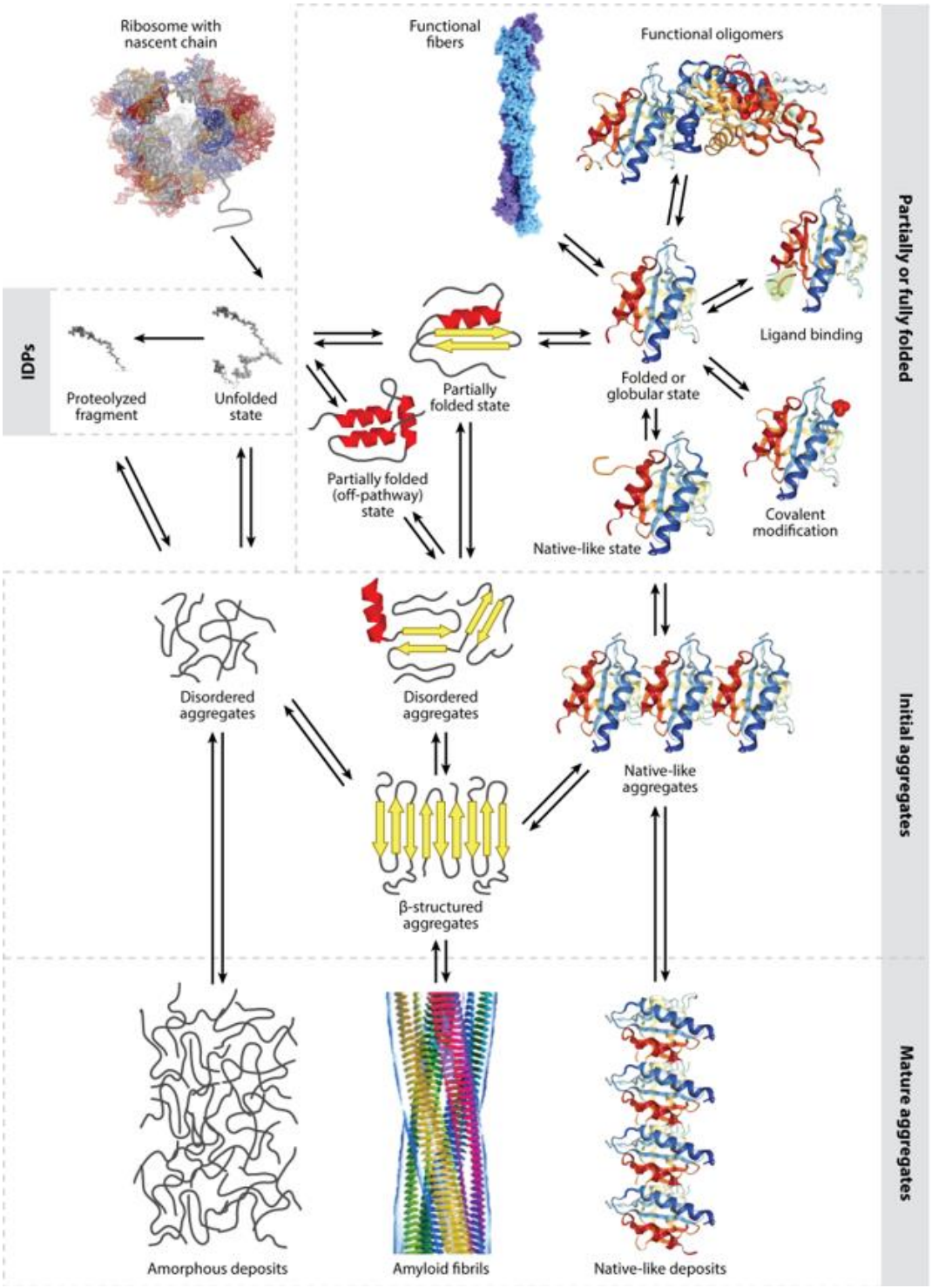

Figure 1.2. Schematic illustration of the various conformational states than can be adopted by a protein after its biosynthesis and the possible transitions between states (Chiti and Dobson, 2017).

1.1.3. Protein deposition diseases

Protein aggregates are highly toxic to eukaryotic cells (Haass and Selkoe, 2007; Chiti and Dobson, 2017). In fact, together with misfolded proteins, they are related to the appearance of a wide range of pathologies known as protein misfolding diseases or conformational diseases (Chiti and Dobson, 2017). These pathologies are caused by the inability of a protein to adopt or maintain a stable native structure, whether it is an ordered structure (secondary or tertiary) or an intrinsically disordered structure. In a large group of misfolding diseases, protein misfolding is associated with protein aggregation with the consequent formation of fibrillar aggregates. These pathologies are called protein deposition diseases. The aggregates can localize in the intracellular environment, forming "intracellular inclusions" with amyloid-like characteristics, or can accumulate in the extracellular environment after secretion of the precursor protein, forming "amyloid fibrils" or "amyloid plaques" (Stefani and Dobson, 2003; Westermark *et al.*, 2005; Chiti and Dobson, 2017).

Protein aggregation diseases can be classified into (i) systemic non-neuropathic amyloidosis, in which aggregates accumulate in various body tissues except the central nervous system (CNS); (ii) localized non-neuropathic amyloidosis, where the aggregates preferentially form in a tissue or organ; (iii) neurodegenerative diseases, where aggregates accumulate in the CNS compromising their functions and giving rise to neurodegenerative conditions (Chiti and Dobson, 2017).

Neurodegenerative diseases constitute an heterogeneous group of pathologies, characterized by the accumulation of different proteins, including Alzheimer's disease (AD), Huntington's disease (HD), Parkinson's disease (PD), amyotrophic lateral sclerosis (ALS) and spongiform encephalopathies (Perl, 2010; Torres *et al*., 2010; Kalia and Lang, 2015; Frost and Li, 2017; Maguire, 2017). In familial forms of amyloid-related diseases,

the aggregation may be caused by mutations in the gene encoding the protein that convert into the amyloid deposits, as in the case of HD and in early-onset AD and PD. However, the majority of cases are sporadic and manifest in an age-dependent manner, apparently facilitated through a decline in the capacity of the proteostasis network that occurs during aging (Douglas and Dillin, 2010; Hipp *et al.*, 2014; Labbadia and Morimoto, 2015).

In order to study neurodegenerative diseases, a cell line model that is widely used is the SH-SY5Y cell line, which is derived from human neuroblastoma cells. These cells are widely used to investigate mechanisms of neurodegeneration because of their human origin, their catecholaminergic (though not strictly dopaminergic) neuronal properties, and their ease of maintenance. In addition, the SH-SY5Y cell line has been used widely in experimental neurological studies, including analysis of neuronal differentiation, metabolism, and function related to neurodegenerative processes, neurotoxicity, and neuroprotection (Schlachetzki *et al.*, 2013).

1.1.4. Alzheimer's diseases

Over 47 million people worldwide live with dementia and AD is one of the major forms of dementia, accounting for 60 to 80% of the cases, which is why it has become an object of great interest in both the medical and social fields (Patterson, 2018).

The vast majority of AD case occurrences are sporadic, but rare gene mutations could originate familiar AD (FAD), which account for less than 1% of cases. FAD is caused by mutations in amyloid precursor protein (APP), presenilin 1 (PSEN1) or presenilin 2 (PSEN2) genes (Ryman *et al.*, 2014), and usually manifest in the early-onset AD (EOAD), which occurs before 65 years and account for fewer than 5% of the pathologically diagnosed AD cases. This often has an atypical presentation and an aggressive course (Mendez, 2017). The more common form of AD is the late-onset AD

(LOAD), which account for about 95% of AD cases and it is considered for the majority sporadic, although allele ε4 of apolipoprotein E (ApoE) has been shown as the strongest genetic risk factor related to LOAD development process, increasing three-fold the risk of developing the disease (Zhu *et al.*, 2015; Kunz *et al.*, 2015; Lane *et al.*, 2018). Other risk factors for LOAD, including TREM2, ADAM10 and PLD3, have been identified using genome wide association studies (GWAS) to implicate nearly 30 genes able to modulate also cholesterol metabolism, endocytosis and immune response, among those with known functions (Karch and Goate, 2015; Jansen *et al.*, 2019). A strong risk factor for AD is aging, with the incidence doubling every five or ten years. Other known risk factors are family history of dementia, head trauma, low level of scholarization, genetic, female sex, vascular diseases and environmental factors (Castellani *et al.*, 2010).

AD is a neurodegenerative disease and its diagnosis first requires evidence of memory loss and cognitive impairment using a specific test, the Folstein Mini-Mental State Examination (MMSE). The MMSE is a 30-question assessment of cognitive function that evaluates attention and orientation, memory, registration, recall, calculation, language and ability to draw a complex polygon (Arevalo-Rodriguez *et al*., 2015). This neurophysiological test is accompanied by other pathological diagnosis, such as the neuroimaging, which plays a key role in the clinical assessment of patients with suspected AD. Computed tomography (CT) and magnetic resonance imaging (MRI) are able to show an insidious onset and inexorable progression of atrophy that is first manifested in the medial temporal lobe. The entorhinal cortex is typically the earliest site of atrophy, followed by the hippocampus, amygdala, and para hippocampus. These losses then spread to involve the temporal neocortex and then all neocortical association areas (Johnson *et al*., 2012).

Currently, the diagnosis of AD is based on the "ATN" system, in which the major AD biomarkers are divided into 3 binary categories: "A" refers to the value of a β-amyloid biomarker; "T" to the value of a tau biomarker; and "N" to biomarkers of neurodegeneration or neuronal injury. Each biomarker category is rated as positive or negative. An individual score might appear as A+/T+/N−, or A+/T−/N−, etc (Jack *et al*., 2016). The +/− categorization does not imply that individuals who fall below the cut point for a particular biomarker have no pathology in the brain. For example, an individual designated as "A" may have amyloid plaques in the brain, but not at a sufficient level to cross the *in vivo* detection threshold of amyloid positron emission tomography (PET). Current biomarker readouts are not sensitive to low but perhaps biologically important levels of early pathology. The +/− designation is a convenient shorthand to facilitate communication, ease of use, and understanding (Jack *et al*., 2016). The ATN system is suited to population studies of cognitive aging because it includes all individuals in any population regardless of the mix of biomarker findings. It does not specify disease labels and thus is not a diagnostic classification system. It is a descriptive system for categorizing multidomain biomarker findings at the individual person level in a format that is easy to understand and use (Jack *et al*., 2016).

There have been different approaches to noninvasively visualize amyloid deposition in human brains with amyloid PET radiotracers able to bind to insoluble fibrillar forms of $A\beta_{40}$ and $A\beta_{42}$ deposits. PET amyloid-β imaging agent could facilitate the clinical evaluation of late-life cognitive impairment by providing an objective measure for AD pathology (Marcus *et al*., 2014). Moreover, brain fluor-deoxy-d-glucose PET (FDG-PET), that quantifies brain function by measuring glucose uptake of neurons and glial cells, can better assess the progression and severity of cognitive decline in people with AD, distinguishing AD from other causes of dementia. In patients with early AD,

the areas of glucose hypometabolism have been commonly observed in the parietotemporal association cortices, posterior cingulate cortex, and the praecuneus (Marcus *et al*., 2014). Moreover, to get an impression of the regional cerebral blood flow, the single-photon emission CT (SPECT) is used. In typical AD cases a bilateral temporoparietal hypoperfusion is seen (Scheltens, 2009).

The post-mortem pathologic diagnosis of AD remains the gold standard for diagnosis (De Ture and Dickson, 2019). Macroscopic and microscopic markers related to AD are known and may help in its characterization, in understanding of the disease pathogenesis. Macroscopically, a cortical atrophy is observed, with primary motor and somatosensory cortices most often unaffected (Perl, 2010). As a result of this atrophy, there is often enlargement of the frontal and temporal horns of the lateral ventricles, and decreased brain weight is observed in most affected individuals (Perl, 2010). A medial temporal atrophy affecting amygdala and hippocampus is also observed, usually accompanied by temporal horn enlargement (Perl, 2010; Serrano-Pozo (1) *et al.*, 2011; Apostolova *et al.*, 2012). Another macroscopic feature commonly observed in AD is the loss of neuromelanin pigmentation in the locus coeruleus (Serrano-Pozo (1) *et al.*, 2011). Microscopically, AD is characterized by the formation of extracellular amyloid plaques, or senile plaques, which are fibrillar deposits of the Aβ peptide, and intracellular aggregation of neurofibrillary tangles (NFTs), composed of hyperphosphorylated microtubule-associated τ. The senile plaque deposit or its oligomeric precursors have pronounced cytotoxic properties which are related to the process of neurodegeneration (Hardy and Higgins, 1992; Li *et al.*, 2012; Stancu *et al.*, 2014; Liu *et al.*, 2015). τ protein, that normally promotes the assembly of tubulin providing microtubule stability (Goedert *et al.*, 2015), undergo subtle changes with high concentrations of Aβ, resulting in the process of its hyperphosphorylation (Stancu *et al.*, 2014). The result of these lesions is

the loss of synapses and then neurons in vulnerable regions leading to the symptoms commonly associated with AD (Perl, 2010; Holtzman *et al.*, 2011; Stancu *et al.*, 2014; Forestier *et al.*, 2015; Liu *et al.*, 2015).

AD in also characterized by altered concentrations of glutamate (Glu) in the posterior cingulate cortex of AD patients, which is one of the major excitatory neurotransmitters in the mammalian brain, as well as the immediate precursor to GABA and glutathione (Conway, 2020). Regulation of brain Glu is primarily governed through the Glu/glutamine cycle (Conway and Hutson, 2016). Following presynaptic neuronal depolarisation, synaptic vesicles, with stored Glu, release it into the synapse, where it can activate a variety of ionotropic and metabotropic receptors on postsynaptic and presynaptic neurons as well as glial cells (Clements *et al*., 1992). The overstimulation is prevented by the rapid and efficient removal carried out by astrocytes that express high levels of the Glu specific transporter (GLAST/EAAT1 and GLT-1/EAAT2). Glu is then converted through amidation to glutamine and, as non-neuroactive, released for reuptake by the pre-synaptic neuron, to replenishes the store of Glu through deamidation. Damage to glutamatergic neurons, together with damage to glutamatergically-innervated cortical and hippocampal neurons, are particularly evident in AD brain (Conway, 2020). Altered expression of glutamatergic transport and receptors were also reported in sporadic AD (Conway, 2020). Pathological accumulation of Glu results in its neurotoxicity, in part due to the time-related exposure, overstimulating the post synaptic response causing an increase in the entry of calcium into neurons predominantly linked with excitotoxicity through the N-methyl-D-aspartate receptors (NMDAr), with a slow neuronal degeneration mediated by Ca^{2+} influx (Conway, 2020).

In the beginning of the disease, there is loss of cholinergic neurons in the basal nucleus and in the entorhinal cortex and more than 90% of them are lost in the advanced

stage of AD, this leads to the appearance of cognitive and non-cognitive symptoms in patients with AD. A marked decrease in acetyltransferase concentration responsible for the synthesis of acetylcholine in the cortex and hippocampus is also observed and is associated with the loss of cholinergic neurons. The dysfunction and cell death of neurons responsible for the maintenance of specific transmission systems leads to the deficiency of acetylcholine, noradrenaline and serotonin (Kasa *et al.*, 1997; Cummings, 2004).

AD is also closely linked to the inflammatory processes. Microglial cells are phagocytes within the brain, which monitor their territories for pathogen exposure or deteriorating neurons and promotes their migration to the site and subsequent activation (Heneka *et al.*, 2015). Under conditions of stress, such as increase of Aβ amyloid fibrils and τ paired helical filaments, they become activated (Heneka *et al.*, 2015). They are observed around senile plaques, and their numbers increase in promotion to neuronal damage associated with NFTs (Wake *et al.*, 2009; Serrano-Pozo (2) *et al.*, 2011; Heneka *et al.*, 2015). Reactive astrocytes represent the other inflammatory response observed in the brains of AD patients (Fig. 1.3) (Heneka *et al.*, 2015). Astrocytes, that normally provide trophic support for the neurons and synapses, are often observed around senile plaques in AD, though in lower abundance compared to microglia, and at a greater distance from the plaque epicentre. It is thought they react to the cytokines and other agents produced by pro-inflammatory microglia, and the changes in the astrocytes are thought to be neurotoxic (Steele and Robinson, 2012; Liddelow *et al.*, 2017).

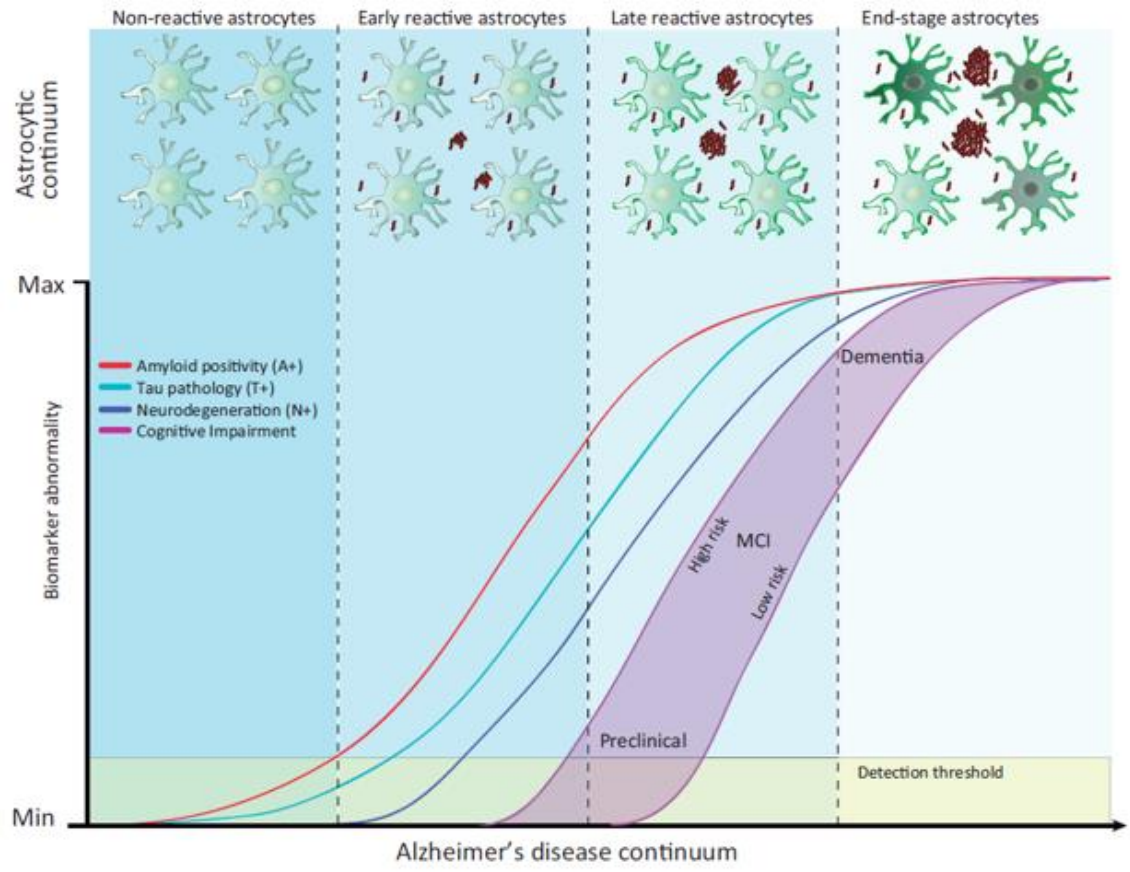

Figure 1.3. Schematic representation of reactive astrocytes in the model of ATN system, with the amyloid biomarkers that become abnormal first (amyloid positivity, A+, red), followed by τ biomarkers (tau positivity, T+, light blue), which leads to neurodegeneration (N+, dark blue), cognitive impairment (violet), and finally dementia. In the absence of pathology, astrocytes exist in their non-reactive state supporting normal brain function. As Aβ pathology begins to develop astrocytes start to react to prevent toxicity to neurons. With further pathological progression late- and end-stage reactive astrocytes can be measured with additional imaging and fluid biomarkers (Carter et al., 2019).

1.1.5. Treatment in Alzheimer's diseases

Several pharmacological treatments for AD have been tested and are currently used as symptomatic drugs in most countries. Some drugs act as inhibitors of cholinesterase (Acetylcholinesterase and Butyrylcholinesterase), which are enzymes responsible for degradation of the acetylcholine in synapses, after transmission of the nervous impulse. Thus, cholinesterase inhibitors increase the availability of these neurotransmitters in the

synaptic cleft, reducing the symptoms of AD. Cholinesterase inhibitors have shown significant improvements in the cognitive process of patients with AD and in the reduction of their symptoms by improving the cholinergic function in neuronal synapses (Anand and Singh, 2013). Typical cholinesterase inhibitors available on the market and administrated to the patients are donepezil, galantamine and rivastigmine.

Another drug, approved by the Food and Drug Administration (FDA), is a non-competitive NMDAr antagonist, named Memantine, which decreases excitotoxicity and neurodegeneration caused by the excessive action of Glu and the resulting entry of Ca^{2+} ions from the extracellular space into the cytosol. It reduces excessive glutamatergic neurotransmission, may decrease hyperphosphorylation of τ and protects against toxicity induced by Aβ peptide (Miguel-Hidalgo *et al.*, 2002; Gordon *et al.*, 2012).

1.1.6. Amyloid fibrils: definition and features

Amyloid fibrils are highly organized structures with persistent lengths of the order of microns and with a very high tension force (Knowles *et al.*, 2007). A high number of proteins, not associated with diseases, can form, under specific *in vitro* conditions, amyloid fibrils (Stefani and Dobson, 2003; Uversky and Fink, 2004). Although they can originate from very different proteins, they have important common structural features that allow them to be classified as such (Dobson, 2003; Chiti and Dobson, 2017).

Amyloid fibrils, whether extracted from patients or generated in the laboratory, present a fibrillary morphology. When observed by electron microscopy (EM) or atomic force microscopy (AFM), they appear as elongated structures whose diameter ranges from 7 to 13 nm (Fig. 1.4A,B). Generally, they comprise from 2 to 8 protofilaments, each of which has approximately a diameter of 2-7 nm. These protofilaments often turn around

each other or associate laterally forming flat ribbons of 2-7 nm high and up to 30 nm wide (Harper (2) *et al.*, 1997; Paravastu *et al.*, 2008; Wasmer *et al.*, 2008).

Amyloid fibrils present a common cross-β structure. They are formed by a structure in β-sheets that run along the entire length of the fibrils, to form a cross-β structure in which these filaments are arranged perpendicularly to the fibrillary axes (Chiti and Dobson, 2017). This structure is visible by X-ray diffraction (Fig. 1.4C). The 4.8 Å diffraction on the meridional direction corresponds to the distance between the β-filaments, while the 10-11 Å diffraction on the equatorial direction corresponds to the distance between the adjacent β-sheets (Harper (2) *et al.*, 1997). This cross-β structure confers to the amyloid fibril mechanical strength and stability (Chiti and Dobson, 2017).

Moreover, the amyloid fibrils present characteristic dye-binding properties. They are capable of binding specific probes such as Thioflavin T (ThT) and Congo red (CR), or their derivatives (Nilsson, 2004) (Fig. 1.4D).

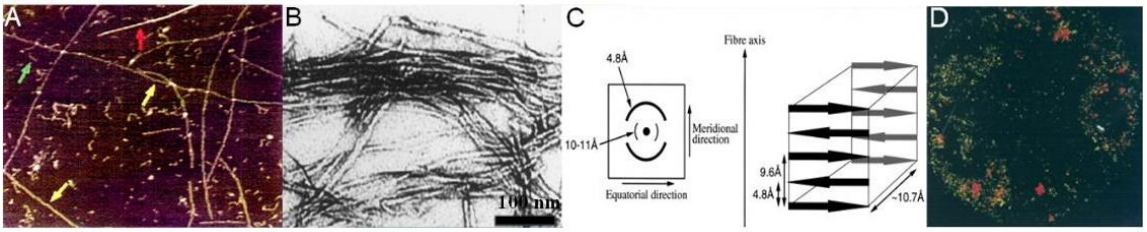

Figure 1.4. Characteristics of amyloid fibrils. Fibrillary morphology observed with (A) AFM (Harper (2) *et al.*, 1997) and (B) TEM (Walsh *et al.*, 1999). (C) Cross-β structure analysed with X-ray diffraction (Serpell, 2000). (D) Green birefringence with polarized light in the presence of CR (Nilsson, 2004).

Although fibrils are less toxic than misfolded protein oligomers (see next section), they do not generally constitute harmless material as they can over-engage the key components of the protein homeostasis network (Labbadia and Morimoto, 2015; Balchin *et al.*, 2016), they can serve as a reservoir of protein oligomers that can be released (Lesnè

et al., 2006; Martins *et al.*, 2008; Koffie *et al.*, 2009; Cremades *et al.*, 2012) and perhaps act as powerful catalysts for the generation of toxic oligomers through secondary nucleation (Knowles *et al.*, 2009; Cohen *et al.*, 2013; Xu *et al.*, 2013; Arosio *et al.*, 2015).

1.1.7. Oligomer toxicity determinants

Significance in the context of amyloid fibril formation are prefibrillar species, termed oligomers, which are thought to represent the most pathogenic species in the diseases associated with amyloid fibril formation. Misfolded oligomers are highly dynamic and exist in equilibrium with monomers and fibrils and it is an ill-defined and heterogeneous group of species ranging from dimers to larger protofibrillar structures. Some oligomers are on-pathway intermediates for amyloid fibril formation, while others might be terminal off-pathway products, some of which could be highly toxic (Rambaran and Serpell, 2008; Breydo and Uversky, 2015; Lesne, 2014). Knowing the structural and the conformational properties of these oligomeric species, it has been possible to elucidate the ways in which they exercise their toxicity (Chiti and Dobson, 2017).

Despite their heterogeneity, oligomers originating from different proteins reduce cell viability in a similar way. This cytotoxicity is attributed in part to their misfolded character or to their common characteristics, rather than to the amino acid sequence (Bucciantini *et al.*, 2002). The exposure of hydrophobic groups on the surface of the oligomers, whose increase determines an increase in cytotoxicity, is an important determinant of oligomer-induced cytotoxicity (Olzscha *et al.*, 2011). By isolating some oligomeric species such as HypF-N (Campioni *et al.*, 2010), $A\beta_{42}$ (Ladiwala *et al.*, 2012), α-synuclein (Cremades *et al.*, 2012) and the NM region of Sup35p (Krishnan *et al.*, 2012), of similar size and morphology but of different degree of toxicity, a significant difference in hydrophobicity exposed to the solvent was observed (Chiti and Dobson, 2017).

Oligomers establish inappropriate interactions with a wide range of cellular components, such as the phospholipid bilayer of cell membranes, protein receptors, soluble proteins, RNA, small metabolites or other molecular species (Chiti and Dobson, 2017). The rapidity with which these aberrant interactions are established is strongly influenced by their size (Mannini *et al.*, 2014). In fact, the dimension is another important toxicity determinant (Chiti and Dobson, 2017). Small size oligomers have higher toxicity, and this is supposed to be due to the high diffusion coefficient of these species. In fact, it determines a more rapid formation of anomalous interactions (Mannini *et al.*, 2014). For example, it has been observed that induced assembly of preformed oligomers of $A\beta_{42}$, IAPP and HypF-N in large protein aggregates, in the absence of any structural reorganization, is associated with a significant reduction in toxicity (Ojha *et al.*, 2011). In some studies of $A\beta_{40}$ and $A\beta_{42}$ oligomers, maximum toxicity, in terms of monomeric equivalents, has been observed for small oligomers such as prefibrillar oligomers (PFOs) of 18-90 kDa (Kayed *et al.*, 2007; Kayed *et al.*, 2009) and the globular oligomers named Aβ-derived diffusible ligands (ADDLs) of 36-72 kDa (Lambert *et al.*, 2001; Gong *et al.*, 2003). This toxicity is reduced with the increase in the size of the oligomers until reaching a fibrillar structure that shows a residual, but significant, toxicity. Interestingly, a correlation between oligomer toxicity and oligomer size, on the one hand, and solvent-exposed hydrophobicity, on the other hand, has been found in a group of HypF-N variants in which one or more charged amino acid residues was replaced with neutral apolar residues, allowing the mutated proteins to aggregate. The most toxic oligomers having high hydrophobicity and small size (Fig. 1.5).

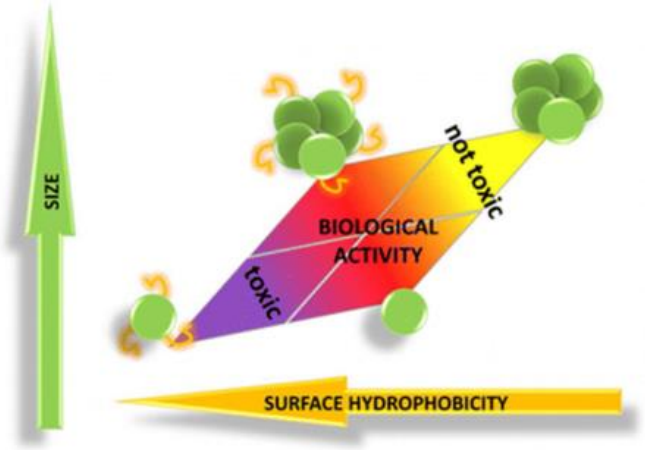

Figure 1.5. Representative images of the correlation between the oligomers toxicity and their surface hydrophobicity and size (Mannini *et al*., 2014).

The different species of oligomers differ not just in exposure of hydrophobic residues and size, but also in the degree of ordered secondary structure. The presence of β-sheet structure in many of the toxic oligomers has led to the hypothesis that such secondary structure is associated with their toxicity, but a recent study, which compares different types of oligomers, has shown that the β-sheet architecture is a favourable structural element but is not an essential prerequisite for toxicity. In fact, oligomers from different protein systems but with similar toxicity, solvent-exposed hydrophobicity, and size, have variable amounts of β-sheet structure and pairs of toxic and nontoxic oligomers from the same protein can have similar contents of β-sheet structure (Vivoli Vega *et al.*, 2019).

Although the toxicity of protein aggregates is considered the primary cause of the onset of cellular dysfunctions, as well as of various pathologies, it is important to underline the fact that this cause cannot be recognized in a single aberrant interaction or mechanism of action, or in a single cascade of cellular events. The toxicity of protein aggregates is rather to be considered as the result of their intrinsically misfolded nature and their structural heterogeneity (Chiti and Dobson, 2017).

1.1.8. Role of calcium in oligomer toxicity

The calcium ion is a second messenger that plays an important role in eukaryotic cells, in particular in excitable cells (Pchitskaya *et al.*, 2018). The blood brain barrier defends extracellular calcium in the brain from changes and at rest brain extracellular calcium is maintained at 1.1 mM, whereas neuronal intracellular calcium is orders of magnitude lower ranging between 50 and 100 nM (Jones and Smith, 2016). The extremely precise control of Ca^{2+} concentration in specific cellular compartments regulate multiple neuronal functions, such as neuronal growth, exocytosis, synaptic plasticity and cognitive functions. These processes involve various Ca^{2+}-conducting channels and a great number of Ca^{2+}-dependent proteins as downstream targets including kinases, phosphatases, transcription factors, enzymes and proteins that induce synaptic vesicle fusion (Brini *et al.*, 2014; Clapham, 2007). Neurons are extremely sensitive to calcium concentration levels and even subtle defects in Ca^{2+} homeostasis can affect their normal function and structure. In fact, it is now known that the destruction of intracellular calcium homeostasis plays an important role in the dynamics of some neuropathology (Chakroborty and Stutzmann, 2014; Pchitskaya *et al.*, 2018).

In studies conducted on cultured cells exposed to prefibrillar protein aggregates of Aβ, a significant increase in intracellular Ca^{2+} levels were found (Mattson, 1999; Tweten *et al.*, 2001; De Felice *et al.*, 2007; Demuro and Parker 2013; Cascella *et al.*, 2017). These events can lead to the activation of apoptosis or other types of cell death (Bucciantini *et al.*, 2004; Stefani, 2010; Cascella *et al.*, 2017). The increase in free cytosolic Ca^{2+} has been often attributed to the involvement of specific ion channels in cell membranes exposed to oligomers (Tozaki *et al.*, 2002; Ye *et al.*, 2003; Demuro *et al.*, 2005; De Felice *et al.*, 2007; Zhao *et al.*, 2009; Decker *et al.*, 2010; Alberdi *et al.*, 2010; Texidò *et al.*, 2011; Sinnen *et al.*, 2016).

Aβ may indeed induce increased Ca^{2+} influx via ion channels in the cellular membrane, such as the NMDAr, a potential source playing an important role in excitatory synaptic neurotransmission (Hardingham and Bading, 2010). It was indeed observed that such toxic oligomers accumulate in regions of the membrane containing high levels of NMDAr and α-amino-3-hydroxy-5-methyl-4-isoxazolepropionic acid receptors (AMPAr) (Decker *et al*., 2010; Cascella *et al*., 2017). Another adverse effect of Aβ is a reduction in NMDAr expression and its enhanced endocytosis (Snyder *et al*., 2005). A potential source for this high level of intracellular Ca^{2+} could also be the direct entry of Ca^{2+} ions across cell membranes, through mechanisms of interaction of these deleterious species with the lipid bilayer and its consequent destabilization or perforation, or though the formation of Ca^{2+}-permeable pores in the plasma membrane mediated by the Aβ peptides (Arispe *et al.*, 1993; Demuro *et al*., 2005; Arispe *et al.*, 2007; Evangelisti *et al*., 2012; Cascella *et al*., 2017).

Toxic α-synuclein oligomers associated with the intraneuronal inclusions called Lewy bodies typical of PD, are capable of forming pore-like structures with non-selective loss of various components (Volles *et al.*, 2001; Quist *et al.*, 2005; Angelova *et al.*, 2016). These effects have an impact on calcium signalling and cell viability (Angelova *et al.*, 2016). Recent studies show that prolonged exposure to α-synuclein oligomers, but not monomers or fibrils, causes an increase in basal synaptic transmission (Diògenes *et al.*, 2012). This occurs through a mechanism dependent on the activation of NMDAr, triggering an increased contribution of calcium permeability of AMPAr (Diògenes *et al.*, 2012).

NMDAr are the main excitatory receptors in the mammalian CNS (Hansen *et al*., 2017). They are heteromeric and constitute integral membrane proteins and they are associated with other types of Glu-type receptors such as AMPAr (Stephenson, 2001).

The molecular mechanisms of NMDAr and AMPAr, therefore, are to be considered strictly responsible for the neuronal death induced by misfolded oligomers (Sattler and Tymianski, 2001).

1.1.9. AMPAr and NMDAr

At excitatory synapses, the postsynaptic effects of Glu are mediated by different types of Glu receptors: the ionotropic Glu receptors (iGluRs) comprising AMPAr, NMDAr and kainate receptors, and the metabotropic Glu receptors (mGluRs). The AMPAr and NMDAr are the most abundant iGluRs in the brain, responsible for mediating the vast majority of excitatory transmission in neuronal networks. They are ligand-gated ion channels that mediate the fast synaptic responses, while mGluRs are coupled to downstream signaling cascades that act on much slower timescales (Sheefhals and MacGillavry, 2018).

The spatial segregation of receptor types has important functional implications as the distinct localization with respect to the presynaptic release site is predicted to greatly impact the activation kinetics of these receptor types (Sheefhals and MacGillavry, 2018). Computational models predict that the AMPAr opening is highest near the vesicle release site suggesting the importance of their density with respect to the presynaptic release site (Franks *et al*., 2003; Raghavachari and Lisman, 2004). Moreover, NMDAr non-saturation has been demonstrated experimentally at different types of synapses, where increasing presynaptic release or focal application of exogenous Glu resulted in larger amplitude responses (Liu *et al*., 1999; McAllister and Stevens, 2000; Pankratov and Krishtal, 2003).

AMPAr are hetero-trameric complexes composed of different combinations of four subunits, i.e. GluA1–4 (Lu *et al*., 2009; Wenthold *et al*., 1996). AMPAr were observed to form distinct subsynaptic regions of high molecular density, of around 70 to

80 nm in diameter, named nanodomains. Most synapses were shown to contain one to three distinct nanodomains, each consisting of around 20 receptors (Sheefhals and MacGillavry, 2018). Additionally, these presynaptic nanodomains are spatially aligned with postsynaptic AMPAr nanodomains, forming a trans-synaptic molecular 'nano-column' (Sheefhals and MacGillavry, 2018). This organization provides a simple, but powerful mechanism to efficiently modulate the efficiency of synaptic transmission.

The NMDAr consist of three different subunits termed GluN1-3, posttranscriptional RNA processing of GluN1 subunits gives rise up to eight different splice variants, GluN2 and N3 subunits are encoded by four (GluN2A-D) and two (GluN3A and B) genes respectively. Functional NMDAr are hetero tetramers containing two obligatory GluN1 subunits in combination with two GluN2 and/or GluN3 subunits (Vyklicky *et al*., 2013). Also, the NMDAr are organized in higher density nanodomains that may serve to optimize the open probability of these receptors by alignment with the presynaptic release site (Sheefhals and MacGillavry, 2018).

1.2. Amyloid β peptide

1.2.1. Aβ structure and relationship of AD

As previously discussed, the amyloid β peptide (Aβ) has an important role in the development of AD, as its characteristic amyloid plaques are mainly composed by aggregated Aβ peptide. It is a normal peptide generated during life, from the APP, an integral transmembrane protein with extracellular domains whose normal function remains unclear (Gouras *et al.,* 2015). Studies with transiently transfected cell lines show that APP moderates cell survival, growth, and motility, along with neurite outgrowth and functions, which are attributed to the release of soluble ectodomains upon normal

cleavage of APP (Thinakaran and Koo, 2008; Oh *et al.*, 2009). APP encodes type 1 transmembrane glycoprotein, which is cleaved either via a nonamyloidogenic pathway (normal state) or via an amyloidogenic pathway (diseased state) (Selkoe, 1994). Aβ production and secretion is stimulated by synaptic activity and its increased level, which lead to the aggregation process and to the amyloid plaque formation, is correlated with an alteration in synapses, particularly evident on microscopy labelling the presynaptic protein synaptophysin in brain (Gouras *et al*., 2015).

APP may be cleaved by a α-secretase, a neuronal protease producing the soluble extracellular sAPPα fragment and the C-terminal fragment C83 in the membrane, which is further cleaved by γ-secretase at residue 711, releasing a soluble P3 peptide (Fig. 1.6) (Solkoe, 2004; Panza *et al.*, 2019). Alternatively, the amyloid pathogenic pathway starts with an altered cleavage of APP by a β-secretase, generating the truncated soluble extracellular sAPPβ fragment and the cell-membrane-bound C99 fragment. The latter is cleaved intracellularly by a γ-secretase, producing the amyloid intracellular domain and the Aβ peptide. Cleavage of both C83 and C99 by γ-secretase releases the APP soluble intracellular domain (AICD) into the cytoplasm, which could translocate to nuclei for further gene-expression function (Fig 1.6) (Solkoe, 2004; Panza *et al.*, 2019).

In the non-amyloidogenic pathway, the α-secretase enzyme cleaves APP at residues 16–17 of the Aβ domain and produces soluble and non-pathogenic precursors. In neurons, the metalloprotease ADAM10 and ADAM17 are considered the major α-secretases (Tiwari *et al*., 2019). The soluble hydrophobic fragment P3, produced in this process, has a role in normal synaptic signalling, but its exact functions are still to be elucidated. The sAPPα produced by α-secretase acts as a neuroprotective factor and has also a role in cell–substrate adhesion (Tiwari *et al*., 2019). The presence of sAPPα is associated with

normal synaptic signalling and adequate synaptic plasticity, learning, memory, emotional behaviour, and neuronal survival (Kimberly *et al*., 2001).

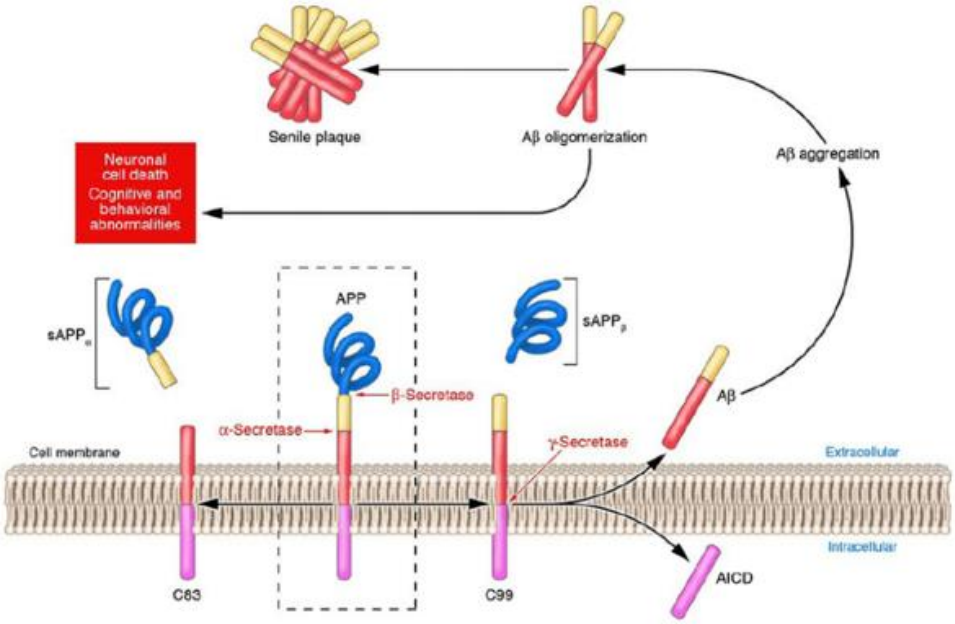

Figure 1.6. Representative scheme of the non-amyloidogenic and amyloidogenic pathways of APP processing. APP is cleaved by α- or β-secretase. In the non-amyloidogenic pathway, the cleavage by α-secretase generates sAPPα and C83 (left). In the amyloidogenic pathway the cleavage by β-secretase generates sAPPβ and C99 (right). C83 is cleaved by gamma-secretase, generating AICD and P3 (not shown). C99 is also cleaved by gamma-secretase, generating AICD and Aβ (right) (Spies *et al*., 2012).

In the amyloidogenic pathway APP is cleaved differently and Aβ is released through sequential cleavages by β-secretase and γ-secretase. The former is the beta-site APP cleaving enzyme 1 (BACE1) and the latter is an intramembrane aspartyl protease that is made up of four proteins: presenilin, nicastrin, anterior pharynx-defective 1 (Aph1), and Psen2 complexed together (Bergmans and De Strooper, 2010). The cleavage by these two secretases leads to the formation of the Aβ peptide that further polymerizes, forming aggregated plaques. There are two main types of Aβ that have a direct role in plaque formation and induced neurotoxicity, which have different length: the 40 amino acid long $A\beta_{40}$ and the 42 amino acid long $A\beta_{42}$. $A\beta_{40}$ is more abundant and less

neurotoxic than $A\beta_{42}$, which is highly insoluble and severely neurotoxic (Panza *et al.*, 2019).

The amino acid sequence of Aβ peptide was discovered in 1984, from extracellular deposits and amyloid plaques of post-mortem brain of AD patients (Glenner and Wong, 1984). It has an amphipathic character, as the N-terminal segment is hydrophilic and the 12-14 C-terminal amino acids are very hydrophobic. This is consistent with the predicted localization of Aβ residues 1–28 in a soluble, extracellular APP domain, while residues 29–42 are contained in a predicted transmembrane helix of APP (Selkoe *et al.*, 2004). The $A\beta_{40}$ peptide contains 17 hydrophobic, 11 polar and 12 charged residues. $A\beta_{42}$ peptide includes two additional hydrophobic residues at the C-terminal, that makes the $A\beta_{42}$ peptide more toxic and aggregation prone (Yoshiike *et al.*, 2003). The Aβ monomer is intrinsically disordered in an aqueous environment and it adopts a large number of conformations (Uversky, 2009; Ball *et al.*, 2011). Structural analysis of Aβ monomers was performed using NMR and molecular dynamics (MD) simulations (Coles *et al.*, 1998). In the membrane-mimicking environment, $A\beta_{40}$ and $A\beta_{42}$ monomers predominantly remain in an α-helical conformation (Coles *et al.*, 1998). The region Asp1-His14 of the $A\beta_{40}$ monomer remains unstructured, and the region between residues Gln15 and Val36 adopts an α-helical conformation with a turn around Gly25-Asn27 (Coles *et al.*, 1998) (Fig. 1.7C). $A\beta_{42}$ monomer contains two α-helix regions, Ser8-Val24 and Lys28-Val38, and a turn region around Gly25-Lys28 (Crescenzi *et al.*, 2002; Janek *et al.*, 2001) (Fig. 1.7B). In an aqueous environment, the $A\beta_{40}$ monomer has an α-helix in the region between His13-Asp23 and an unstructured region in the N- and C-terminal (Vivekanandan *et al.*, 2011) (Fig. 1.7A), while in the $A\beta_{42}$ monomer, the region between Try10-Asp23 remained in α-helix conformation and the region between Leu34-Gly38 contains a certain degree of helical structure, whilst the Gly25-Lys28 region forms

a turn (Tomaselli *et al.*, 2006) (Fig. 1.7D). The Aβ peptide present in the micelle-like environment has the highest α-helix content, whilst the Aβ peptide present in 100% aqueous environment has the lowest α-helix content. MD simulation studies have shown that hydrophobicity, flexibility, and mobility of the N-terminal region is important for obtaining the misfolded structure. The C-terminal region of both peptides ($A\beta_{40}$ and $A\beta_{42}$) favours a membrane environment, while the N-terminal region favours an aqueous region and forms a coil (Luttmann and Fels, 2006; Agrawal and Skelton, 2017; Valerio *et al.*, 2005; Miyashita *et al.*, 2009).

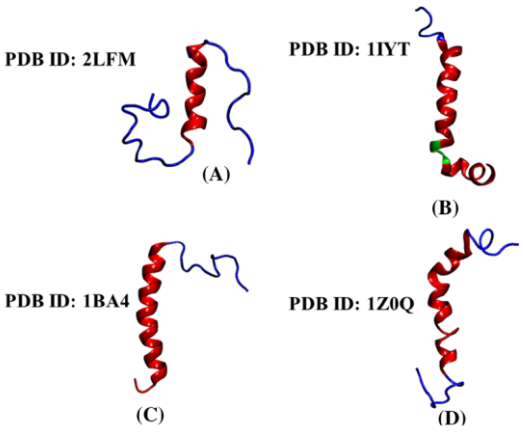

Figure 1.7. Cartoon representation of (A) $A\beta_{40}$ monomer structure (PDB ID: 2LFM) in a complete aqueous environment; (B) $A\beta_{42}$ monomer structure (PDB ID: 1IYT) in a membrane-mimicking environment; (C) $A\beta_{40}$ monomer structure (PDB ID: 1BA4) in a membrane-mimicking environment; (D) $A\beta_{42}$ monomer structure (PDB ID: 1Z0Q) in an aqueous environment. The α-helix region has shown in red colour, the unstructured region in blue colour and turns region in green (Agrawal and Skelton, 2019).

$A\beta_{40}$/$A\beta_{42}$ aggregation in the extracellular space results in blocked ion channels, altered calcium homeostasis, increased mitochondrial oxidative stress, and diminished energy metabolism and glucose regulation, which contributes to deterioration of neuronal health and finally to neuronal cell death (Panza *et al.*, 2019). Aβ deposition in the brain drives τ phosphorylation, NFTs formation in the intracellular space, synaptic loss, neuronal death, and cognitive impairment. The relatively rare early onset familial AD is

caused by autosomal-dominant mutations in PSEN1, PSEN2, or APP genes. These alterations either increase the Aβ production, the production of the most toxic $A\beta_{42}$ form, or increase the propensity of Aβ aggregate (Panza *et al.*, 2019). In the late onset sporadic AD, Aβ is not caused by specific mutations, although a number of genetic risk factors have been disclosed, in addition to a number of risk life styles (Panza *et al.*, 2019).

1.2.2. Aβ aggregation process

Enormous efforts have been made to identify how Aβ aggregates into fibrils and to characterize the intermediates formed in the process. In the process of fibrillation, three stages are distinguished: the lag-period, in which the formation of nuclei (nucleation) and oligomers of different sizes takes place, the growth of fibrils, in which fibrils grow from these nuclei through the addition of monomers, and the plateau phase, in which the process reaches equilibrium and most soluble proteins are converted into fibrils (Chiti and Dobson, 2017; Galzitskaya *et al.*, 2018). Early studies were mainly focused on the formation and toxicity of mature Aβ fibrils, but it was found that instead various prefibrillar, soluble oligomeric forms of Aβ are more likely to be the pathological species. This is supported, among various lines of evidence, by a weak correlation between the number of fibrillar deposits and severity of AD (DeKosky and Scheff, 1990; Terry *et al.*, 1991), and by a better correlation between levels of soluble forms of Aβ and cognitive impairment (Lue *et al.*, 1999; McLean *et al.*, 1999).

A large number of $A\beta_{40}$ and $A\beta_{42}$ oligomers have been observed to form following *in vitro* experiments of Aβ aggregation. The smallest type of oligomers for both $A\beta_{40}$ and $A\beta_{42}$ are the low-n oligomers, from dimers to tetramers (Walsh *et al*., 2005). Stable Aβ dimers have been detected in *in vitro* experiments with synthetic $A\beta_{40}$ and $A\beta_{42}$ (Garzon-Rodriguez *et al*., 1997; Hilbich *et al.*,1992), human brain homogenates (Roher *et al*.,

1996) and cell culture media (Podlisny *et al.*, 1995). Aβ dimers detected *in vivo* are supposed to form intracellularly (Walsh *et al.*, 2000). These low-n oligomers are SDS-resistant and are apparently secreted by cultured cells (Podlisny *et al.*, 1995). They have been shown to inhibit hippocampal long-term potentiation when injected into the rat brain (Walsh *et al.*, 2002). Small Aβ oligomers have been found in *in vitro* experiments, in the growth medium of Aβ-secreting cells and in human brain homogenate (Kuo *et al.*, 1996; Walsh *et al.*, 2002; Bitan *et al.*, 2003). They comprise oligomers of 3-50 subunits and inhibit long term potentiation in rat hippocampal slices.

It has been observed that the initial phase of oligomerization of $A\beta_{42}$ *in vitro*, in contrast to that of $A\beta_{40}$, involves the formation of pentamers/hexamers termed paranuclei, mostly unstructured (Bitan *et al.*, 2003; Levine, 1995). Further small oligomeric species of around 60 kDa, termed $A\beta_{42}$ globulomers, have been identified *in vivo* in murine and in human brain as well as *in vitro* (Barghorn *et al.*, 2005). They were suggested to be built up in a micellar-like manner with the hydrophobic C-terminal part of Aβ buried in the interior and the more hydrophilic N-terminal part facing the surrounding solvent (Barghorn *et al.*, 2005).

ADDLs are nonfibrillar and neurotoxic Aβ oligomers, with a size from 17 to 42 kDa. They were found in *in vitro* fibrillization experiments and in soluble extract of human and murine brain tissue with a correlation between their level and the cognitive defects of AD patients (Lambert *et al.*, 1998; Chromy *et al.*, 2003; Klein *et al.*, 2004; Georganopoulou *et al.*, 2005). ADDLs contain primarily trimers to hexamers and larger species up to 24mers and morphologically resemble spherical protofibrils (Harper *et al.*, 1999).

Annular Aβ structures have been found when incubating synthetic Aβ *in vitro* and they are found to be toxic in cell culture, with a membrane-disrupting process. They are

pore-like structures with an outer diameter of 8-12 nm and a molecular size around 150-200 kDa (Kagan *et al*., 2002; Lashuel *et al*., 2002; Quist *et al*., 2005).

Protofibrils seem to be true intermediates on the pathway to fibrils and the largest form of soluble species, observed primarily *in vitro*, they can be rapidly converted to Aβ fibrils when seeded by a small amount of preformed fibrils (Harper (1) *et al*., 1997). They are shorter (< 200 nm) and slightly thinner than mature fibrils and have been shown to induce neurotoxicity (Harper (2) *et al*., 1997; Walsh *et al*., 1997; Hartley *et al*., 1999). They have a core resistant to hydrogen exchange and weakly bind the dyes CR and ThT, suggesting a significant β-sheet content (Arimon *et al*., 2005; Kheterpal *et al*., 2003; Walsh *et al*., 1997; Williams *et al.*, 2005; Harper (1) *et al*., 1997; Harper (2) et al., 1997; Harper *et al*., 1999). Protofibrils appear to be in a dynamic equilibrium with lower-order oligomers (Walsh *et al*., 1999) and several studies indicate that they are also neurotoxic species in AD (Harper (1) *et al*., 1997, Rochet and Lansbury, 2000).

These are just a few examples of the Aβ oligomers so far described in the literature, as isolated and characterized species *in vitro*. This long list also includes amylospheroids (ASPDs), pentamers (5mers), A11-positive PFOs, OC-positive fibrillar oligomers (FOs) and spherical amyloid intermediates (Kayed *et al*., 2003; Kayed *et al*., 2007; Hoshi *et al*., 2003; Chimon *et al*., 2007; Ahmed *et al*., 2010).

Aβ fibrils are thermodynamically stable, structurally organized, highly insoluble, filamentous protein aggregates, with repeating units of β-strands aligned perpendicular to the fibre axis and a distinctive X-ray diffraction pattern consistent with high β-sheet content (Ross and Poirier, 2005). Aβ fibrils bind CR and ThT (Klunk *et al.*, 1999; LeVine, 1999) and those formed *in vitro* are similar to those extracted from human AD plaques (Hilbich *et al*., 1992; Kirschner *et al*., 1987). They are composed of multiple protofilaments twisted around each other aligned in a perfect parallel fashion, which

results in filamentous structures with a diameter of 7–13 nm (Chiti and Dobson, 2017). Aβ has the ability to form multiple fibrillar structures, as different fibril morphologies with different molecular structures can be obtained *in vitro* by varying the aggregation conditions (Petkova *et al*., 2005; Garai and Frieden, 2013). The insoluble Aβ fibrils accumulate extracellularly in deposits called amyloid plaques, characteristic of AD patients and in murine brain. They represent the final state of the Aβ aggregation process *in vivo* (Weissmann, 2004).

1.2.3. Aβ oligomer toxicity

The oligomeric forms of Aβ accumulating as intermediates in the aggregation process or released by mature fibrils have a variety of pathogenic effects, as they are able to interact with a number of biological targets (Benilova *et al*., 2012; Selkoe and Hardy, 2016). The damage caused by the Aβ oligomers in brain tissue, combined with accumulating τ pathology, results in irreversible neurodegeneration. Many mechanisms have been described through which Aβ oligomers mediate their cytotoxic effect.

The Aβ oligomers-derived synaptotoxicity, with the impairment of the hippocampal long term potentiation (LTP) and long term depression (LTD), is correlated with the Aβ oligomer-induced hyperexcitability of postsynaptic AMPAr and NMDAr (Li *et al.*, 2011; Yamin, 2009). Mechanistically, the levels of the AMPAr subunit GluA1, a critical mediator of LTP expression, have been shown to be increased in AD hippocampus (Marcello *et al.*, 2012). GluA1 phosphorylation and GluA3 levels are both increased in young AD model mice (Megill *et al.*, 2015; Cantanelli *et al*., 2014), but their levels are significantly decreased in old AD model mice. Aβ might initially target the calcium-permeable GluA2-lacking AMPAr to induce synaptic alterations and after its activation other AMPAr subunits will be involved in the excess synaptic activity (Gilbert *et al.*,

2016; Whitcomb *et al.*, 2015). The impairment of LTP is also correlated with a decrease of the GABAergic inhibitory activity mediated by the Aβ oligomers, with a GABAergic interneuron loss and dysfunction (Villette *et al*., 2012; Wu *et al.*, 2014), which may be due to Aβ-mediated GABA receptor internalization (Ulrich, 2015). The induction of LTD requires activation of NMDAr or mGlu receptor in the hippocampus (Collingridge *et al*., 2010; Connor and Wang, 2016). An increase in intracellular calcium can trigger signalling cascades involved in LTD induction (Connor and Wang, 2016).

Several studies investigating the mechanisms of Aβ oligomer–induced toxicity start from the assumption that the oligomers are stable structures that interact specifically with receptors. They can apparently affect several cell-surface neuronal receptors, such as NMDAr, AMPAr, mGlu, insulin, nAChRs, β-adrenergic and GABA receptors, and alter numerous signalling pathways. Cellular prion protein (PrP^C) is a glycoprotein highly expressed in the brain (Barry *et al*., 2011; Freir *et al*., 2011; Klyubin *et al.*, 2014), whose binding with the Aβ oligomers has been reported in AD brain tissue and it was confirmed in mouse studies (Dohler *et al*., 2014; Kostylev *et al*., 2015; Balducci *et al.*, 2010; Calella *et al*., 2010; Lauren *et al*., 2009). It has been proposed that such binding mediates the toxic effects of Aβ oligomers at synapses as it allows the oligomers to reach these critical sites. Interestingly, Aβ oligomers, but not monomers, were found to increase the localization of PrP^C to the cell surface in several cell lines and hippocampal neurons (Caetano *et al*., 2011). Aβ oligomers were also found to interact with various receptors of microglial cells and increase the levels of inflammatory cytokines like tumour necrosis factor-alpha, interleukins (IL-1, IL-6), interferon-γ, and chemokines (Domingues *et al*., 2017; Lyons *et al*., 2007). These changes likely boost microglial activation and make microglia more susceptible to secondary stimuli.

Several AD studies are focused on Aβ-induced glutamatergic excitotoxicity. The physiological clearance of Glu can prevent the excitotoxicity mediated by excessive NMDAr activation, particularly extrasynaptic NMDAr activation. Aβ oligomers have been shown to alter this process in various experimental systems (Lanznaster *et al.*, 2017; Li *et al*., 2009; Matos *et al*., 2008; Piermartiri *et al*., 2010; Tong *et al.*, 2017), with several different mechanisms, such as decreasing Glu uptake and inducing rapid Glu transporter mislocalization and internalization in astrocytes, leading to the reduction of Glu clearance (Lanznaster *et al*., 2017; Li *et al*., 2009; Matos *et al*., 2012; Hascup and Hascup, 2016; Scimemi *et al*., 2013). In addition, the cystine/Glu transporter (xCT) mediating the release of Glu by astrocytes is upregulated, leading to the increase of its release (Qin *et al*., 2006). The increased extracellular Glu levels could activate extrasynaptic NMDAr and leads to LTP impairment, LTD enhancement, and synapse loss. The pro-inflammatory cytokines potentially released from activated microglial cells in the presence of Aβ oligomers have been shown to alter the ability for glial Glu uptake (Carmen *et al*., 2009; Dumont *et al*., 2014; Sulkowski *et al*., 2009; Tong *et al*., 2017; Verma *et al*., 2010).

The maintenance of plasma membrane integrity is critical for cell viability and an increase in its permeability has long been associated with amyloid pathogenesis. Aβ oligomers were found to interact with the phospholipid bilayer, causing its destabilization and perforation (Kawahara *et al*., 2000; Demuro *et al.*, 2005; Sepùlveda *et al*., 2014; Cascella *et al*., 2017; Arispe *et al*., 1993; Arispe *et al*., 2007). Aβ can be incorporated into membranes and form a pore, causing the disruption of ion homeostasis, such as calcium, promoting numerous degenerative processes, including free radical formation and phosphorylation of τ, thereby accelerating neurodegeneration (Kawahara *et al*., 2000; Yatin *et al*., 1998; Takashima *et al.*, 1993). The membrane permeabilization could be caused also by a channel-independent disruption of the integrity of the phospholipid

bilayer, without the formation of pores, with a consequent penetration of the oligomers in the cells, where they similarly disrupt intracellular membranes (Bucciantini *et al*., 2004; Demuro *et al*., 2005). Other studies showed the ability of the soluble oligomers to increase the membrane conductance in a conformation-specific manner, which could lead to depolarization of the plasma membrane, which would be injurious to the function of cells, especially for neuronal function (Kayed *et al*., 2004).

In addition to extracellular Aβ, there is evidence demonstrating the intracellular accumulation of Aβ in AD patients, transgenic mice, and cultured cells (Glabe, 2001; LaFerla *et al*., 2007; Gouras *et al*., 2010; D'Andrea *et al*., 2001; Gouras *et al*., 2000; Gyure *et al*., 2001; Langui *et al*., 2004; Wirths *et al*., 2001). The Aβ accumulation in neurons was observed to inhibit the activities of the proteasome and deubiquitinating enzymes. The inhibition of the ubiquitin-proteasome system (UPS) impairs the endocytic trafficking of neuronal receptors and may be the cause of synaptic dysfunction in AD (Almeida *et al*., 2006). Furthermore, the inhibition of UPS leads to an increase of Aβ levels (Oh *et al*., 2005; Tseng *et al*., 2008). Accumulation of Aβ has also been observed in mitochondria, related to diminished enzymatic activity (Manczak *et al*., 2006; Caspersen *et al*., 2005).

1.2.4. Calcium role in Aβ oligomer cytotoxicity

In neuronal cells the extremely precise control of Ca^{2+} concentration is a well defined requisite, mediating vital physiological processes and controlling the synaptic plasticity, and defects on Ca^{2+} homeostasis can lead to destructive consequences and alter normal neuronal activity leading to neurodegeneration, such as in AD (Berridge, 1998).

Many mechanisms have been described through which Aβ oligomers cause an increase of Ca^{2+} levels in AD. As described above, in the phenomenon known as

excitotoxicity, Aβ oligomers were found to increase the release of Glu by astrocytes (Acosta *et al*., 2017). Astrocytic Ca^{2+} elevations in response to neuronal activity lead to Ca^{2+}-dependent release of gliotransmitters, such as Glu (Acosta *et al*., 2017). Chronic Aβ exposure leads to a modulation of Ca^{2+} responses to chemical transmitters and enhance expression of genes encoding receptors that induce astrocytic Ca^{2+} signalling (Xiu *et al*., 2005). Application of Aβ oligomers to hippocampal astrocytes induced Ca^{2+} elevations mediated by the nicotinic acetylcholine receptor α7 (α7nAChR) causing an increase in Glu release (Talantova *et al*., 2013). Moreover, the Aβ activation of astrocytic mGluR5 might produce sustained astrocyte Ca^{2+} signalling increasing the frequency of hippocampal and cortical NMDAr mediated slow inward currents (SICs) in AD mouse models, indicative of enhanced glutamatergic gliotransmission and, therefore, of dysregulated astrocyte–neuron signalling (Gomez-Gonzalo *et al*., 2017). Aβ oligomers were also found to reduce the Glu uptake in astrocytic cells by the excitatory amino acid transporters 1 and 2 (EAAT-1 and EAAT-2), which are the human homologs of rodent Glu/aspartate transporter (GLAST) and Glu transporter-1 (GLT-1), respectively. This reduction may be due to Aβ oligomer-dependent reductions of GLT-1 and GLAST expression or their cell surface localization (Acosta *et al*., 2017). The combined effects of impaired Glu uptake and enhanced Glu release cause an excessive Glu concentration in perisynaptic space, which activates iGluRs acting as Ca^{2+} channels on neuronal membranes, particularly extrasynaptic NMDAr, leading to a rise in intraneuronal Ca^{2+} concentration (Zhang *et al*., 2016; Wang and Reddy, 2017; Acosta *et al*., 2017).

Aβ oligomers have also been found to induce a Glu independent Ca^{2+} influx from the extracellular space to the cytosol across the cell membrane. One possible explanation is the direct passage through the lipid bilayer (Fig. 1.8), or through Ca^{2+}-permeable pores formed in the plasma membrane by the Aβ oligomers (Fig. 1.8) (Arispe *et al*., 1993;

Arispe *et al*., 2007). Aβ may induce increased calcium influx via the activation of the voltage-gated Ca^{2+} channels, in particular the activation of L-type VGCCs (Ueda *et al*., 1997), but it was also reported a suppression of P/Q-type VGCCs calcium currents (Nimmrich *et al*., 2008). Another potential source for intracellular calcium is the Glu-independent overactivation of the NMDAr (Snyder *et al*., 2005; De Felice *et al*., 2007; Deshpande *et al*., 2009; Alberdi *et al*., 2010; Decker *et al*., 2010; Rönicke *et al*., 2011; Texidò *et al*., 2011; Sinnen *et al*., 2016; Arbel-Ornath *et al*., 2017) and AMPAr (Tozaki *et al*., 2002; De Felice *et al*., 2007; Zhao *et al*., 2009; Alberdi *et al*., 2010), whose activation mechanism is not yet clear. Aβ oligomers were also found to augment the transient receptor potential melastatin 2 (TRPM2) current, a Ca^{2+}-permeable nonselective cation channel most highly expressed in the CNS. Several mechanisms of activation are suggested, such as the oxidative stress occurring via the production of its agonist, NAD^{+}-derived ADPR associated with mitochondrial damage, or the elevated Ca^{2+} or the aberrant NMDAr stimulation (Ostapchenko *et al*., 2015). Moreover, the Ca^{2+} hyperactivity caused by Aβ oligomers involve the activation of transient receptor potential A1 (TRPA1), which might be directly targeted by Aβ oligomers or might be secondarily activated through an oligomer-induced oxidative stress and/or through its mechanosensory properties if Aβ oligomers bind to the plasma membrane (Bosson *et al*., 2017).

In addition to adverse Aβ effects, mutated presenilin directly cause Ca^{2+} dysregulation in AD with an overfilling of the ER with Ca^{2+} and the excessive Ca^{2+} release through the inositol trisphosphate receptor (IP_3R) (Ito *et al*., 1994; Leissring (1) *et al*., 1999; Leissring (2) *et al*., 1999; Nelson *et al*., 2007; Stutzmann *et al*., 2006). Mutant presenilin could directly affect IP_3R gating, store-operated Ca^{2+} entry (SOCE), ryanodine receptor (RyR) or sarco-endoplasmic reticulum calcium ATPase (SERCA), or forms ER calcium leaking pore inducing ER Ca^{2+} overfilling (Pchitskaya *et al*., 2018). Recent

results suggest a significant role for neuronal SOCE pathway in AD pathogenesis, activated following depletion of ER Ca^{2+} levels. Reduced expression levels of SOCE ER Ca^{2+} sensor STIM2 were discovered in experiments with AD patient fibroblasts (Pchitskaya *et al.*, 2018).

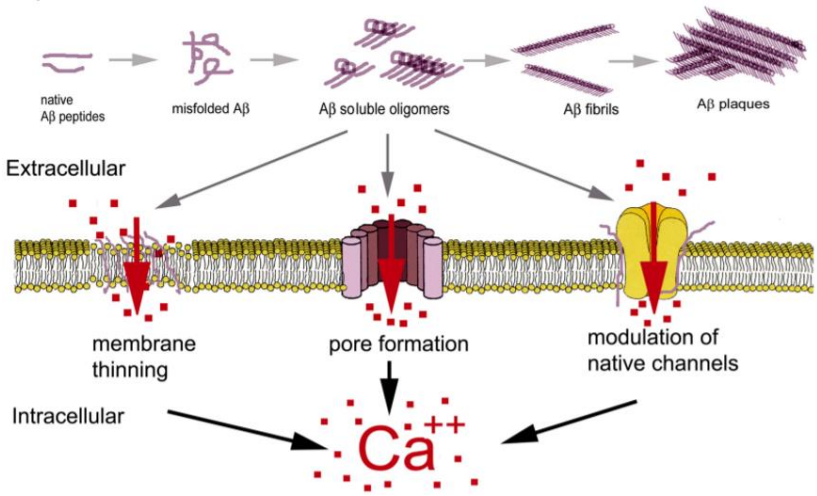

Figure 1.8. Schematic representation of Aβ oligomers induced mechanism of intracellular Ca^{2+} increase by the direct passage through the lipid bilayer, or through Ca^{2+}-permeable pores formed in the plasma membrane or by the activation of specific Ca^{2+} permeable channels (Demuro *et al.*, 2010).

1.3. The HypF-N model protein

1.3.1. Structure and function of HypF-N

HypF is a large multi-domain protein of about 82 KDa, present in *E. Coli* and other bacteria, whose function is required for the synthesis, folding and maturation of active NiFe-hydrogenases (Paschos *et al.*, 2002; Blokesch (2) *et al.*, 2004). HypF is characterized by several domains: a N-terminal acylphosphatase domain encompassing residues 1-91 (Paschos *et al.*, 2002; Rosano *et al.*, 2002), a Zn-finger domain comprising two almost identical Zn fingers (residues 107–136 and 157–186) essential for HypF

function in hydrogenase maturation (Paschos *et al*., 2002; Petkun et al., 2011), a middle domain (residues 188–378) with structural similarity to the YrdC-like proteins (Petkun *et al*., 2011) and a C-terminal domain (residues 379–746) with a motif characteristic of carbamoyl transferases (Paschos *et al*., 2002; Petkun *et al*., 2011).

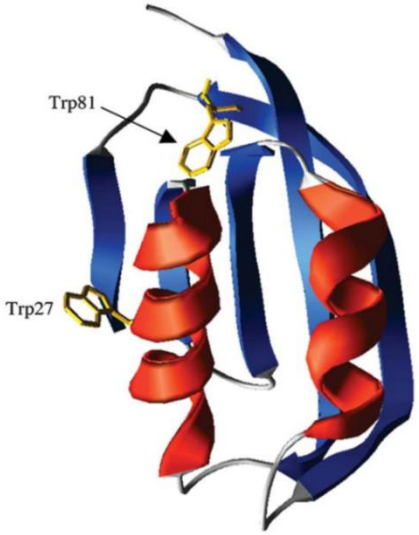

Figure 1.9. Three-dimensional structure of native HypF-N from X-ray crystallography (Rosano *et al*., 2002). The red and blue colours indicate α-helices and β-strands, respectively. The two tryptophan residues of the protein (Trp27 and Trp81) are shown in yellow (Marcon *et al*., 2005).

NiFe-hydrogenases require a set of complementary and regulatory proteins for correct folding and maturation processes, which include HypF as one of the essential proteins (Friedrich and Schwartz, 1993). NiFe-hydrogenases have an Ni-Fe site in which the iron has one carbon monoxide (CO) and two cyanide (CN-) groups as ligands (Reissmann *et al*., 2003). Synthesis of these ligands requires the activity of HypF, which support the conversion of carbamoyl phosphate into CO and CN-, promoting coordination of these ligands to the hydrogenase metal cluster (Blokesch (1) *et al*., 2004; Reissmann *et al*., 2003).

The N-terminal domain of HypF (HypF-N) is a small 11 kDa α/β protein of 91 residues, which belongs to the acylphosphatase superfamily (Chiti *et al*., 2001; Rosano *et al*., 2002). The crystallographic analysis revealed the existence of a ferredoxin-like

folding (Rosano *et al*., 2002). HypF-N is structured in a βαββαβ topology (plus an additional β-strand-5), with high compact and globular shape stabilized by intramolecular contacts of the two antiparallel amphipathic α-helices, which pack their hydrophobic residues against the inner face of the β-sheet, without leaving core cavities in the protein structure (Rosano *et al*., 2002). The HypF-N protein domain has β-sheet edge strands that are either very short (β5) or highly twisted (β4), the latter due to the presence of a proline, Pro78. Additionally, there is a cluster of charged residues (Asp72, Glu75-Arg76-Glu77) (Rosano *et al*., 2002). These structural elements are protective against native-like aggregation occurring through the propagation of β-β interaction at edge β-strands (Soldi *et al*., 2008).

HypF-N is not related with any human pathology, but it is a good model used to investigate the structural basis of the cellular dysfunction caused by misfolded protein oligomers, as it can be purified at a high yield, has relatively low costs and provides highly reproducible results in studies based on protein aggregation and on oligomer toxicity (Bucciantini *et al*., 2002; Campioni *et al*., 2008; Campioni *et al*., 2010; Zampagni *et al*., 2011; Mannini *et al*., 2012; Cascella *et al*., 2013; Tatini *et al*., 2013). HypF-N, under conditions that destabilize its native state or promote its co-operative unfolding into partially structured species, is able to form oligomers, protofibrils and amyloid-like fibrils *in vitro* and the premature oligomers have the same morphological, structural and tinctorial features as those formed by disease-related peptides and proteins (Chiti *et al*., 2001; Relini *et al*., 2004; Marcon *et al*., 2005; Campioni *et al*., 2008). These oligomers are sufficiently stable and maintain their morphological and structural properties even in very different conditions from those that promote their formation, allowing depth biophysical studies and cellular biology investigations (Campioni *et al*., 2010; Evangelisti *et al*., 2012; Tatini *et al*., 2013; Mannini *et al*., 2014). Moreover, HypF-N oligomers

formed *in vitro* and added to the extracellular medium of cultured cells (Bucciantini *et al*., 2002; Cecchi *et al*., 2005; Campioni *et al*., 2010; Mannini *et al*., 2012; Mannini *et al*., 2014), or injected into the mouse brain (Baglioni *et al*., 2006; Zampagni *et al*., 2011; Tatini *et al*., 2013), damage cell viability similarly to the oligomers related to many amyloid diseases.

1.3.2. *In vitro* aggregation of HypF-N

Monomeric HypF-N, under conditions that destabilized its native state, is able to form *in vitro* two different types of stable oligomers (Campioni *et al*., 2010). In particular, if the protein is incubated at the concentration of 48 μM for 4 hours at 25 °C in a solution with 50 mM acetate buffer, 12% (v/v) trifluoroethanol (TFE), 2 mM DTT, pH 5.5, it forms toxic oligomers known as type A oligomers (Campioni *et al*., 2010). If, instead, the protein is incubated at the concentration of 48 μM for 4 hours at 25 °C in a solution with 20 mM trifluoroacetic acid (TFA), 330 mM NaCl, pH 1.7, it forms non toxic oligomers known as type B oligomers (Campioni *et al*., 2010).

Both type A and B oligomers are able to bind ThT, an amyloid specific dye, increasing its fluorescence to similar extents, suggesting that both types of oligomers have an extensive intramolecular β-sheet structure. This ability to bind ThT is preserved when the oligomers are placed under physiological conditions, indicating an absence of re-solubilization (Campioni *et al*., 2010). Tapping-mode AFM (TM-AFM) images revealed the presence of spherical bead-like aggregates with heights in the range of 2–6 nm for type A oligomers (Fig. 1.10A) and 2–7 nm for type B oligomers (Fig. 1.10B) (Campioni *et al*., 2010).

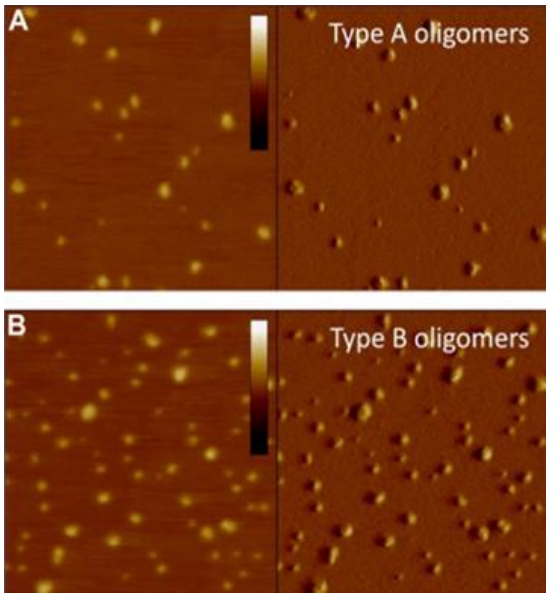

Figure 1.10. TM-AFM images (left, height data; right, amplitude data) of type A (A) and type B (B) oligomers of HypF-N resuspended at pH 7.0. Scan size, 500 nm. The colour bar corresponds to a Z range of 7 nm. These images represent the formation of spherical bead-like aggregates with heights in the range of 2-6 nm (A) and 2-7 nm (B) (Campioni *et al.*, 2010).

In order to identify the structural differences of the two types of oligomers, protein engineering and structural mapping techniques were used. In particular, the pyrene moiety (PM) was used, which allows to investigate the proximity between a pair of labelled residues. When two PM moieties are about 10 Å apart, they are able to form excited-state dimers, or excimers, which give rise to a band in the 430-470 nm region of the PM fluorescence emission spectrum (Krishnan and Lindquist, 2005). The studies were focused on 18 mutational variants of HypF-N, all carrying a single cysteine residue in different positions along the polypeptide chain and labelled with pyrene (PM). Each labelled variant was then aggregated separately under the two different conditions, and the fluorescence spectra of the resulting samples were acquired and analysed (Campioni *et al.*, 2010). The analysis of the fluorescence emission spectra of type B oligomers of HypF-N labelled with PM at the different residues allow to calculate the ratio between the intensity of the peak at 440 nm (excimer peak) and the intensity of the peak at 375 nm

(monomer peak) for each labelled residue (Fig. 1.11A). The results obtained indicate three specific regions of the molecule (corresponding the residues 22–34, 55–59 and 75–87) tightly and loosely packed at the structural core level of the non-toxic and toxic HypF-N oligomers, respectively (Fig. 1.11). Furthermore, a clear correlation was observed between the localization of these three regions (Fig. 1.11A) and the three main peaks shown in the hydropathy profile of HypF-N (Fig. 1.11B). These results demonstrate that the regions of the polypeptide sequence with greater hydrophobicity contribute to the formation of the structural core of the non-toxic HypF-N aggregates and that the level of ordered intermolecular packing between corresponding hydrophobic regions of the adjacent HypF-N molecules is less marked in the case of the toxic aggregates (Campioni *et al*., 2010).

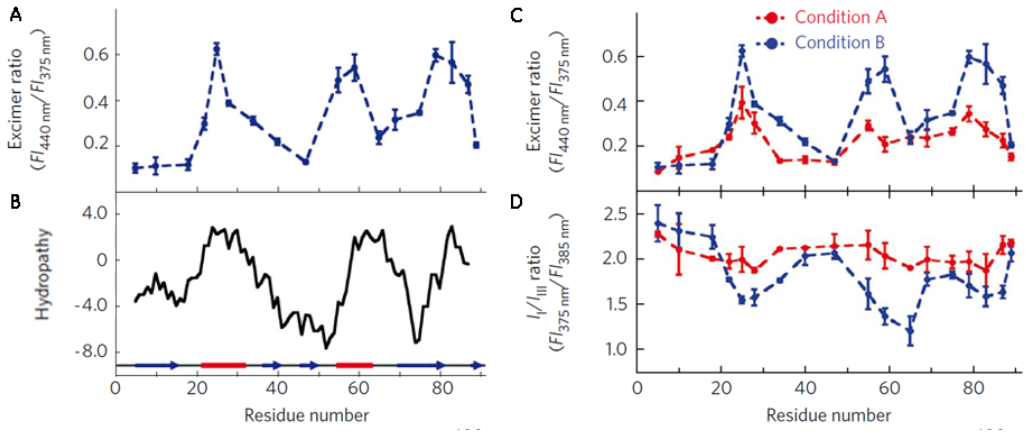

Figure 1.11. (A) Ratio between the fluorescence intensities measured at 440 nm (excimer peak) and 375 nm (monomer peak) for all the labelled positions along the HypF-N sequence. Error bars correspond to s.d. of at least two independent experiments per position. (B) Hydropathy profile of HypF-N calculated using the Roseman hydrophobicity scale (Roseman, 1988). In red the positions of α-helices and in blue the position of β-strands in the native structure. (C) Excimer ratio profiles of type A (red) and type B (blue) oligomers. Error bars correspond to s.d. of at least two independent experiments per position. (D) Ratio between the fluorescence intensities measured at 375 nm (I_I) and 385 nm (I_{III}) for all the labeled positions along the HypF-N sequence. Error bars correspond to s.d. of at least two independent experiments (Campioni *et al*., 2010).

To investigate the polarity of the environment explored by the PM moieties in the type A and B oligomers, the fluorescence intensity ratio at 350 nm (I_I) and 385 nm (I_{III}) was calculated for all the labelled positions along the HypF-N sequence (Dong and Winnik, 1984) (Fig.1.11D). The I_I/I_{III} ratio obtained for the two types of HypF-N oligomers indicate that the PM fractions are more accessible to the solvent (higher I_I/I_{III} ratio) in toxic oligomers rather than in non-toxic ones. In particular, this is observed at the level of the three main hydrophobic regions (Fig. 1.11D). The results of the excimers and the values of the I_I/I_{III} ratio indicate that in toxic oligomers the hydrophobic regions are more highly disorganized from a structural point of view and more exposed to the solvent than those in non-toxic oligomers (Campioni *et al*., 2010).

More recently, various biophysical techniques were used to characterise both types of oligomers in residue-specific structural detail (Capitini *et al*., 2018). Type A and B oligomers have a similar structural core, based on a β-sheet structure, which is more organized and compact in type A than type B oligomers, as determined with solid-state NMR (Capitini *et al*., 2018). The three-dimensional structures of the two oligomer types were probed using the analysis of Förster Resonance Energy Transfer (FRET), by determining the intermolecular interactions between pairs of residues labelled with 1,5-IAEDANS, used as the donor, and 6-IAF, used as the acceptor, located in different molecules and at different positions in the polypeptide chain. The results showed that the intermolecular distances between the N-terminus and other portions of the sequence in adjacent protein molecules in the oligomers are longer in the case of type B oligomers, suggesting a high degree of flexibility of the N-terminal region compared to type A oligomers. By contrast, the FRET efficiency values (E) measured for many of the distances between hydrophobic regions are higher in type B oligomers (Fig. 1.12, red boxes), indicating that the donor and acceptor fluorophores are, on average, closer

together and the three main hydrophobic regions (regions 18–30, 55–65, 75–87) appear to interact more closely in type B oligomers than in type A oligomers (Capitini *et al*., 2018). The greater structural flexibility of the non-toxic oligomers could induce the hydrophobic residues of the protein, which are free to move to form a compact hydrophobic nucleus, with the hydrophobic residues hidden inside. The greater rigidity of the toxic oligomers, on the other hand, prevents the formation of a compact hydrophobic nucleus, causing a fraction of the hydrophobic residues to remain exposed to the solvent, and allowing the establishment of aberrant intermolecular interactions with the cell membrane or with other possible cellular components (Capitini *et al*., 2018).

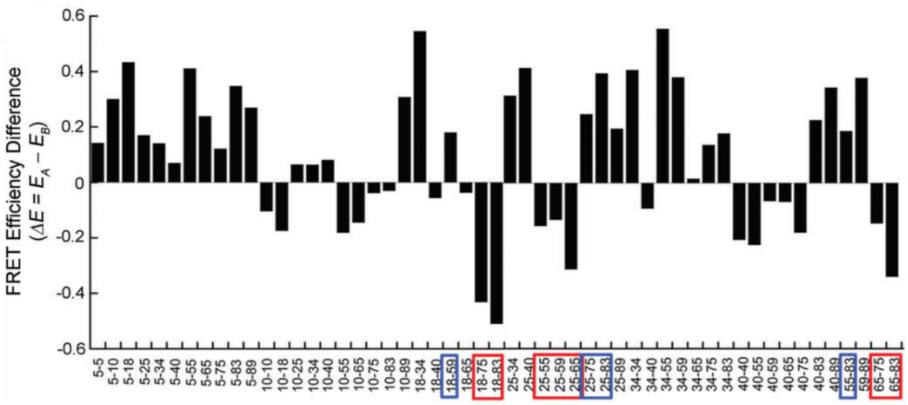

Figure 1.12. Differences between the E values of type A and type B oligomers ($\Delta E = E_A - E_B$) for the pairs of residues reported on the x axis; the pairs in boxes indicate interactions between hydrophobic residues with $\Delta E < 0$ (red) or $\Delta E > 0$ (blue) (Capitini *et al*., 2018).

In another study, HypF-N mutants were produced in order to increase the hydrophobicity of the three main hydrophobic regions of the sequence (Mannini *et al*., 2014). The results showed that SH-SY5Y cells exposed to the mutant type A oligomers generally determined higher levels of viability than cells treated with wild-type type A oligomers and that mutant type B oligomers appeared toxic in some cases. To clarify the link between the oligomer toxicity and their structural properties, the extent of exposed

hydrophobic surface areas of the various mutant oligomers was tested by using ANS and their size was tested by using light scattering (Mannini *et al*., 2014). Oligomer toxicity was found to correlate, in a three-dimensional plot, with both solvent-exposed hydrophobicity and size of the oligomers, indicating that both parameters play an important role in determining the deleterious effects of HypF-N misfolded oligomers (Mannini *et al*., 2014).

1.3.3. HypF-N oligomer toxicity

The biological activity of the type A and B oligomers were investigated transferring the pre-formed aggregates to physiological conditions and adding them to the cell culture media of human neuroblastoma cells (SH-SY5Y) and mouse endothelial cells (Hend) (Campioni *et al*., 2010).

First, the viability of the cells was monitored using the 3-(4,5-dimethylthiazol-2-yl)-2,5-diphenyltetrazolium bromide (MTT) reduction inhibition assay, a colorimetric assay for measuring cell mitochondrial activity based on the ability of NADPH-dependent cellular oxidoreductase enzymes to reduce the tetrazolium dye MTT to its insoluble formazan, which has a purple colour. The type A oligomers were found to decrease the MTT reduction in both cell lines, compared with the untreated cells and the native protein; by contrast, the type B oligomers have essentially no effect on the ability of both the cell lines to reduce MTT (Fig. 1.13A) (Campioni *et al*., 2010).

The SH-SY5Y cells were also stained with the apoptotic marker Hoechst 33342, which binds to the highly condensed chromatin present in the nuclei of apoptotic cells, giving rise to a strong fluorescence signal and allowing the visualization of abnormal nuclei. Fluorescence microscopy images indicate that the nuclei of the cells treated with type A HypF-N oligomers were significantly stained with this dye and appeared abnormal

in shape (Fig. 1.13B), by contrast, the nuclei of cells treated with the type B oligomers or with the native protein exhibited a much lower degree of staining, similar to that of untreated cells (Campioni *et al*., 2010).

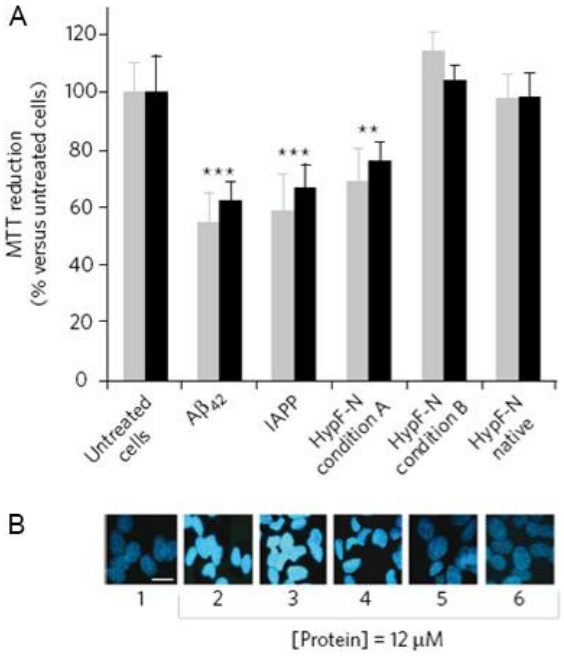

Figure 1.13. (A) MTT reduction assay on SH-SY5Y (grey) and Hend (black) cells left untreated (lane 1) or treated with $A\beta_{42}$ oligomers (lane 2), IAPP oligomers (lane 3), type A (lane 4) and B (lane 5) oligomers of HypF-N, and native HypF-N (lane 6). Error bars correspond to the s.d. values of four independent experiments. Double and triple asterisks refer to P values lower than 0.01 and 0.001, respectively. (B) Hoechst staining of SH-SY5Y cells left untreated (image 1) or treated with $A\beta_{42}$ oligomers (image 2), IAPP oligomers (image 3), type A (image 4) and B (image 5) oligomers of HypF-N and native HypF-N (image 6). The protein concentration reported refers to monomer concentrations. The scale bar represents 20 μm (Campioni *et al*., 2010).

The cytotoxicity of the oligomers was further investigated analysing the reactive oxygen species (ROS) levels in SH-SY5Y cells. Type A oligomers induce a rapid increase of ROS levels in the cells, clearly detectable after only 5 min incubation and reaching a plateau after 30-60 min. By contrast, this increase is not observed after the treatment with type B oligomers (Zampagni *et al*., 2011). It was also observed that type A toxic oligomers are able to increase the membrane lipid peroxidation, to increase the

intracellular Ca^{2+} level and to release the calcein from the intracellular space in SH-SY5Y cells, changes that are not observed after the treatment with the type B oligomers (Zampagni *et al*., 2011). Moreover, to investigate the ability of the two oligomeric species to induce apoptosis, the caspase-3 activity was analysed, a well-recognised apoptotic marker. Type A oligomers induce the activation of caspase-3 already after 3 h of treatment, and more markedly after 24 h in SH-SY5Y cells. On the other hand, negligible caspase-3 activation was detected when cells were treated for different lengths of time with type B oligomers (Zampagni *et al*., 2011). In order to investigate the necrotic cell death, the release of LDH was analysed, a widely used necrotic marker. A significant, albeit weak, increase in LDH release was observed only in cells exposed to type A oligomers for 48 h, supporting the presence of a minor and late necrotic outcome in this case (Zampagni *et al*., 2011).

Experiments performed in rat models show that the two types of stable oligomers have different abilities to affect cholinergic neuronal cells, in agreement with their different toxicities observed in neuroblastoma cultured cells. In particular, only the type A oligomers are capable to induce a dysfunction and/or reduction of cholinergic neuronal cells after the injection in rat brain, as detected using choline acetyltransferase (ChAT) immunohistochemistry (Zampagni *et al*., 2011).

Type A oligomers are also able to induce the typical early synaptic dysfunction characteristic of various neurodegenerative diseases, in particular AD (Tatini *et al*., 2013). This has been demonstrated by observing the ability of these species to inhibit LTP in hippocampal rat sections, to colocalize with post-synaptic markers in cultured rat hippocampal primary neurons and to cause damage to the spatial memory of rat resulting in cognitive decline, when microinjected *in vivo* into the brain (Tatini *et al*., 2013).

The toxic and non-toxic oligomers have different abilities to penetrate the cell membrane when transferred to the extracellular medium of SH-SY5Y cells (Campioni *et al*., 2010; Zampagni *et al*., 2011). In particular, it was found that only the toxic oligomers have sufficiently high structural plasticity and hydrophobic surface to penetrate the cell membrane and be internalized into the cells, with a rapid increase of such oligomers after only 5 min of treatment. Whereas the non-toxic ones interact with the cell surface without crossing the membrane even after prolonged incubation of the oligomers with the cells.

The oligomer-mediated cytotoxicity depends not only on the specific structural properties of the oligomers, but also on the biochemical and biophysical properties of the cellular membrane they interact with, in a delicate and complex interplay between the structural and physicochemical features of both (Evangelisti *et al*., 2012; Evangelisti *et al*., 2016; Oropesa-Nuñez *et al*., 2016). It was previously observed that the toxicity of type A oligomers and their internalization are significantly reduced after an enrichment of the cell plasma membrane with cholesterol (Evangelisti *et al*., 2012). If cholesterol was depleted from the cell membrane, the cells not only increased their apoptotic status when exposed to type A oligomers, but also became apoptotic even in the presence of type B oligomers (Evangelisti *et al*., 2012). By contrast, the cell vulnerability to type A oligomers is suppressed after a reduction in the membrane GM1 content, a monosialoganglioside that is abundant in neuronal cell membranes, particularly in lipid rafts (Evangelisti *et al*., 2012; Evangelisti *et al*., 2016; Oropesa-Nuñez *et al*., 2016). The increase in membrane GM1 does not modify the toxicity of type A oligomers, whereas it causes type B oligomers to become significantly more toxic, and able to induce caspase-3 activation (Evangelisti *et al*., 2012; Evangelisti *et al*., 2016; Oropesa-Nuñez *et al*., 2016). The high affinity observed between oligomers and GM1-enriched membrane is

driven mainly by the sialic acid moiety of GM1, through a mechanism that remain to be clarified (Evangelisti *et al*., 2012; Oropesa-Nuñez *et al*., 2016).

HypF-N oligomers co-localise with protein dense regions in the postsynaptic membrane of cultured neurons and a different capability of both oligomer types to interact with the protein and lipid components of the cell was observed (Campioni *et al*., 2010; Zampagni *et al*., 2011). In particular, type A oligomers were found to interact and destabilize the lipid bilayer of the membrane, consistent with their higher hydrophobicity (Campioni *et al*., 2010; Zampagni *et al*., 2011). By contrast, type B oligomers were found primarily to remain attached to the cell surface without penetrating the lipid bilayer (Campioni *et al*., 2010; Zampagni *et al*., 2011) and were found to be unable to interact with a supported lipid bilayer reconstituted in the absence of membrane proteins (Oropesa-Nunez *et al*., 2018). Moreover, a pull-down assay and mass spectrometry analysis revealed that type B oligomers bind more strongly to membrane proteins than do type A oligomers, this is likely to arise from the lower degree of solvent-exposed hydrophobic regions of the former species that makes their surfaces more hydrophilic. In fact, it is well established that extracellular domains of membrane proteins are hydrophilic as they bury their hydrophobic patches on the interior and therefore are likely to have a higher affinity for type B than type A oligomers (Mannini *et al*., 2019). It therefore appears that type B oligomers bind to the cell membrane by interacting with their protein component in the absence of a significant interaction with the lipid bilayer and ability to cross it. By contrast type A oligomers have a lower affinity for membrane proteins, but they are able to interact with, and destabilize, the lipid bilayer of the membrane (Mannini *et al*., 2019).

1.3.4. Role of calcium in HypF-N cytotoxicity

As described in the previous section, the cytotoxicity of type A oligomers of HypF-N is determined by their ability to interact with the cell membrane, particularly the lipid bilayer, altering its permeability and compromising its structure. These damages cause important biochemical variations such as a significant and early increase in the levels of intracellular free Ca^{2+} (Fig. 1.14), followed by an increase in intracellular ROS levels and the activation of apoptotic pathways (Campioni *et al*., 2010; Zampagni *et al*., 2011, Evangelisti *et al*., 2012; Evangelisti *et al*., 2016). These results, observed by treating cell cultures with toxic oligomers, have also been confirmed using reconstituted liposomes and synthetic membranes of phospholipids, without proteins, which were permeabilized by toxic HypF-N oligomers, causing an influx of Ca^{2+} from outside to inside liposomes (Relini *et al*., 2004).

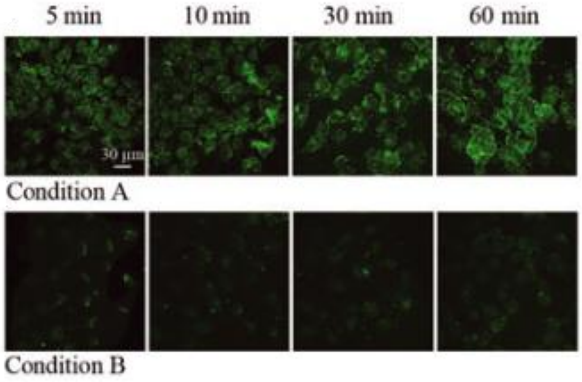

Figure 1.14. Representative confocal microscope images showing intracellular Ca^{2+} levels in SH-SY5Y cells exposed for the indicated time lengths to type A and B oligomers (Zampagni *et al*., 2011).

It was observed that the influx of extracellular Ca^{2+} into the cytosol is a primary causative role in the apoptotic pathway, because in cholesterol-depleted cells exposed to aggregates, either in the presence of the intracellular Ca^{2+} chelator or in Ca^{2+}-free

medium, the caspase-3 activation was prevented (Evangelisti *et al*., 2012). The Ca^{2+} spike is also strictly correlated with the ROS levels: in fact, if the treatment with the oligomers is performed in a medium without extracellular Ca^{2+}, there is a complete inhibition of the ROS production; moreover, a pre-treatment of the cells with vitamin E able to reduce the oxidative stress, prevents the Ca^{2+} spike (Zampagni *et al*., 2011).

The increase of the intracellular Ca^{2+} levels is associated with the ability of the oligomers to bind the membrane. Variation of membrane GM1 content was found to be able to change both the binding of the oligomers to the membrane and the cell vulnerability to HypF-N oligomers, significantly altering the intracellular Ca^{2+} influx after the exposure to the oligomers (Evangelisti *et al*., 2016). Besides, toxic oligomers of HypF-N accumulate in membrane regions containing both types of AMPAr and NMDAr (Cascella *et al*., 2017). Using specific inhibitors of such receptors, it was observed a reduction, even if partial, of this influx, suggesting their role in this early biochemical change mediated by the toxic oligomers (Evangelisti *et al*., 2016; Cascella *et al*., 2017).

1.4. Aim of the thesis

As described in section 1.1.7., the cytotoxicity of misfolded protein oligomers is closely related to their ability to establish inappropriate interactions with components of the lipid bilayer of the cell membrane or of the proteins associated with it, causing a consequent damage that determines important biochemical variations and, in particular, a rapid influx of extracellular calcium ions into the cytosol. This early and significant variation in intracellular free calcium levels has an impact on its signalling and on the activation of apoptotic pathways. The influx of Ca^{2+} caused by protein misfolded oligomers bound to the membrane could be non-specific, involving just the lipid component, or specific,

involving membrane receptors. Although the involvement of different calcium channels has been described in the oligomer-mediated Ca^{2+} entry and its associated toxicity, such as the AMPAr and NMDAr, it is not fully understood how the oligomers activate them, whether with a direct interaction causing their opening, through other mechanisms mediated by unknown protein factors, or through an oligomer-induced destabilization of the membrane, which is sensed by the channels themselves. In addition, it is not clear the extent to which the Ca^{2+} influx is caused by protein receptors relative to a non-specific destabilization of the lipid bilayer.

In addition to misfolded protein oligomers formed by $A\beta_{40}$ and $A\beta_{42}$, i.e. the zinc-stabilized $A\beta_{40}$ oligomers and the ADDLs oligomers, respectively, the possibility of obtaining toxic oligomers from the HypF-N model protein placed in specific experimental conditions, with the same biochemical, electrophysiological, histopathological localization and cognitive impairment in animal models as those formed by Aβ, allows us to analyse in detail the mechanisms through which oligomers cause an entry of Ca^{2+}.

Using neuroblastoma cultured cells (SH-SY5Y) and microglial cells (N13) it was possible to study the involvement of different calcium channels, some of them interacting directly with the oligomers, while others engaging no apparent interactions with them, as found in previous interactome studies. These channels, together with the AMPAr and NMDAr, were analysed using specific receptor inhibitors and observing intracellular calcium variations by means of specific probes visible under a confocal microscope. The attention was then focused on the AMPAr and NMDAr, as they were found to be involved in the early stages of Ca^{2+} influx, in particular their activation mechanism was investigated. FRET experiments allowed to obtain more information on the presence or absence of direct interactions between the toxic oligomers and AMPAr and NMDAr. Given the absence of interaction, we evaluated other mechanisms of activation

considering the mechanosensitivity of the receptors and we performed experiments to modify the membrane composition, using specific lipids able to induce membrane stretch and compression. Moreover, the fluidity of the membrane in the presence of the oligomers was also investigated analysing the anisotropy of the TMA-DPH probe, embedded within the polar region of the bilayer. Our results indicate an activation through a change in membrane tension caused by the oligomers and transmitted mechanically to the receptors via the lipid bilayer.

The analysis performed in this thesis allowed to identify the ion channels mediating the Ca^{2+} influx induced by the three types of oligomers, to identify the molecular mechanism by which the oligomers activate them, and to establish that a non-specific mechanism independent of Ca^{2+} channel activation, based on the direct interaction of the oligomers with the membrane, is also in part involved.

2. Materials and methods

2.1. Purification of wild-type and C7S/C65A HypF-N

Competent *E. Coli* XL1 Blue cells were transformed with the pQE30-Th plasmid encoding the N-terminal His-tagged HypF-N or the N-terminal His-tagged C7S/C65A HypF-N mutant (Calloni *et al*., 2005; Campioni *et al*., 2010). The latter is a single cysteine mutant of HypF-N carrying the cysteine residue at position 40, which was previously produced by Dr. Silvia Campioni using the QuikChange site-directed mutagenesis kit (Stratagene, La Jolla, CA, USA). Briefly, two of the three cysteine residues of the wild-type protein, located at positions 7 and 65 of the amino acid sequence, were substituted with serine and alanine, respectively, to create a mutant with only one cysteine residue at position 40 (Campioni *et al*., 2010).

Cultures of *E. Coli* XL1 Blue cells were grown overnight at 37 °C under shaking in 20 g/L LB medium (Sigma-Aldrich, St. Louis, MO, USA) with 100 μg/ml of Ampicillin (Sigma-Aldrich), to select clones harbouring the plasmid. The cells were then diluted 1:20 in fresh medium and grown at 25 °C under shaking until they reached the value of optical density at 600 nm (OD600) of ~ 0.6, monitored using a Jasco V-630 UV-VIS Spectrophotometer (Tokyo, Japan). The protein expression was induced overnight at 25 °C under shaking by adding 1 mM isopropyl β-Dthiogalactopyranoside (IPTG, Thermo Scientific, Waltham, MA, USA). The day after, the bacterial cells were harvested by centrifugation for 15 min at 7000 g at 4 °C and the pellet was resuspended in ~ 40 ml of lysis buffer (50 mM sodium phosphate, 300 mM sodium chloride, 10 mM imidazole, pH 8.0) and stored at -20 °C overnight in order to improve the bacterial lysis.

The pellet was defrosted in a Thermo Haake C25P water bath (Karlsruhe, Germany) at 37 °C and lysed by an incubation of 1 h with 1 mg/ml of lysozyme (Sigma-

Aldrich) in ice under shaking, followed by 5 cycles of sonication at 50 kHz for 30 s alternated to 30 s in ice. The cellular lysate was then centrifuged for 45 min at 38700 g at 4 °C and the supernatant containing the protein was filtered using filters with a cut-off of 0.45 µM. The supernatant was then applied at 4 °C to an affinity chromatography column packed with HIS-Select Nickel Affinity Gel (Sigma-Aldrich), previously equilibrated with the lysis buffer. The His-tag present in the fusion protein has a high affinity for divalent ions of nickel because the ring of the imidazole side chain in histidine is able to establish coordination bonds with the metal ion. The column was then washed at 4 °C with the washing buffer (50 mM sodium phosphate, 300 mM sodium chloride, 20 mM imidazole, pH 8.0) to remove the proteins that form non-specific bonds to the resin, equilibrated at 4 °C with the cutting buffer (50 mM sodium phosphate, 50 mM sodium chloride, pH 8.0) and incubated with a solution containing 50 units of human thrombin (Sigma-Aldrich) in 5 ml of cutting buffer for 1 h at 37 °C, and then overnight at 4 °C under slight shaking. The pure protein, separated from His-tag, was eluted at 4 °C with the elution buffer (50 mM sodium phosphate, 50 mM sodium chloride, 10 mM imidazole, pH 8.0) and its concentration was measured with Jasco V-630 UV-VIS Spectrophotometer (Tokyo, Japan) by evaluating the absorbance value at 280 nm (HypF-N contains two tryptophan residues and one tyrosine). Protein concentration was calculated using the Lambert-Beer law:

$$A = \varepsilon_\lambda \, c \, I \qquad (1)$$

where A is the absorbance value at 280 nm, ε_λ is the molar extinction coefficient (ε_{280} of HypF-N = 12490 $M^{-1}cm^{-1}$), c is the protein concentration in mol/L and I is the optical path in cm of the quartz cuvette used for the measurement.

The protein was buffer-exchanged in 20 mM potassium phosphate, 2mM dithiothreitol (DTT), pH 7.0 for the wild-type form or in 20 mM potassium phosphate, 2

mM tris(2-carboxyethyl)phosphine hydrochloride (TCEP), pH 7.0 for the C7S/C65A HypF-N mutant, and concentrated at 4 °C using an ultrafiltration cell with a 3000 Da cut-off cellulose membrane (Biorad, Hercules, CA, USA). The obtained samples were centrifuged for 10 min at 16100 g to eliminate any aggregates and/or impurities, and the concentration of the supernatant was calculated using the absorbance value at 280 nm. Samples were then stored at -80 °C until use.

2.2. Labelling of HypF-N mutant with Alexa Fluor 555 maleimide

In order to label the HypF-N C7S/C65A mutant with the Alexa Fluor 555 maleimide (Life Technologies/Thermo Fisher Scientific, Waltham, MA, USA), able to conjugate the dye to the cysteine residue of the protein, the mutant was diluted to reach the final concentration of 120 μM in 20 mM potassium phosphate buffer, 2 mM TCEP, pH 7.0. Alexa Fluor 555 maleimide was then added to the sample, to a final concentration of 360 μM, in order to obtain 3-fold molar excess of the dye. The reaction mixture was left in dark on a mechanical shaker for 2 h at room temperature and then overnight at 4 °C. The labelled sample was dialysed in the dark, using a membrane with a cut-off of 3 kDa, against 1 L of 20 mM potassium phosphate buffer, pH 7.0 for 8 h and then 1 L of the same buffer overnight. It was then centrifuged to remove any precipitate.

The concentration of the dye was determined spectrophotometrically, using ε_{555} = 158000 M^{-1} cm^{-1}. The protein concentration was also determined spectrophotometrically using ε_{280} = 12490 M^{-1} cm^{-1}, after subtraction of the absorbance contribution of the probe at the same wavelength of 280 nm. We estimate this contribution as:

$$y = 0.0092582 + 0.0016448x \quad (2)$$

where x represents the molar concentration of the dye, and y is the absorbance of the dye at 280 nm.

2.3. Preparation of HypF-N oligomers, $A\beta_{42}$ ADDLs and zinc-stabilised $A\beta_{40}$ oligomers

HypF-N and its mutant were converted into toxic (type A) and nontoxic (type B) oligomers, as previously described (Campioni *et al*., 2010). According to this previous report, the protein was incubated for 4 h at 25 °C without agitation and at the concentration of 48 μM in the two different experimental condition: 50 mM acetate buffer, 12% (v/v) trifluoroethanol (TFE), 2 mM DTT, pH 5.5 for the type A oligomers and 20 mM trifluoroacetic acid (TFA), 330 mM NaCl, pH 1.7 for the type B oligomers. For the FRET experiments, type A oligomers were formed by mixing mutant HypF-N labelled with Alexa Fluor 555 and unlabelled HypF-N, at a molar ratio of 1:5. Each type of oligomer was then diluted at the monomer equivalent concentration of 12 μM when added to the SH-SY5Y cell culture media, and of 0.1 μM when added to the N13 cell culture media.

Lyophilised $A\beta_{42}$ (Bachem, Bubendorf, Switzerland) was dissolved in HFIP to 1.0 mM and incubated for 1 h at room temperature to allow complete peptide monomerization. Then, $A\beta_{42}$ was converted into ADDLs oligomers as previously described (Lambert *et al*., 2001). The HFIP was evaporated with a gentle flow of N_2 and the dried protein was resuspended at the concentration of 5 mM with DMSO and then diluted with F-12 HAM at the concentration of 100 μM. The sample was then incubated at 4 °C for 24 h. The day after, the sample was centrifugated at 12000 g for 10 min and

the supernatant with the oligomers was immediately diluted in the appropriate medium and added to the SH-SY5Y cell culture media at the concentration of 1 μM.

Lyophilized $A\beta_{40}$, expressed and purified as previously described (Mannini *et al*., 2018), was kindly provided by Prof. Michele Vendruscolo (Centre for Misfolding Diseases, University of Cambridge, UK) and stored at −80 °C until use. 1 mg of lyophilized $A\beta_{40}$ was dissolved in 300 μl of HFIP, sonicated for 5 sec and then incubated overnight at 4 °C. The day after, the solvent was evaporated with a gentle flow of N_2 and the dried protein was resuspended in DMSO at the concentration of 2.2 mM, sonicated twice for 10 min at room temperature and then centrifugated at 14000 g for 5 min. The supernatant with the protein was diluted in 20 mM sodium phosphate buffer, at pH 6.9, with 200 μM $ZnCl_2$ to a final concentration of $A\beta_{40}$ of 100 μM, incubated without shaking at 20 °C for 20 h in a final volume of 275 μL and centrifuged at 15000g for 15 min at 20 °C. The pellet containing the oligomers was resuspended in 20 mM phosphate buffer at pH 6.9, with 200 μM $ZnCl_2$. The Zn^{2+}-stabilized $A\beta_{40}$ oligomers were diluted in the appropriate medium and added to the SH-SY5Y cell culture media at the concentration of 5 μM.

2.4. Cell cultures

Human SH-SY5Y neuroblastoma cells (A.T.C.C., Manassas, VA, USA) were cultured in Dulbecco's Modified Eagle's Medium (DMEM), F-12 HAM with 25 mM N-2-hydroxyethylpiperazine-N-2-ethanesulfonic acid (HEPES) and NaHCO3 (1:1) and supplemented with 10% fetal bovine serum (FBS), 2 mM glutamine and 1% antibiotics. Cell cultures were maintained in a 5% CO_2 humidified atmosphere at 37 °C and grown until they reached 80% confluence for a maximum of 20 passages.

Murine N13 microglial cells (RRID CVCL_5G93) were cultured in DMEM, F-12 HAM with 25 mM HEPES and NaHCO3 (1:1) and supplemented with 10% heat-inactivated FBS, 2 mM glutamine, 1% antibiotics and 1% non-essential amino acids. Cell cultures were maintained in a 5% CO_2 humidified atmosphere at 37 °C and grown until they reached 80% confluence for a maximum of 20 passages.

Primary rat cortex neurons (Life Technologies/Thermo Fisher Scientific) were plated in 24-well plate at the density of 200,000 cells per well and maintained in neuronal basal plus medium (Life Technologies/Gibco, Thermo Fisher Scientific) supplemented with GlutaMAX (Gibco) at the concentration of 0.5 mM and 2% (v/v) B-27 serum-free complement (Gibco), at 37 °C in a 5.0% CO_2 humidified atmosphere. Every 4 days medium was partially replaced with fresh one. All the experiments were performed 12-16 days after plating.

2.5. MTT reduction assay

The MTT reduction assay is a standard colorimetric assay used to measure cell viability based on the mitochondrial activity of specific enzymes (Berridge *et al*., 2005). In particular, it is able to monitor the ability of the NAD(P)H-dependent oxidoreductase to reduce the MTT to formazan, with a colour change from yellow (MTT) to blue (formazan) (Berridge *et al*., 2005), this ability is lost in dead cells.

MTT assay was performed in SH-SY5Y and N13 cells seeded in 96-well plate at a density of 10000 cells per well. SH-SY5Y and N13 cells were treated with type A and type B oligomers and the native protein at the monomer equivalent concentration of 12 μM or 0.1 μM, respectively. The aggregates were transferred from the solution in which they were formed into the normal cultured medium, a transition that is known to maintain

their morphological and structural properties (Campioni *et al*., 2010), or in a medium without Ca^{2+} and then added to the cells. 24 h after the treatment the cells were incubated at 37 °C with 0.5 mg/ml of MTT solution in RPMI for 4 h, then were incubated for 1 h at 37 °C with the lysis buffer (20% SDS, 50% N,Ndimethylformamide, pH 4.7). Cell viability was determined with the absorbance at 595 nm and expressed as the percentage of MTT reduction relative to the untreated cells, taken as 100%.

2.6. Expression of AMPAr and NMDAr

The expression of AMPAr and NMDAr was checked in SH-SY5Y cells plated in 6-well plates containing coverslips at a density of 40,000 cells per well. After 24 h cells were washed with PBS, fixed with 2% (v/v) paraformaldehyde for 10 min at room temperature and incubated for 1 h at 37 ° C in PBS and 1% FBS with 1:150 diluted rabbit polyclonal anti-AMPAr antibody or with 1:100 diluted rabbit polyclonal anti-NMDAr antibody, both labelled with ATTO488 (Alomone Labs, Jerusalem, Israel).

2.7. Measurement of cytosolic free Ca^{2+} level

The cytosolic Ca^{2+} levels were measured in living SH-SY5Y cells and N13 cells loaded with 4 μM Fluo-4 AM (Life Technologies/Thermo Fisher Scientific), a cellular permeable probe able to bind Ca^{2+} ions and increase 100 times its fluorescence. The probe was detected after excitation at 488 nm by a TCS SP8 scanning confocal microscopy system equipped with an argon laser source (Leica Microsystems, Mannheim, Germany). A series of 1 μm thick optical sections (1024 x 1024) were taken through the cell depth for each sample using a Leica Plan Apo 63x oil immersion objective and projected as a single

composite image by superimposition (Leica). 10-22 cells, in three different experiments, were analysed using Image J software.

SH-SY5Y and N13 cells were seeded in 6-well plates at a density of 40000 cells per well. In one set of experiments, SH-SY5Y cells were treated with 12 μM native HypF-N for 15 min, 12 μM type B oligomers (monomer equivalents) for 15 min, 12 μM type A oligomers, 1 μM $A\beta_{42}$ ADDLs and 5 μM of zinc-stabilized $A\beta_{40}$ oligomers for 5, 10, 15, 30, 60, 90, 120 and 180 min. In a separate set of experiments, the SH-SY5Y cells were treated for 10 or 60 min with 12 μM of type A oligomers (monomer equivalent) in a medium with or without Ca^{2+}.

In another set of experiments, the SH-SY5Y cells were treated for 10 min with 1 mM NMDA or with 50 μM AMPA, with or without pre-treatment for 60 min with 10 μM memantine (NMDAr inhibitor) or 5 μM CNQX (AMPAr inhibitor), respectively.

In another set of experiments, before the treatment with the various oligomers (12 μM type A oligomers of HypF-N, 1 μM $A\beta_{42}$ ADDLs and 5 μM zinc-stabilized $A\beta_{40}$ oligomers), the SH-SY5Y cells were pre-treated for 1 hr with 5 μM CNQX (AMPAr antagonist) or 10 μM memantine (NMDAr inhibitor) and analysed after 5, 10, 15, 30, 60, 90, 120 and 180 min of oligomers treatment. The SH-SY5Y cells were also pre-treated with 1 μg/ml Anti-ANO6 Antibody (SCAN channel inhibitor), 0.6 μg/ml Anti-P2RX4 Antibody (P2X4 inhibitor), 5 μM GsMTx4 (FAM38A inhibitor), 3 μM FTY720 (LTrpC-7 inhibitor), 10 μM Cd^{2+} (VGCCs inhibitor), 10 μM Synta66 (CRAC inhibitor), 100 nM α-bungarotoxin (α7nAChR inhibitor), or 100 μM erastin (xCT inhibitor) and analysed after 5, 10 and 60 min of type A oligomers of HypF-N treatment and after 5 and 60 min of $A\beta_{42}$ ADDLs and zinc-stabilized $A\beta_{40}$ oligomers treatment. Before the treatment with 12 μM type A oligomers or 1 μM $A\beta_{42}$ ADDLs for 10 min, the SH-SY5Y cells were also

pre-treated for 2 h with 0.05, 0.1, 1.0 and 2.0 μM L-α-lysophosphatidylcholine (LPC) or 10 μM AA, the latter in the presence or in the absence of 10 μM memantine.

The experiments described above were performed also using N13 cells with the difference that 0.1 μM of type A oligomers were used. In addition, the N13 cells were also treated for 5 or 60 min with 0.1 μM of type A oligomers in a medium without Ca^{2+}, after 1 h of pre-treatment with 10 μM CGP-37157, or with 100 μM 2APB, or with both inhibitors in a medium with or without Ca^{2+}, to inhibit the release of the Ca^{2+} from the intracellular compartments. Moreover, the N13 cells were also treated with 175 μM probenecid (TrpV2 activator), 75 μM tranilast (TrpV2 inhibitor), or both, to observe the effective inhibition of the channel after its activation.

The experiments with 1 μM $A\beta_{42}$ ADDLs for 10 and 60 min with or without 5 μM CNQX or 10 μM memantine, and with or without 2.0 μM LPC or 10 μM AA were also performed in the primary rat cortex neurons.

2.8. RNA interference

Small-interfering RNA (siRNA) was used to perform the silencing of NMDAr type subunit 2B (GRIN2B) gene in SH-SY5Y cells. siRNA is a class of double-strand RNA molecules (20-25 base pairs in length) that interferes with the expression of specific genes with complementary nucleotide sequences. They function by breaking down mRNA after transcription, resulting in lack of translation (Agrawal *et al*., 2003).

SH-SY5Y cells were plated in 6-well plates containing coverslips at a density of 40000 cells per well. After 24 h, they were washed with PBS and transfected using 25 nM Stealth RNAi™ siRNA against NMDAr GRIN2B (Life Technologies/Thermo Fisher Scientific), 7 μl of Lipofectamine, 10 μl of 5 mg/L transferrin in DMEM for 3 h in a 5%

CO_2 humidified atmosphere at 37 °C. The cells were also transfected with vehicle (transfection mix without siRNA), and with 25 nM Stealth RNAi™ siRNA negative controls (Life Technologies/Thermo Fisher Scientific). 3 h after transfection the DMEM was replaced with fresh complete medium, and the cells were incubated for 72 h. The cells were then washed and incubated for 60 min at 37 °C with 1:400 diluted mouse monoclonal anti-NMDAr 2B antibody (Life Technologies/Thermo Fisher Scientific) in PBS and 1% FBS, and for 90 min with 1:1000 diluted Alexa Fluor 488-conjugated anti-mouse secondary antibodies (Life Technologies/Thermo Fisher Scientific) in PBS and 1% of FBS. The cytosolic Ca^{2+} levels after the treatment with 1 μM $A\beta_{42}$ ADDLs were also measured in silenced cells after 72 h of incubation, using the protocol described above.

2.9. FRET analysis

Förster Resonance Energy Transfer is an electrodynamic phenomenon that occurs when the emission spectrum of a fluorophore, called donor (D), overlaps with the absorption spectrum of another molecule, called acceptor (A). The donor emits at shorter wavelengths than the acceptor, and its emission spectrum overlaps with the absorption spectrum of the acceptor. The rate of FRET depends on the extent of the spectral overlap between donor and acceptor, the quantum yield of the donor, the relative orientation between the donor and acceptor transition dipoles, and the distance between the donor and the acceptor. In this thesis, the FRET technique was used to study the interaction between the HypF-N oligomers and the AMPAr and NMDAr located on the cell membrane.

SH-SY5Y cells were seeded in 6-well plate at a density of 40000 cells per well and then treated with type A oligomers (12 μM monomer equivalents) labelled with Alexa

Fluor 555 (Life Technologies/Thermo Fisher Scientific) as an acceptor (A) for 15 min, then fixed with 2% buffered paraformaldehyde for 10 min at room temperature and then permeabilized with PBS, 0.5% (v/v) Triton-X and 0.5% bovine serum albumin (BSA) for 7 min at room temperature. After washing, the cells were stained with 1:150 diluted rabbit polyclonal anti-AMPAr antibody or with 1:100 diluted rabbit polyclonal anti-NMDAr antibody, both labelled with ATTO488 (Alomone Labs, Jerusalem, Israel) as a donor (D), in PBS and 1% FBS, for 60 min at 37 °C. A positive control was performed in the absence of oligomers using the same experimental protocol described above and then incubating the cells for 60 min at 37 °C with 1:900 diluted Alexa Fluor 594-conjugated anti-rabbit secondary antibody (Life Technologies/Thermo Fisher Scientific). Cells were analysed using a Leica TCS SP8 confocal scanning microscopy (Leica Microsystems), as described above. The optical sections were acquired in the donor channel (excitation at 488 nm and emission at 499-55 nm), in the acceptor channel (excitation at 543 nm and emission at 560-610 nm) and in the FRET channel (excitation at 488 nm and emission at 560-610 nm).

2.10. TMA-DPH labelling and anisotropy

The (1-(4-trimethylammoniumphenyl)-6-phenyl-1,3,5-hexatriene p-yoluenesulfonate) (TMA-DPH, Life Technologies/Thermo Fisher Scientific) is a hydrophobic fluorescent probe, which is rapidly incorporated into the plasma membrane near the polar head group regions due to its charged group. These properties offer promising applications in membrane fluidity studies and in monitoring exocytosis kinetics (Illinger *et al*., 1995).

SH-SY5Y cells, seeded on glass coverslips at a density of 40000 cells per well, were loaded for 15 min with 5 µM trodusquemine labelled with Alexa Fluor 594

succinimidyl ester in a 10:1 (trodusquemine:dye) molar ratio, to label the membrane, and the last 5 min 2 μM TMA-DPH was added. Cells were analysed using a Leica TCS SP8 confocal scanning microscopy (Leica Microsystems), as described above.

Cells loaded with 2 μM TMA-DPH, with or without the treatment with 1 μM $A\beta_{42}$ ADDLs for 10 min, were recovered after trypsinization using PBS with $MgCl_2$ and $CaCl_2$, and the fluorescence anisotropy values (*r*) were measured at 430 nm, after excitation at 355 nm, using a 10X4 path length quartz cuvette and an the Agilent Cary Eclipse spectrofluorimeter (Agilent Technologies, Santa Clara, CA, USA) equipped with a thermostated cell holder attached to a Agilent PCB 1500 water Peltier system.

2.11. Statistical analysis

All data were expressed as means ± S.E.M. (standard error of the mean). Pairwise comparisons between the different groups were performed by unpaired t-test using Graphpad Prism software (GraphPad Software). The single, double and triple asterisks or symbols refer to p values <0.05, <0.01 and <0.001, respectively.

3. Results

3.1. Ca^{2+} dependent toxicity of type A HypF-N oligomers

In order to elucidate the mechanism of the calcium influx event in determining the cellular toxicity mediated by the oligomers, we primarily analysed the model oligomers formed by the protein HypF-N. In particular, the type A oligomers were used, which were found to be highly stable, versatile and easy to isolate, to have similar effect to those of Aβ oligomers in cell and animal models, and which have a non-toxic type B counterpart useful as a negative control (Campioni *et al*., 2010; Zampagni *et al*., 2011; Evangelisti *et al*., 2012; Tatini *et al*., 2013).

First, the cellular stress induced by type A and type B HypF-N oligomers and native protein was assessed on SH-SY5Y neuroblastoma cells after 24 h treatment using the MTT reduction assay, which is an indicator of the mitochondrial activity (Mosmann, 1983). Results of MTT reduction assays obtained with this cell and oligomer types have been found to correlate well with those of other cell stress readout assays (Zampagni *et al*., 2011). The aggregates were transferred from the solution in which they were formed into the cultured medium, a transition that is known to maintain their morphological and structural properties (Campioni *et al*., 2010), and then added to the cells. The treatment of the cells with the native protein or with type B oligomers (12 μM monomer equivalents) did not affect the ability of the cells to reduce the MTT molecule, whereas the same dose of type A oligomers caused a 27±5% reduction of mitochondrial activity (Fig. 3.1A), a significant reduction compared with the untreated cells, confirming previous results (Campioni *et al*., 2010; Zampagni *et al*., 2011). When the experiment was repeated in extracellular medium without Ca^{2+}, such a reduction was not observed and the level of cellular viability after the treatment with the type A oligomers is similar

to the untreated cells (Fig. 3.1B). This result was also confirmed in another cell line, the N13 murine microglial cells, which showed a higher susceptibility to lower concentration of type A oligomers, 0.1 μM, compared to SH-SY5Y cells (Fig. 3.1C). Overall, the data indicate that the cellular toxicity induced by the oligomers is mediated by the calcium ions present in the extracellular space.

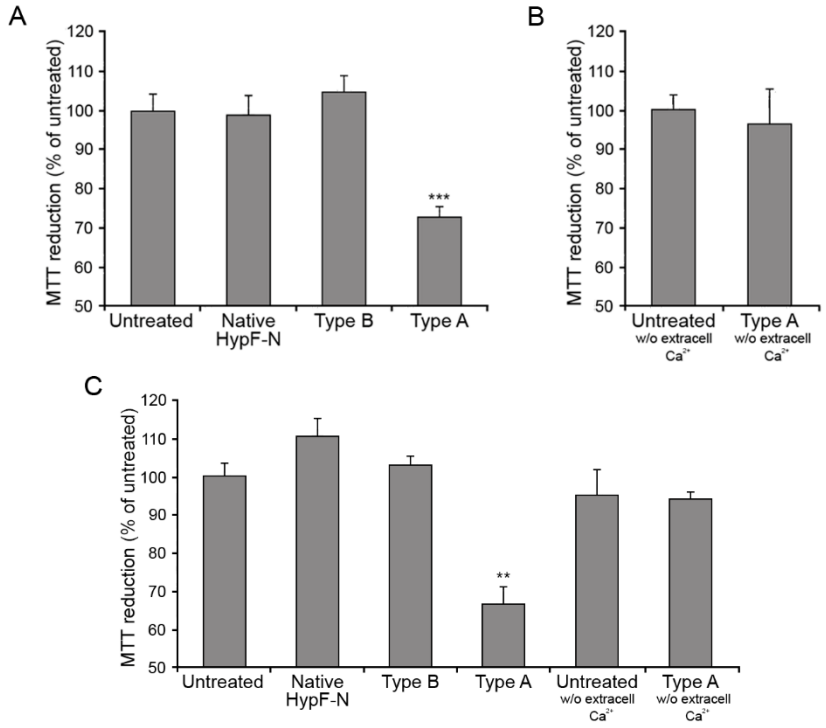

Figure 3.1. MTT reduction assay in (**A**) SH-SY5Y cells treated for 24 h with native HypF-N (12 μM), type A and type B HypF-N oligomers (12 μM, monomer equivalents), (**B**) in medium without Ca^{2+}, with or without 24 h treatment with type A oligomers and in (**C**) microglial N13 cells treated for 24 h with native HypF-N (0.1 μM) and type A and type B oligomers (0.1 μM, monomer equivalents) and in medium without Ca^{2+}, with or without 24 h treatment with type A oligomers. Error bars: S.E.M. The double (**) and triple (***) asterisk refers to p values <0.01 and <0.001 relative to the untreated cells, respectively.

3.2. Ca^{2+} dyshomeostasis induced by type A HypF-N oligomers

To investigate the mechanism of oligomer-induced and calcium-mediated toxicity, the intracellular Ca^{2+} level in SH-SY5Y cells treated with HypF-N oligomers (12 μM

monomer equivalents) was monitored using the Fluo-4 AM probe able to bind the intracellular Ca^{2+} ions. The treatment with type B HypF-N oligomers or the native protein show an intracellular Ca^{2+} level similar to the untreated cells (Fig. 3.2A,B). By contrast, the results after the treatment with the type A HypF-N oligomers show a gradual increase of the intracellular Ca^{2+} concentration, which reached maximum level after 180 min of treatment (Fig. 3.2A,B). When these experiments were carried out in a Ca^{2+} free medium, the cytoplasmic Ca^{2+} did not increase to any detectable extent (Fig. 3.2C), indicating the extracellular origin of Ca^{2+}.

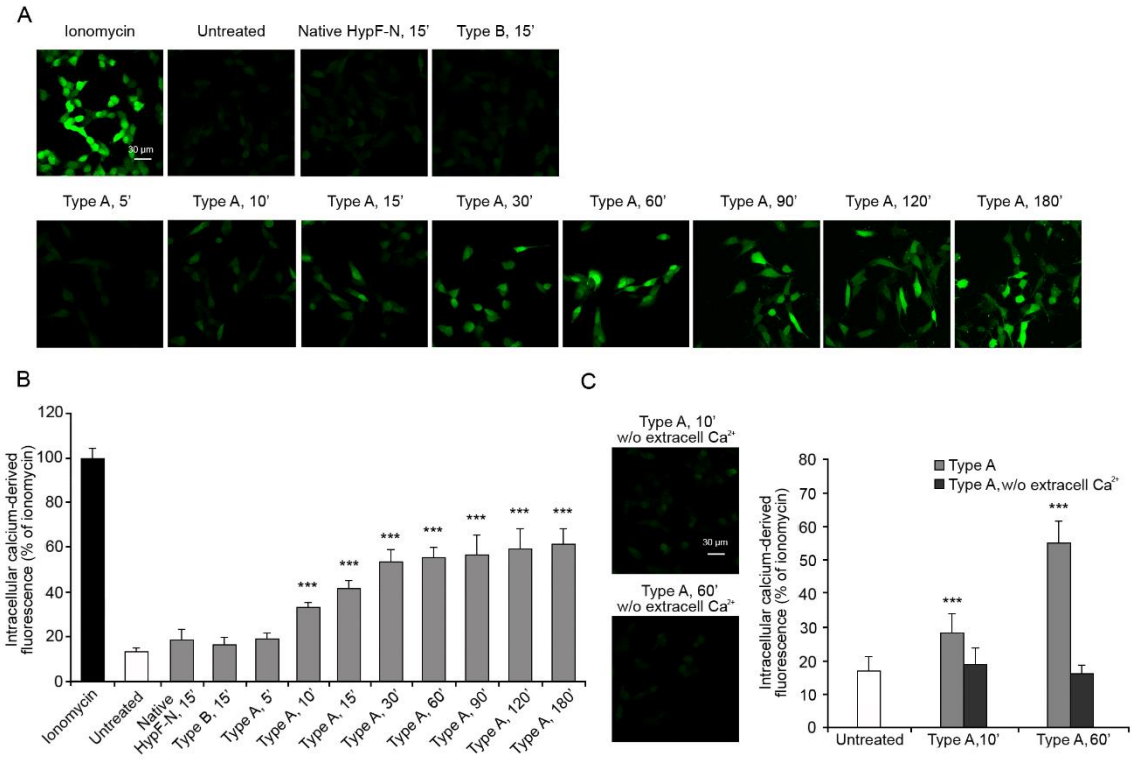

Figure 3.2. (**A**) Representative confocal scanning microscopy images showing the level of intracellular free Ca^{2+} in SH-SY5Y cells treated with 1 µM ionomycin, no treatment, 12 µM native HypF-N for 15 min, 12 µM type B oligomers for 15 min, 12 µM type A oligomers for 5, 10, 15, 30, 60, 90, 120 and 180 min. The green fluorescence arises from Ca^{2+} binding to the Fluo-4 probe. (**B**) Semi-quantitative analysis of intracellular free Ca^{2+}-derived fluorescence. (**C**) Representative confocal scanning microscopy images of the intracellular free Ca^{2+} level following the treatment with 12 µM type A oligomers for 10 and 60 min in a medium without Ca^{2+} and semi-quantitative analysis of intracellular free Ca^{2+}-derived fluorescence. Variable numbers of cells (12-22) in three different experiments were analysed for each condition. Error bars: S.E.M. The triple (***) asterisks refer to p values <0.001 relative to the untreated cells.

The experiments were repeated on the N13 microglial cells, where we observed an absence of increase of intracellular Ca^{2+} level after the treatment with the native HypF-N and the type B HypF-N oligomers, and a more rapid increase in the intracellular free Ca^{2+} levels within the first 5 min of treatment with type A oligomers, which then remained almost constant up to 60 min (Fig. 3.3A,B).

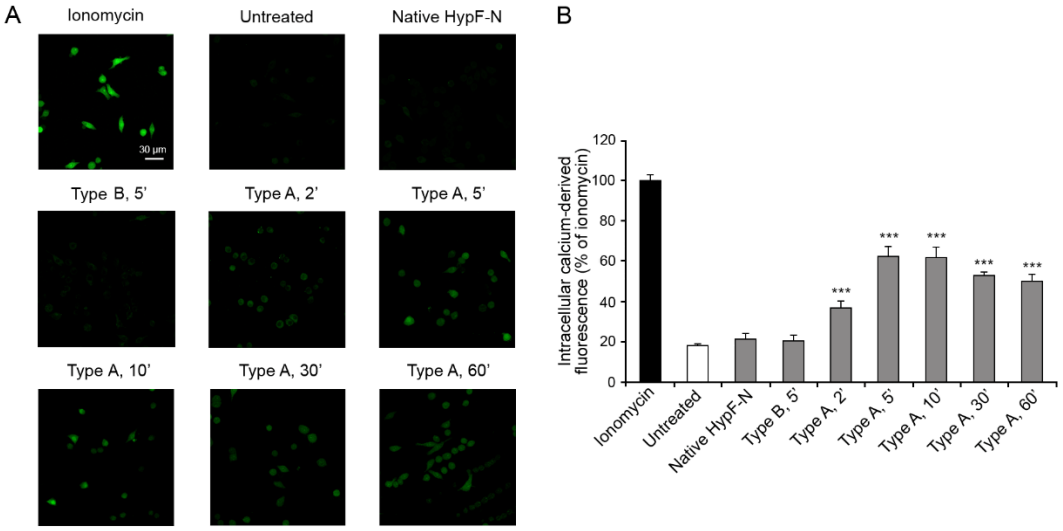

Figure 3.3. (**A**) Representative confocal scanning microscopy images of N13 cells showing the levels of intracellular free Ca^{2+} following the treatment with 1 µM ionomycin, no treatment, 0.1 µM native HypF-N for 5 min, 0.1 µM (monomer equivalents) type B oligomers for 5 min, 0.1 µM (monomer equivalents) type A oligomers for 2, 5, 10, 15, 30 and 60 min. The green fluorescence arises from Ca^{2+} binding to the intracellular Fluo-4 probe. (**B**) Semi-quantitative analysis of intracellular free Ca^{2+}-derived fluorescence. Variable numbers of cells (12-22) in three different experiments were analysed for each condition. Error bars: S.E.M. The triple (***) asterisks refer to p values <0.001 relative to untreated cells.

In a Ca^{2+} free medium, the intracellular Ca^{2+} level after 5 min of treatment with type A oligomers were slightly lower than those observed after the treatment in the normal medium, but significantly higher than those of untreated cells (Fig. 3.4A,B), suggesting that the cytosolic Ca^{2+} increment in the microglial cells could arise in a large part from intracellular compartments.

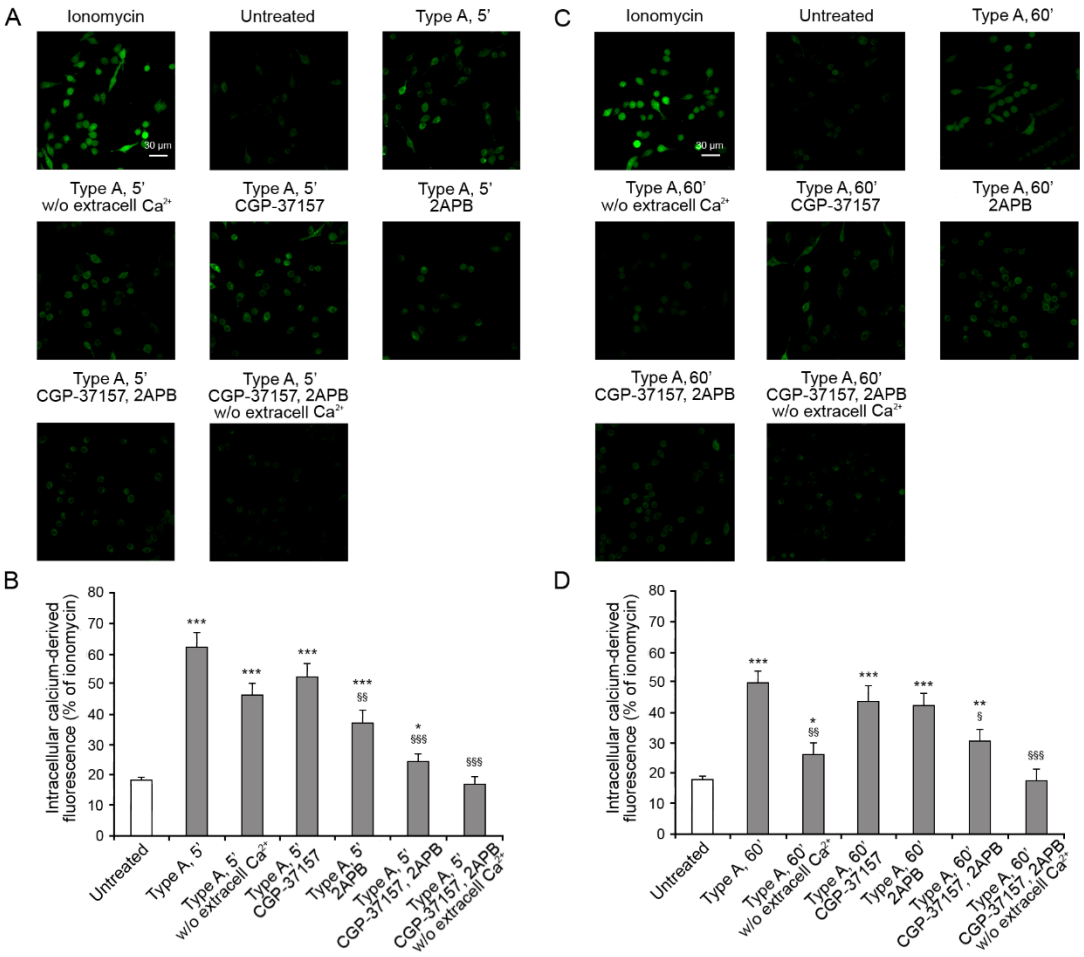

Figure 3.4. (**A**,**C**) Representative confocal scanning microscopy images of intracellular free Ca^{2+} level in N13 microglial cells following the treatment with 1 µM ionomycin, no treatment, 0.1 µM (monomer equivalents) type A oligomers for (**A**) 5 min or (**C**) 60 min w/o inhibitors and type A oligomers for (**A**) 5 min or (**C**) 60 min in different conditions: in a medium w/o Ca^{2+}, with 10 µM CGP-37157, with 100 µM 2APB, with CGP-37157 in a medium w/o Ca^{2+}, with 2APB in a medium w/o Ca^{2+}, with both inhibitors and with both inhibitors in a medium w/o Ca^{2+}. (**B**,**D**) Semi-quantitative analysis of intracellular free Ca^{2+}-derived fluorescence. Variable numbers of cells (12-22) in three different experiments were analysed for each condition. Error bars: S.E.M. The single (*), double (**) and triple (***) asterisks refer to p values <0.05, <0.01 and <0.001, respectively, relative to the untreated. The double (§§) and triple (§§§) symbol refer to p values <0.01 and <0.001, respectively, relative to type A oligomers, 5 min or 60 min.

To assess this possibility, specific channels involved in the mechanism of release of Ca^{2+} from the intracellular compartments were inhibited in the N13 cells before the treatment with type A oligomers. In particular, CGP-37157 to inhibit the mitochondrial Na^{+}/Ca^{2+} exchange and the sarcoplasmic reticulum calcium stimulated ATPase (Neumann *et al.*, 2011; Palty and Sekler, 2012), and 2-aminoethyl diphenylborinate

(2APB) to inhibit the intracellular D-myo-inositol 1,4,5-trisphosphate (IP3)-induced calcium release from the endoplasmic reticulum (Maruyama *et al*., 1997) were used.

Both the inhibitors reduce the intracellular Ca^{2+} levels following 5 min of treatment with type A oligomers, compared with the treatment without inhibitors. This reduction was further exacerbated if the treatment was performed with both inhibitors at the same time, and even more using both inhibitors and the free Ca^{2+} medium, where the levels of cytosolic Ca^{2+} are comparable to the untreated cells (Fig. 3.4A,B).

After 60 min of treatment with type A oligomers there is a low intracellular Ca^{2+} level in the treatment with free Ca^{2+} medium, suggesting a higher contribution of Ca^{2+} from the extracellular space and a lower one from the internal sources (Fig. 3.4C,D). Again, the pre-treatment with both 2APB and CGP-37157 inhibitors and the use of the Ca^{2+} free medium did not cause any increase of cytosolic Ca^{2+} following the treatment with type A oligomers (Fig. 3.4C,D).

Therefore, type A HypF-N oligomers appear to induce an increase of cytosolic Ca^{2+} in both neuroblastoma SH-SY5Y and microglial N13 cells. However, in the first case the increase is due almost exclusively to the extracellular Ca^{2+} crossing the cell membrane, whereas in the second case the source of cytosolic Ca^{2+} is both the extracellular medium and the intracellular stores.

3.3. Early Ca^{2+} influx induced by type A HypF-N oligomers is mediated by glutamate receptors

In the search for potential Ca^{2+} channels mediating the influx of Ca^{2+} from the extracellular space upon exposure to type A HypF-N oligomers, we first considered the ligand-gated Ca^{2+} channels of glutamatergic type, such as the NMDAr and AMPAr,

whose involvement in the influx of Ca^{2+} mediated by toxic Aβ oligomers was extensively studied in literature (Tozaki *et al*., 2002; De Felice *et al*., 2007; Zhao *et al*., 2009; Alberdi *et al*., 2010; Decker *et al*., 2010; Rönicke *et al*., 2011; Texidó *et al*., 2011; Sinnen *et al*., 2016; Arbel-Ornath *et al*., 2017; Deshpande *et al*., 2009; Snyder *et al*., 2005).

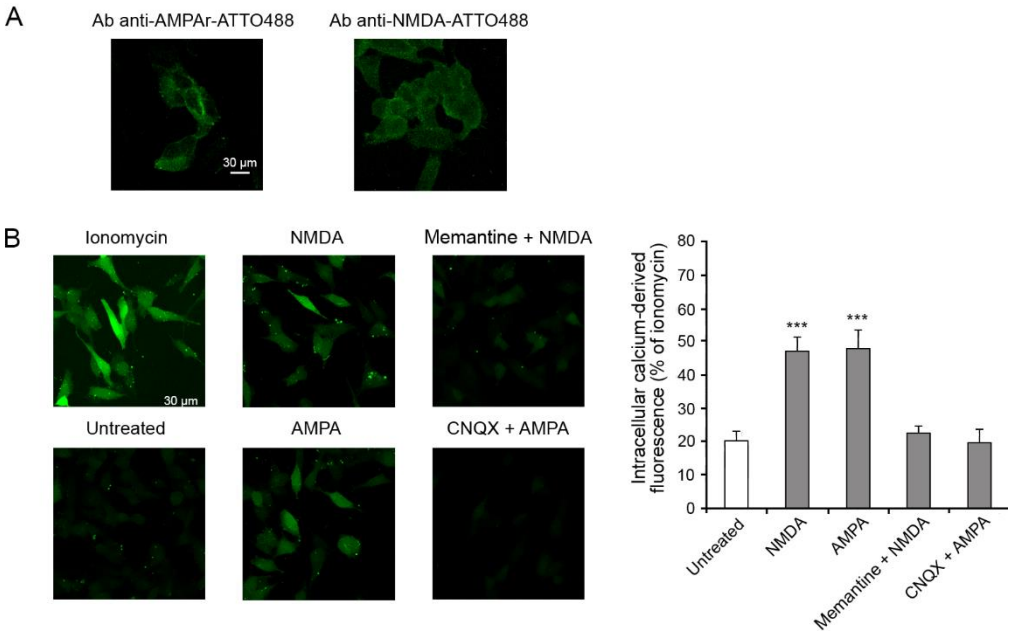

Figure 3.5. (**A**) Representative confocal scanning microscopy images of SH-SY5Y cells following the treatment with primary antibody against AMPAr and NMDAr, both labelled with ATTO488. (**B**) Representative confocal scanning microscopy images of intracellular Ca^{2+} level following the treatment with 1 µM ionomycin, no treatment, 1 mM NMDA, 50 µM AMPA, 1 mM NMDA preceded by pre-treatment with 10 µM memantine, and 50 µM AMPA preceded with 5 µM CNQX. The histogram reports the semi-quantitative analysis of intracellular free Ca^{2+}-derived fluorescence. Variable numbers of cells (12-22) in three different experiments were analysed for each condition. The triple (***) asterisks refer to p values <0.001 relative to untreated cells.

In order to verify the presence of the NMDAr and AMPAr on the SH-SY5Y cellular membrane, we probed them with their specific antibodies, observing their expression (Fig 3.5A). To assess whether the expressed receptors were also functional and active, we activated them using their specific agonists NMDA and AMPA, finding that both small molecules can induce an increase of the intracellular Ca^{2+} levels (Fig. 3.5B), an influx that was inhibited if the cells were pre-treated with the NMDAr

uncompetitive inhibitor memantine and the AMPAr competitive antagonist 6-cyano-7-nitroquinoxaline-2,3-dione (CNQX), respectively, (Fig. 3.5B).

We therefore pre-treated the SH-SY5Y cells with CNQX or with memantine and then we treated the cells with type A oligomers for different time intervals (Fig. 3.6). CNQX determined a slight reduction of the cytoplasmic Ca^{2+} levels in the early stages, up to 10 min, compared to the normal time course without inhibitors (Fig. 3.6). This reduction was more significant following treatment with memantine, with which we observed Ca^{2+} levels similar to those of untreated cells up to 10 min of treatment, and then a gradual increase which remained significantly different from that observed without inhibitors starting from 15 min, reaching comparable levels at 60 min of treatment (Fig. 3.6). These slowing down of the Ca^{2+} influx kinetic (Fig. 3.6C) suggest that in the early stages of the Ca^{2+} influx from the extracellular space the extrasynaptic AMPAr and NMDAr play an important role, particularly the latter, whereas in the late stages of the influx these receptors do not seem to give a significant contribution to the massive entrance of Ca^{2+} ions into the cells. This finding legitimates the use of SH-SY5Y cells for this study, as they do not contain synaptic NMDAr/AMPAr that might interfere with the analysis.

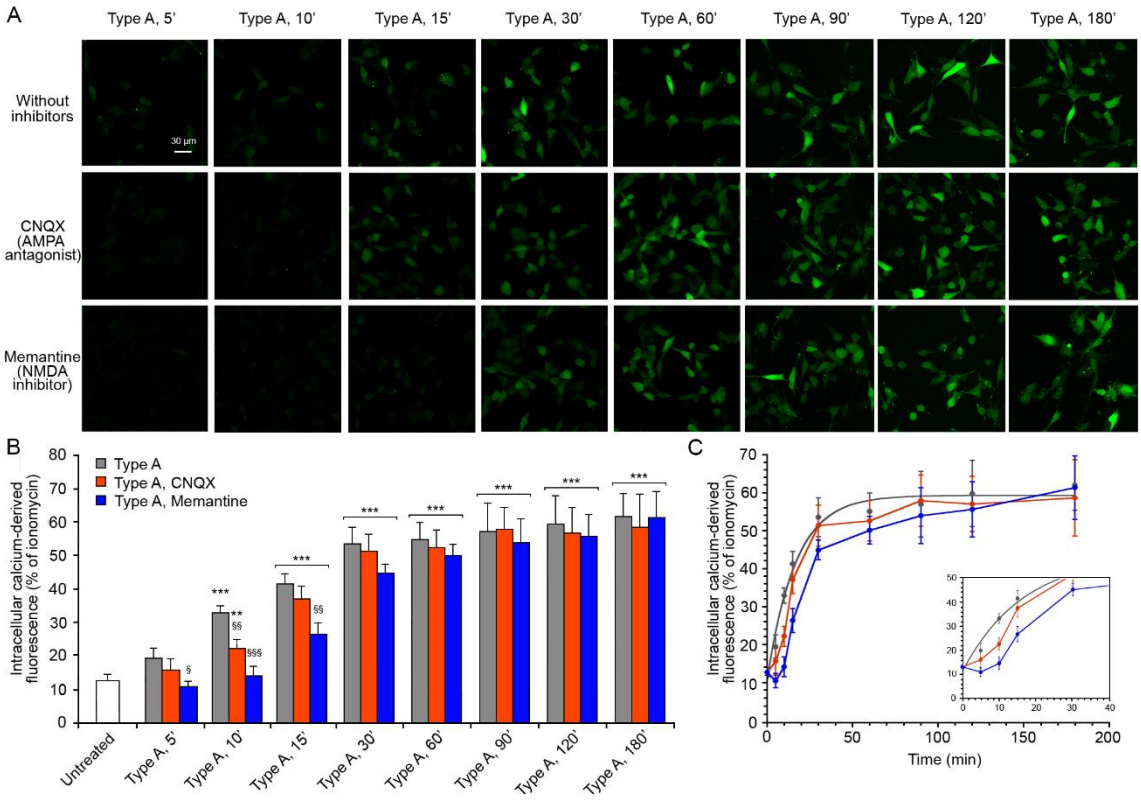

Figure 3.6. (**A**) Representative confocal scanning microscopy images of intracellular free Ca^{2+} level in SH-SY5Y neuroblastoma cells following the treatment with no inhibitors (first row), 5 µM CNQX (second row) and 10 µM memantine (third row), and analysed after 5, 10, 15, 30, 60, 90, 120 and 180 min of treatment with 12 µM (monomer equivalents) type A oligomers. (**B**) Semi-quantitative analysis of intracellular free Ca^{2+}-derived fluorescence. Variable numbers of cells (12-22) in three different experiments were analysed for each condition. The double (**) and triple (***) asterisks refer to p values <0.01 and <0.001, respectively, relative to the untreated. The single (§), double (§§) and triple (§§§) symbol refer to p values <0.05, <0.01 and <0.001, respectively, relative to type A oligomers without inhibitors. Error bars: S.E.M. (**C**) Kinetic plots showing the fluorescence versus time as reported in panel B.

The involvement of extrasynaptic AMPAr and NMDAr in the early stages of the influx of Ca^{2+} induced by type A oligomers were confirmed in the N13 cells. After 5 min of treatment with CNQX or memantine, we observed a reduction of the cytosolic free Ca^{2+} in the cells, compared to those without inhibitors (Fig. 3.7). This reduction was similar to that observed in the treatment without Ca^{2+} described before at corresponding time-lengths (Fig. 3.4). After 60 min of treatment with the type A HypF-N oligomers, the cytosolic Ca^{2+} levels were the same with or without the inhibitors (Fig. 3.7).

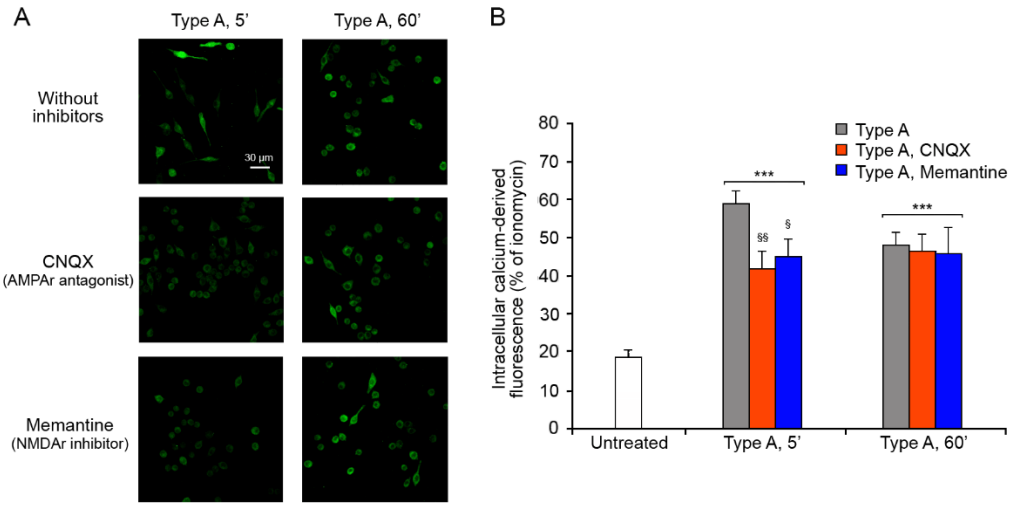

Figure 3.7. (**A**) Representative confocal scanning microscopy images of intracellular free Ca^{2+} level in N13 microglial cells following the treatment with no inhibitors (first row), 5 µM CNQX (second row) and 10 µM memantine (third row), and analysed after 5 and 60 min of treatment with 0.1 µM (monomer equivalents) type A oligomers. (**B**) Semi-quantitative analysis of intracellular free Ca^{2+}-derived fluorescence. Variable numbers of cells (12-22) in three different experiments were analysed for each condition. The single triple (***) asterisks refer to p values <0.001 relative to the untreated. The single (§) and double (§§) symbol refer to p values <0.05 and <0.01, respectively, relative to type A oligomers. Error bars: S.E.M.

3.4. Type A HypF-N oligomers do not directly interact with AMPAr and NMDAr

To investigate the mechanism of activation of extrasynaptic AMPAr and NMDAr channels by type A HypF-N oligomers, we checked if there was a direct interaction between the oligomers and the receptors using a FRET analysis. We use only the SH-SY5Y cells for this analysis because they are a better cell model for the neurodegenerative diseases, and the influx Ca^{2+} observed arise completely from the extracellular space.

The AMPAr and NMDAr were labelled with the donor probe (D) ATTO488-conjugated-primary antibody, and the type A oligomers were labelled with the acceptor probe (A) Alexa Fluor 555 covalently linked to a cysteine residue of the HypF-N

sequence. In the presence of only D, SH-SY5Y cells were excited at 488 nm (D excitation wavelength) and the fluorescence was observed at 499-535 nm (D emission range, Fig. 3.8A, left). Then we excited the samples at 488 nm, but we observed the emission at 560-610 nm (A emission range), to observe the bland contribution of D in the FRET channel (Fig. 3.8A, right). In the presence of only A, we excited at 543 nm (A excitation wavelength) and observed the emission at 560-610 nm (Fig. 3.8B, left); then we observed the bland emission at 560-610 nm in the FRET channel exciting at 488 nm (D excitation wavelength, Fig. 3.8B, right). In the presence of both D and A, we acquired images in the donor channel (ex 488 nm, em 499-535 nm), in the acceptor channel (excitation 543 nm, emission 560-610 nm), in the FRET channel (excitation 488 nm, emission 560-610 nm) and finally overlapped the donor and acceptor channels to obtain the colocalization image (Fig. 3.8C).

The comparison between the FRET channel with only A or both D and A (Fig. 3.8D) did not show any variation of the A fluorescence. Moreover, the comparison of the D fluorescence in the areas enriched with the A-labelled oligomers (F_{DA}, Fig. 3.8E, yellow circle) with the surrounding areas (F_D, Fig. 3.8E, blue circle) showed similar values of D fluorescence. By calculating the FRET efficiency (E) value as:

$$E = 1 - \frac{F_{DA}}{F_D} \quad (1)$$

we obtained a value close to 0, suggesting the lack of any direct interaction between type A oligomers and NMDAr.

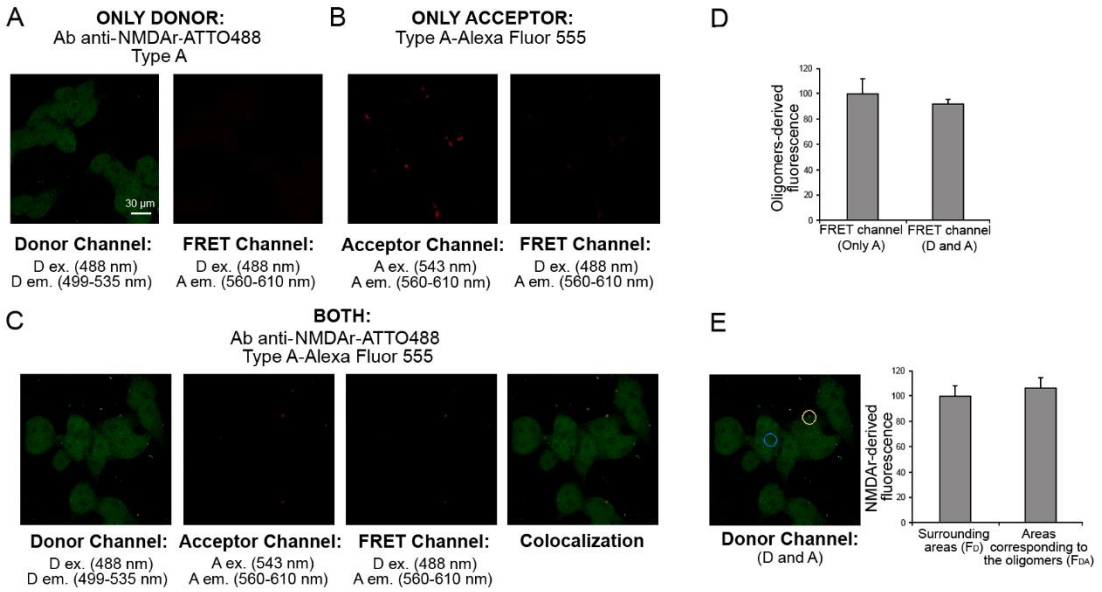

Figure 3.8 (**A**) SH-SY5Y cells treated with unlabelled oligomers in the presence of primary antibody against NMDAr labelled with D on the donor channel (left, ex: 488 nm; em: 499-535 nm) and FRET channel (right, ex: 488; em: 560-610 nm). (**B**) SH-SY5Y cells treated with the oligomers labelled with A, in the absence of D on the acceptor channel (left, ex: 543 nm; em: 560-610 nm) and FRET channel (right, ex: 488; em: 560-610 nm). (**C**) SH-SY5Y cells treated with the D and A. From left to right the donor channel, the acceptor channel, the FRET channel and the colocalization image, obtained by overlapping the donor and acceptor channels. (**D**) Semi-quantitative analysis of the oligomers-derived fluorescence in the FRET channel in the presence of only A or both D and A. (**E**) Representative confocal scanning microscopy image of donor channel in the presence of both D and A (left). The blue and yellow circles indicate representative areas without oligomers (F_D) and with type A oligomers (F_{DA}), respectively. Semi-quantitative analysis of the NMDAr-derived fluorescence in the areas corresponding to the oligomers, compared with the surrounding areas (right). Error bars: S.E.M.

The same experiments were performed also with the AMPAr and the type A HypF-N oligomers (Fig. 3.9) and, similarly, analysing the FRET channel with only A or both D and A (Fig. 3.9D) and comparing of the D fluorescence in the areas enriched with the A-labelled oligomers (F_{DA}, Fig. 3.9E, yellow circle) with the surrounding areas (F_D, Fig. 3.9E, blue circle), we did not detect any direct interaction between the receptors and the oligomers.

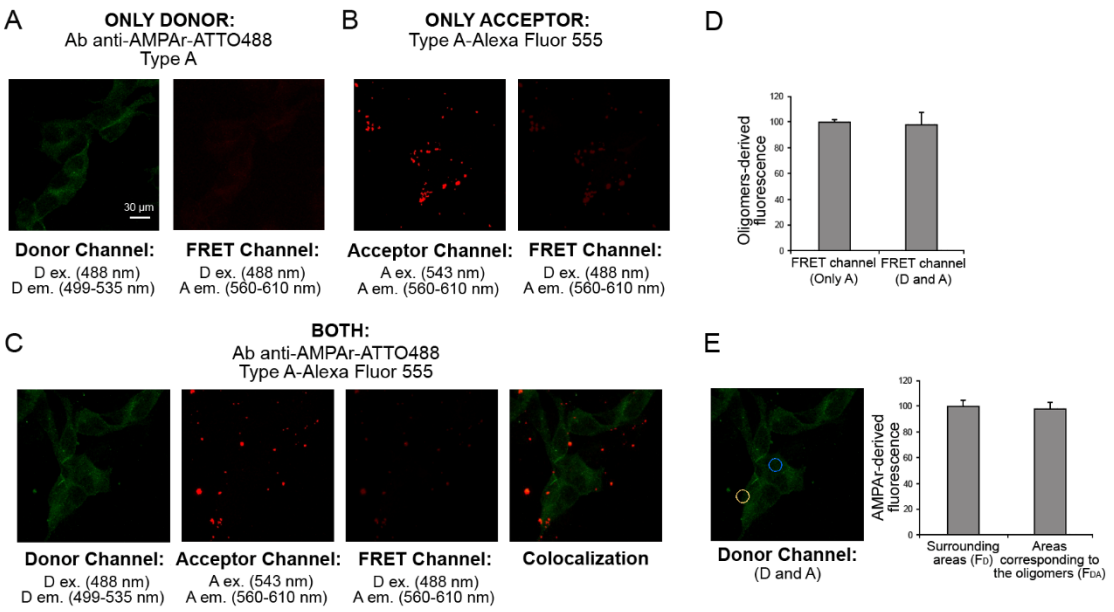

Figure 3.9. (**A**) SH-SY5Y cells treated with oligomers in the presence of primary antibody against AMPAr labelled with D on the donor channel (left, ex: 488 nm; em: 499-535 nm) and FRET channel (right, ex: 488; em: 560-610 nm). (**B**) SH-SY5Y cells treated with oligomers labelled with A, in the absence of D on the acceptor channel (left, ex: 543 nm; em: 560-610 nm) and FRET channel (right, ex: 488; em: 560-610 nm). (**C**) SH-SY5Y cells treated with D and A. From left to right the donor channel, the acceptor channel, the FRET channel and the colocalization image obtained by overlapping the donor and acceptor channels. (**D**) Semi-quantitative analysis of the oligomer-derived fluorescence in the FRET channel in the presence of only A or both D and A. (**E**) Representative confocal scanning microscopy image of D in the presence of both D and A (left). The blue and yellow circles indicate representative areas without oligomers (F_D) and with type A oligomers (F_{DA}), respectively. Semi-quantitative analysis of the AMPAr-derived fluorescence in the areas corresponding to the oligomers, compared with the surrounding areas (right). Error bars: S.E.M.

To rule out technical issues in the experiments described above that could be responsible for the lack of FRET signal, we carried out a positive control of FRET using an anti-AMPAr antibody labelled with ATTO488 and the Alexa Fluor 594-conjugated anti-rabbit secondary antibody as D and A, respectively (Fig. 3.10). In the presence of only A, the fluorescence in the FRET channel was lower compared to that in the presence of both D and A (Fig. 3.10E); moreover, the D fluorescence in the donor channel was higher with only D compared to that with both D and A (Fig. 3.10D), proving the presence of energy transfer between D and A.

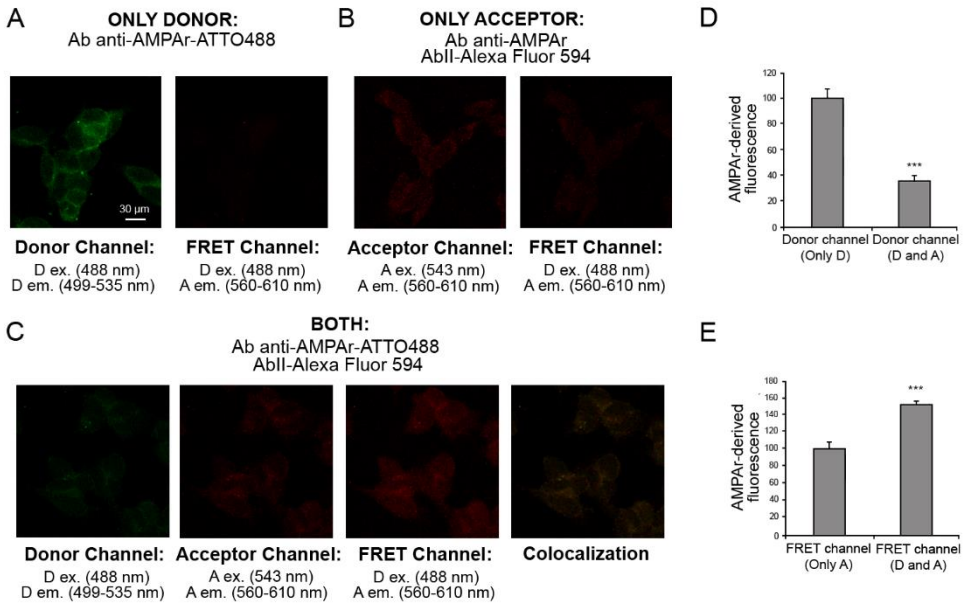

Figure 3.10. (**A**) SH-SY5Y cells treated with primary antibody against AMPAr labelled with D on the donor channel (left, ex: 488 nm; em: 499-535 nm) and FRET channel (right, ex: 488; em: 560-610 nm). (**B**) SH-SY5Y cells treated with unlabelled primary antibody against AMPAr and secondary antibody labelled with A, in the absence of D on the acceptor channel (left, ex: 543 nm; em: 560-610 nm) and FRET channel (right, ex: 488; em: 560-610 nm). (**C**) SH-SY5Y cells treated with D and A. From left to right the donor channel, the acceptor channel, the FRET channel and the colocalization image, obtained by overlapping the donor and acceptor channels. (**D**) Semi-quantitative analysis of the green AMPAr-derived fluorescence in the donor channel in the presence of only D or both D and A. (**E**) Semi-quantitative analysis of the red AMPAr-derived fluorescence in the FRET channel in the presence of only A or both D and A. Error bars: S.E.M. The triple (***) asterisks refer to p values <0.001 relative to the channels in the presence of only the acceptor or only the donor.

3.5. Mechanical stimuli propagated through the lipid bilayer are responsible for type A HypF-N oligomers-induced activation of NMDAr

The absence of direct interaction of extrasynaptic NMDAr and AMPAr with the oligomers may suggest an activation mediated by the involvement of other proteins and/or messengers. However, the rapidity of their activation, highlighted by the absence of a lag phase in the time-dependent rise of intracellular Ca^{2+} ions (Fig. 3.2), rather leads to the

alternative hypothesis that the membrane deformation caused by the interaction with the oligomers is transmitted mechanically to the receptors via the lipid bilayer. Indeed, NMDAr are well known to be mechanosensitive and be potentiated by well-defined mechanical stimuli such as membrane depression, hypotonic solutions and lateral membrane stretch, and be inhibited by the opposite stimuli (Paoletti and Ascher, 1994; Casado and Ascher, 1998; Chaban *et al*., 2004; Kloda *et al*., 2007; Singh *et al*., 2012).

To assess this possibility, we used again the SH-SY5Y cells and enriched them with LPC and AA, which are known to cause a membrane compression and stretch, respectively, because of their opposite shapes: LPC has the shape of cone, large hydrophilic head and narrow hydrophobic tail, whereas AA is an inverted cone, narrow hydrophilic head and large, highly unsaturated, hydrophobic tail (Casado and Ascher, 1998; Chernomordik *et al*., 1993). They therefore cause an inhibition and potentiation of the NMDAr, respectively (Casado and Ascher, 1998). It was previously observed that the use of LPC can cause an increase in intracellular Ca^{2+} levels through the signaling of GPR55 (Drzazga *et al*., 2017), a receptor, which is, however, not expressed (Human Protein Atlas source) or weakly expressed (Harmonizome source) in SH-SY5Y cells.

The SH-SY5Y cells were treated with various concentrations of LPC (0-2 μM) for 2 h, washed with cell medium and then incubated with 12 μM monomer equivalent of type A HypF-N oligomers for 10 min. A concentration of 2 μM LPC was found to inhibit the oligomer-induced Ca^{2+} entry through the NMDAr (Fig. 3.11A,B). The ability of a bilayer-embedded compound, such as LPC, to counteract the oligomer-induced NMDAr opening, despite the lack of any specific interaction between the lipid and the receptors, suggests that the oligomers induce a mechanical stimulus upon binding to the membrane, that is transmitted down to the NMDAr via the lipid bilayer causing their opening. The

opposing force exerted by LPC effectively inhibits the mechanical signal generated by the action of the oligomers onto the membrane.

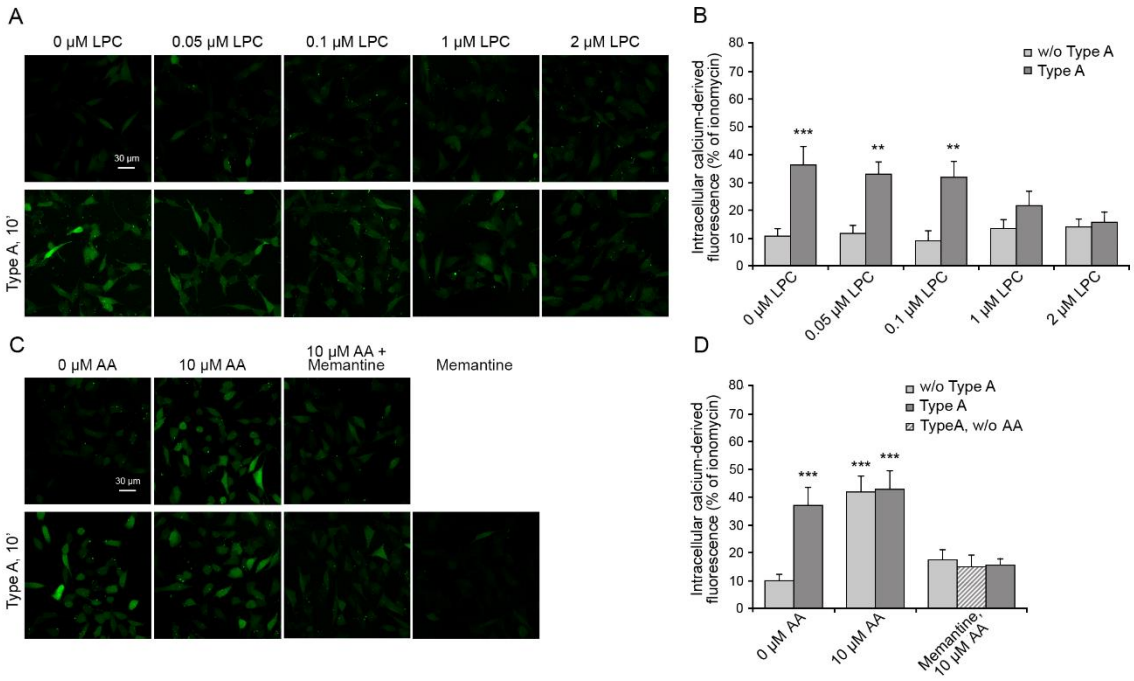

Figure 3.11. (**A**) Representative confocal scanning microscopy images of intracellular free Ca^{2+} in SH-SY5Y cells following the treatment for 2 h with 0, 0.05, 0.1, 1.0 and 2.0 µM LPC with or without 10 min treatment of type A oligomers, and (**B**) semi-quantitative analysis of intracellular free Ca^{2+}-derived fluorescence. (**C**) Representative confocal scanning microscopy images of intracellular free Ca^{2+} in SH-SY5Y cells following the treatment for 2 h with 0 and 10 µM AA with or without 10 min treatment of type A oligomers and after pre-treatment with 10 µM Memantine for 1 h and (**D**) semi-quantitative analysis of intracellular free Ca^{2+}-derived fluorescence. Variable numbers of cells (12-22) in three different experiments were analysed for each condition. The double (**) and triple (***) asterisks refer to p values <0.01 and <0.001, respectively, relative to the untreated.

We then incubated incubating the cells for 2 h with 10 µM AA before the addition of the oligomers. AA alone was found to be enough to activate an NMDAr-mediated influx of Ca^{2+} ions, even in the absence of oligomers (Fig. 3.11C, D), in agreement with the literature reporting its mechanical action on the membrane (Paoletti and Ascher, 1994; Casado and Ascher, 1998). The influx of Ca^{2+} ions was not further increased after the addition of 12 µM monomer equivalent of type A oligomers in the presence of AA pre-

treatment (Fig. 3.11C, D), in agreement with the idea that an occlusion exists if two mechanical stimuli of the same type are applied to the membrane to modulate NMDAr (Casado and Ascher, 1998). Importantly, all three effects are inhibited by memantine indicating that they all result from an ionic influx involving the NMDAr (Fig. 4C, D).

3.6. Ion channels interacting with type A HypF-N oligomers are not involved in the Ca^{2+} influx

In the search for others potential Ca^{2+} channels involved in the observed influx of Ca^{2+} from the extracellular medium, we considered a recent interactome-wide study in which more than 2500 membrane proteins of N13 cells interacting with type A HypF-N oligomers were identified (Mannini *et al*., 2019). Among them, we did not find any subunits of NMDAr and AMPAr, in agreement with our FRET results, but we identified five different Ca^{2+} channels: anoctamin-6 (SCAN channel), transient receptor potential cation channel subfamily V member 2 (TrpV2), P2X purinoceptor 4 (P2X4), piezo-type mechanosensitive ion channel component 1 (FAM38A) and transient receptor potential cation channel subfamily M member 7 (LTrpC-7). Four of them were found to be expressed also in SH-SY5Y cells, except for TrpV2 (Human Protein Atlas source; Uhlén *et al*., 2015).

To investigate their possible role in the influx of Ca^{2+} induced by type A HypF-N oligomers in SH-SY5Y cells, before the treatment for 5, 10 or 60 min with the type A oligomers we inhibited them one by one, using specific inhibitors: Anti-ANO6 Antibody (SCAN channel inhibitor), Anti-P2RX4 Antibody (P2X4 inhibitor), GsMTx4 (FAM38A inhibitor) and FTY720 (LTrpC-7 inhibitor). In all cases, we did not observe any variation

in the influx of Ca^{2+}, indicating that none of the four channels are involved directly, either in the early or in the late stages of Ca^{2+} influx (Fig. 3.12).

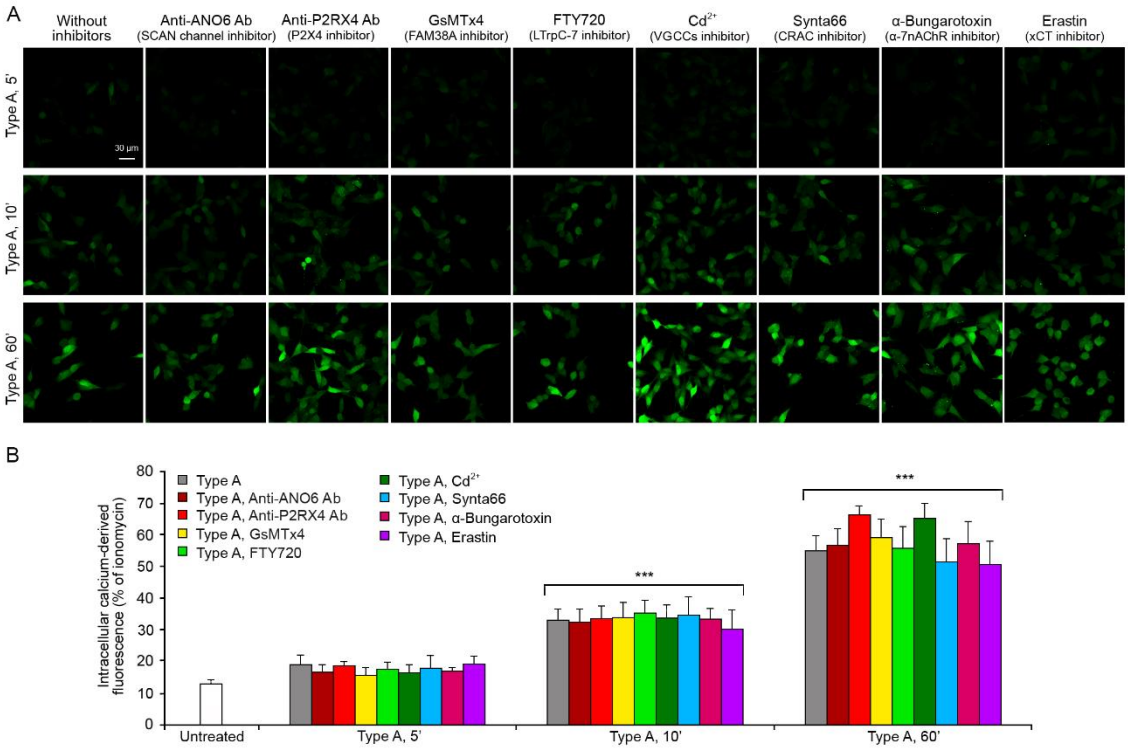

Figure 3.12. (**A**) Representative confocal scanning microscopy images of intracellular free Ca^{2+} level in SH-SY5Y cells following the treatment with no inhibitors, 1 µg/ml Anti-ANO6 Antibody (SCAN channel inhibitor), 0.6 µg/ml Anti-P2RX4 Antibody (P2X4 inhibitor), 5 µM GsMTx4 (FAM38A inhibitor), 3 µM FTY720 (LTrpC-7 inhibitor), 10 µM Cd2+ (VGCCs inhibitor), 10 µM Synta66 (CRAC inhibitor), 100 nM α-bungarotoxin (α7nAChR inhibitor) and 100 µM erastin (xCT inhibitor) and analysed after 5 min (first row) or 10 min (second row) or 60 min (third row) of treatment with 12 µM (monomer equivalents) type A oligomers. (**B**) Semi-quantitative analysis of intracellular free Ca^{2+}-derived fluorescence. Variable numbers of cells (12-22) in three different experiments were analysed for each condition. Error bars: S.E.M. The triple (***) asterisks refer to p values <0.001 relative to the untreated cells.

We also investigated other channels, which were not found to interact directly with type A HypF-N oligomers in the interactome study (Mannini *et al.*, 2019), but are known to be important in some circumstances for Ca^{2+} homeostasis and thus potentially relevant in the present context: the voltage-gated calcium channels (VGCCs), the calcium release-activated channels (CRAC), the nicotinic acetylcholine receptor α7 (α7nAChR)

and the cystine/Glu transporter (xCT) (Ueda *et al*., 1997; Quan *et al*., 2016; Qin e*t al*., 2006; Talantova *et al*., 2013; Feske, 2019). In these cases, we pre-treated the SH-SY5Y cells with Cd^{2+} (VGCCs inhibitor), with Synta66 (CRAC channel inhibitor), with α-bungarotoxin (α7nAChR inhibitor) or with erastin (xCT inhibitor), and then we treated the cells with type A oligomers for 5, 10 or 60 min. The pattern of Ca^{2+} influx was similar to that observed without inhibitors at all time points (Fig. 3.12), ruling out their involvement in the Ca^{2+} influx induced by type A oligomers.

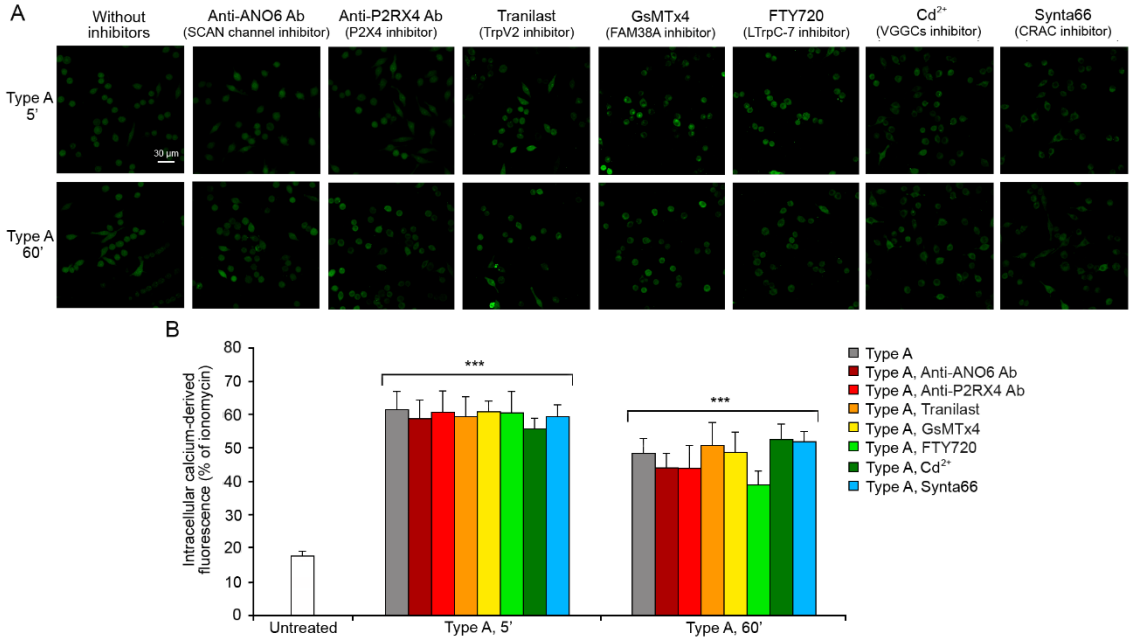

Figure 3.13. (**A**) Representative confocal scanning microscopy images of intracellular free Ca^{2+} level in N13 cells following the treatment with no inhibitors, 1 µg/ml Anti-ANO6 Antibody (SCAN channel inhibitor), 0.6 µg/ml Anti-P2RX4 Antibody (P2X4 inhibitor), 75 µM tranilast (TrpV2 inhibitor), 5 µM GsMTx4 (FAM38A inhibitor), 3 µM FTY720 (LTrpC-7 inhibitor), 10 µM Cd2+ (VGCCs inhibitor) and 10 µM Synta66 (CRAC inhibitor) and analysed after 5 min (first row) or 60 min (second row) of treatment with 0.1 µM (monomer equivalents) type A oligomers. (**B**) Semi-quantitative analysis of intracellular free Ca^{2+}-derived fluorescence. Variable numbers of cells (12-22) in three different experiments were analysed for each condition. Error bars: S.E.M. The triple (***) asterisks refer to p values <0.001 relative to the untreated.

The entire analysis was also performed on N13 cells, confirming the same results, without any involvement of all the analysed channels in the Ca^{2+} influx (Fig. 3.13). On

this cell line we also used the TrpV2 inhibitor, tranilast, channels not expressed in the SH-SY5Y cells (Fig 3.13), and combinations of inhibitors (Fig. 3.14A,B), but without any significant variations in the Ca^{2+} levels. As a positive control, we treated N13 cells with probenecid and then with a combination of probenecid and tranilast, acting as specific activator and inhibitor of the TrpV2 channel, respectively, in both cases in the absence of HypF-N oligomers. We observed an increase of intracellular Ca^{2+} in the presence of probenecid, and a restoration to the levels observed in the untreated cells after the treatment with tranilast (Fig. 3.14C,D).

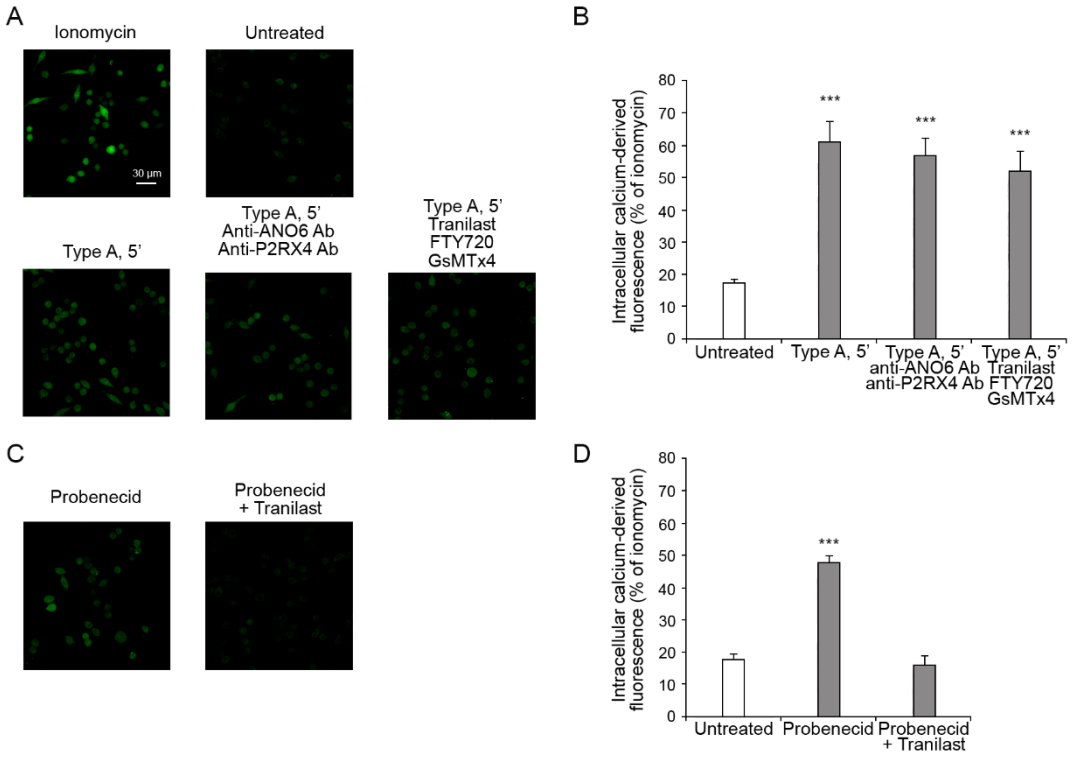

Figure 3.14. (**A**) Representative confocal scanning microscopy images of intracellular free Ca^{2+} level in N13 cells treated with 1 µM ionomycin, no inhibitors, 0.1 µM (monomer equivalents) type A oligomers without or with the indicated inhibitors. (**B**) Semi-quantitative analysis of intracellular free Ca^{2+}-derived fluorescence. (**C**) Representative confocal scanning microscopy images of intracellular free Ca^{2+} level in N13 cells treated with 175 µM probenecid (TrpV2 activator) and 175 µM probenecid plus 75 µM tranilast (TrpV2 activator and inhibitor, respectively). (**D**) Semi-quantitative analysis of intracellular free Ca^{2+}-derived fluorescence. Variable numbers of cells (12-22) in three different experiments were analysed for each condition. Error bars: S.E.M. The triple (***) asterisks refer to p values <0.001 relative to the untreated cells.

3.7. Experiments with zinc-stabilised $A\beta_{40}$ oligomers and $A\beta_{42}$ ADDLs confirm the involvement of NMDAr and AMPAr

The analysis performed with type A HypF-N oligomers was extended to 5 μM monomer equivalents of the zinc-stabilised $A\beta_{40}$ oligomers (Mannini *et al*., 2018) and to 1 μM of $A\beta_{42}$ ADDLs (Lambert *et al*., 2001).

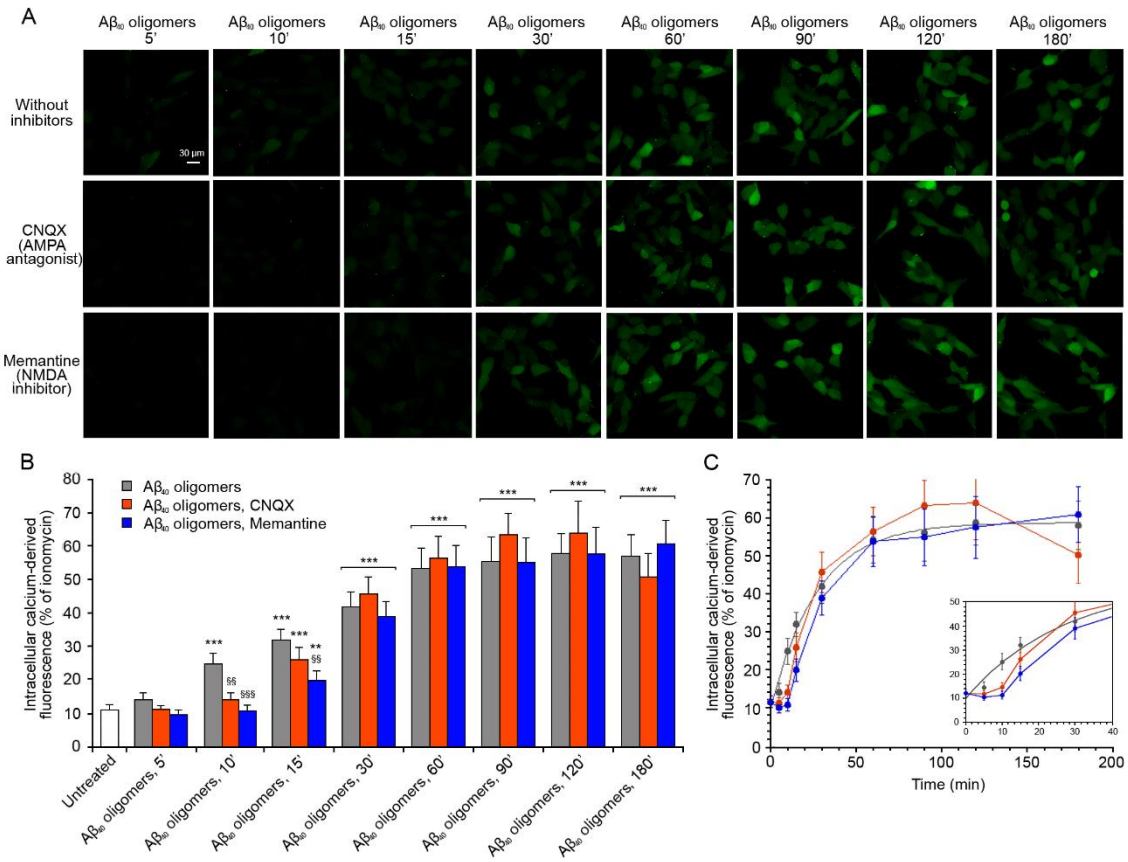

Figure 3.15. (**A**) Representative confocal scanning microscopy images of intracellular free Ca^{2+} in SH-SY5Y cells treated with no inhibitors (first row), 5 μM CNQX (second row) and 10 μM memantine (third row), and analysed after 5, 10, 15, 30, 60, 90, 120 and 180 min of treatment with 5 μM zinc-stabilized $A\beta_{40}$ oligomers. (**B**) Semi-quantitative analysis of intracellular free Ca^{2+}-derived fluorescence. Variable numbers of cells (12-22) in three different experiments were analysed. Error bars: S.E.M. The double (**) and triple (***) asterisks refer to p values <0.01 and <0.001, respectively, relative to the untreated. The double (§§) and triple (§§§) symbol refer to p values <0.01 and <0.001, respectively, relative to oligomers without inhibitors. (**C**) Kinetic plots showing the fluorescence values versus time as reported in panel B.

The treatment of SH-SY5Y cells with the zinc-stabilized $A\beta_{40}$ oligomers induced a gradual increase of intracellular Ca^{2+} levels, which reached the maximum value after 180 min of treatment (Fig. 3.15). The inhibition of AMPAr and NMDAr, using their specific inhibitors CNQX and memantine, respectively, confirmed the involvement of these channels in the early stage of the influx of Ca^{2+}, with a reduction of Ca^{2+} level up to 10 min of treatment for the AMPAr inhibition and 15 min for the NMDAr inhibition, compared with the treatment without inhibitors (Fig. 3.15B), as they slowed down the kinetics of the Ca^{2+} increase (Fig. 3.15C).

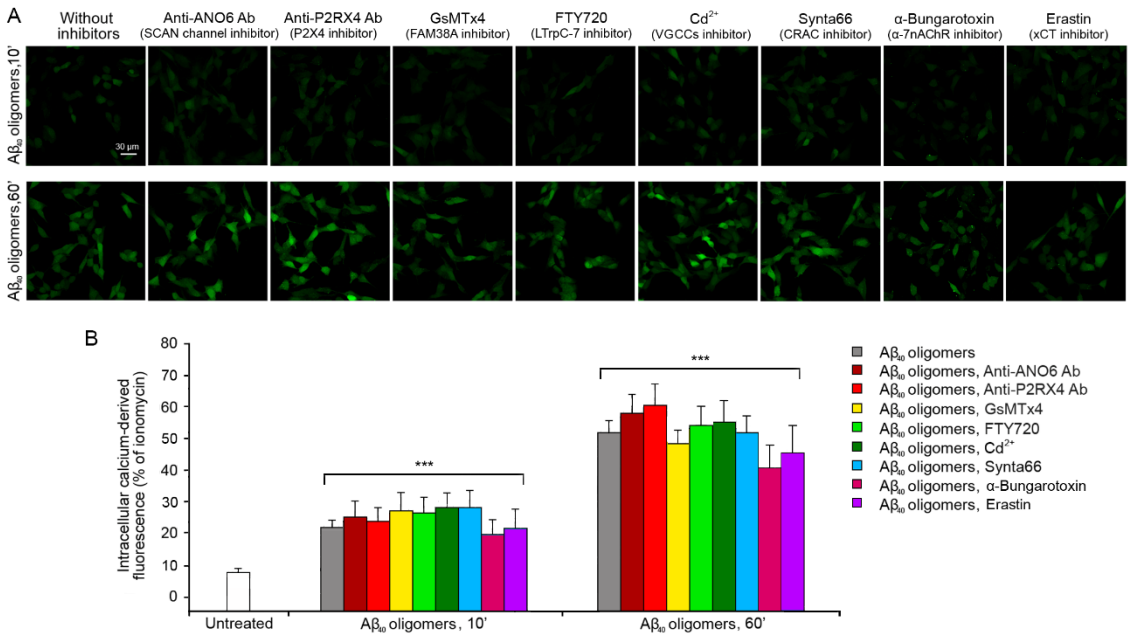

Figure 3.16. (**A**) Representative confocal scanning microscopy images of intracellular free Ca^{2+} level in SH-SY5Y cells treated with no inhibitors, 1 μg/ml Anti-ANO6 Antibody (SCAN channel inhibitor), 0.6 μg/ml Anti-P2RX4 Antibody (P2X4 inhibitor), 5 μM GsMTx4 (FAM38A inhibitor), 3 μM FTY720 (LTrpC-7 inhibitor), 10 μM Cd2+ (VGCCs inhibitor), 10 μM Synta66 (CRAC inhibitor), 100 nM α-bungarotoxin (α7nAChR inhibitor) and 100 μM erastin (xCT inhibitor) and analysed after 10 min (first row) or 60 min (second row) of treatment with 5 μM (monomer equivalents) zinc-stabilized $A\beta_{40}$ oligomers. (**B**) Semi-quantitative analysis of intracellular free Ca^{2+}-derived fluorescence. Variable numbers of cells (12-22) in three different experiments were analysed for each condition. Error bars: S.E.M. The triple (***) asterisks refer to p values <0.001 relative to the untreated.

Moreover, we analysed the four Ca^{2+} channels found to interact with the type A oligomers of HypF-N in the N13 cells, as well as the VGCCs, the CRAC channels, the α7nAChR and the xCT, using their respective specific inhibitors and protocols described before. The results confirmed those observed with the type A oligomers of HypF-N, that is the lack of involvement of these channels in the influx of Ca^{2+} (Fig. 3.16).

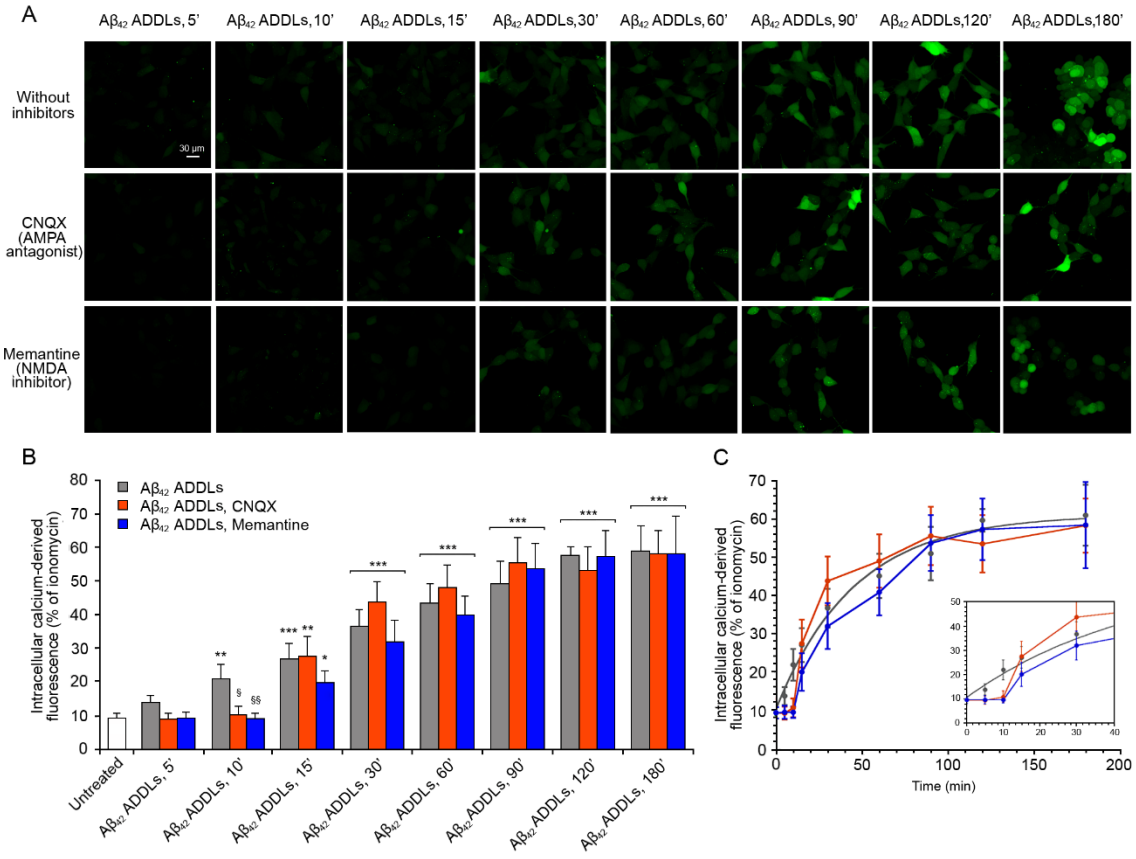

Figure 3.17. (**A**) Representative confocal scanning microscopy images of intracellular free Ca^{2+} in SH-SY5Y cells treated with no inhibitors (first row), 5 μM CNQX (second row) and 10 μM memantine (third row), and analysed after 5, 10, 15, 30, 60, 90, 120 and 180 min of treatment with 1 μM Aβ42 ADDLs oligomers. (**B**) Semi-quantitative analysis of intracellular free Ca^{2+}-derived fluorescence. Variable numbers of cells (12-22) in three different experiments were analysed. Error bars: S.E.M. The single, double (**) and triple (***) asterisks refer to p values <0.05, <0.01 and <0.001, respectively, relative to the untreated. The single (§) and double (§§) symbol refer to p values <0.05 and <0.01, respectively, relative to oligomers without inhibitors. (**C**) Kinetic plots showing the fluorescence values versus time as reported in panel B.

The $A\beta_{42}$ ADDLs had a similar behaviour, causing an increase in the intracellular Ca^{2+} level up to 180 min after the treatment of the SH-SY5Y cells (Fig. 3.17). Similarly to the zinc-stabilised $A\beta_{40}$ oligomers described above, the inhibition of the AMPAr and NMDAr determined a reduction of Ca^{2+} up to 10 min and 15 min of treatment with the oligomers, respectively (Fig. 3.17).

Moreover, inhibition of any of the other Ca^{2+} channels, before the treatment with $A\beta_{42}$ ADDLs, did not have any such effects on the influx of Ca^{2+} induced by the oligomers, similar to the results observed with the type A HypF-N oligomers and the zinc-stabilised $A\beta_{40}$ oligomers (Fig. 3.18).

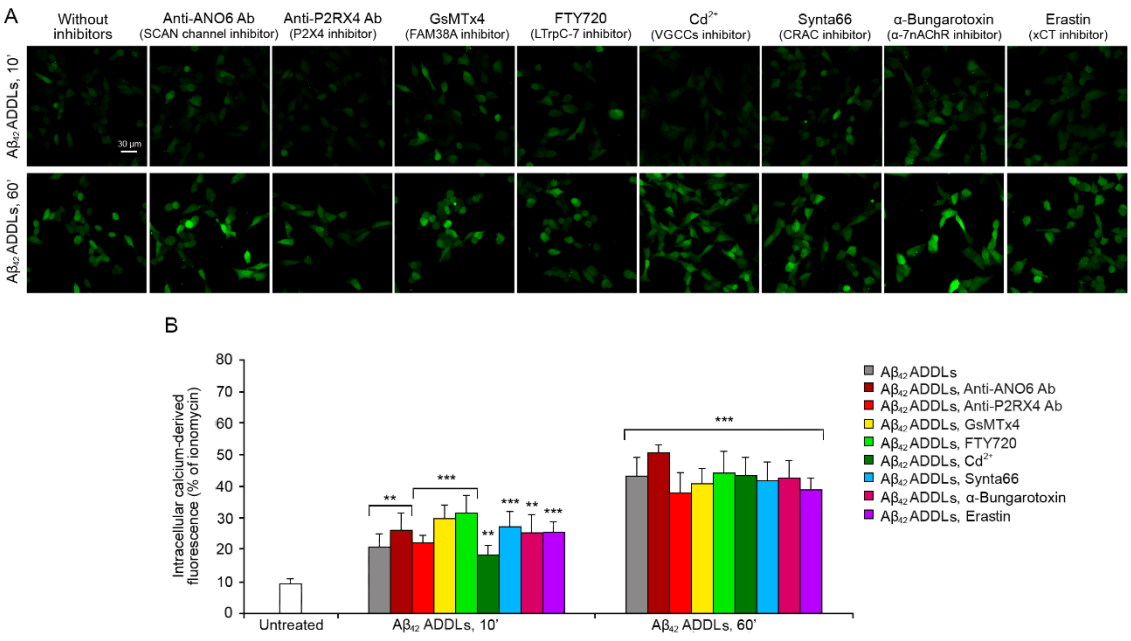

Figure 3.18. (**A**) Representative confocal scanning microscopy images of intracellular free Ca^{2+} level in SH-SY5Y cells treated with no inhibitors, 1 μg/ml Anti-ANO6 Antibody (SCAN channel inhibitor), 0.6 μg/ml Anti-P2RX4 Antibody (P2X4 inhibitor), 5 μM GsMTx4 (FAM38A inhibitor), 3 μM FTY720 (LTrpC-7 inhibitor), 10 μM Cd2+ (VGCCs inhibitor), 10 μM Synta66 (CRAC inhibitor), 100 nM α-bungarotoxin (α7nAChR inhibitor) and 100 μM erastin (xCT inhibitor) and analysed after 10 min (first row) or 60 min (second row) of treatment with 1 μM (monomer equivalents) $A\beta_{42}$ ADDLs oligomers. (**B**) Semi-quantitative analysis of intracellular free Ca^{2+}-derived fluorescence. Variable numbers of cells (12-22) in three different experiments were analysed for each condition. Error bars: S.E.M. The double (**) and triple (***) asterisks refer to p values <0.01 and <0.001, respectively, relative to the untreated.

The effect on Ca^{2+} dyshomeostasis of the $A\beta_{42}$ ADDLs after 10 and 60 min of treatment was tested also in primary rat cortex neurons (Fig. 3.19). Along the same line, 10 min of treatment with the oligomers was sufficient to induce an increase of the intracellular Ca^{2+} level, which increased further after 60 min of treatment (Fig. 3.19). The inhibition of the AMPAr and NMDAr determined a significant reduction of the Ca2+ level after 10 min of treatment with the $A\beta_{42}$ ADDLs, confirming the involvement of the receptors in the Ca^{2+} influx (Fig. 3.19).

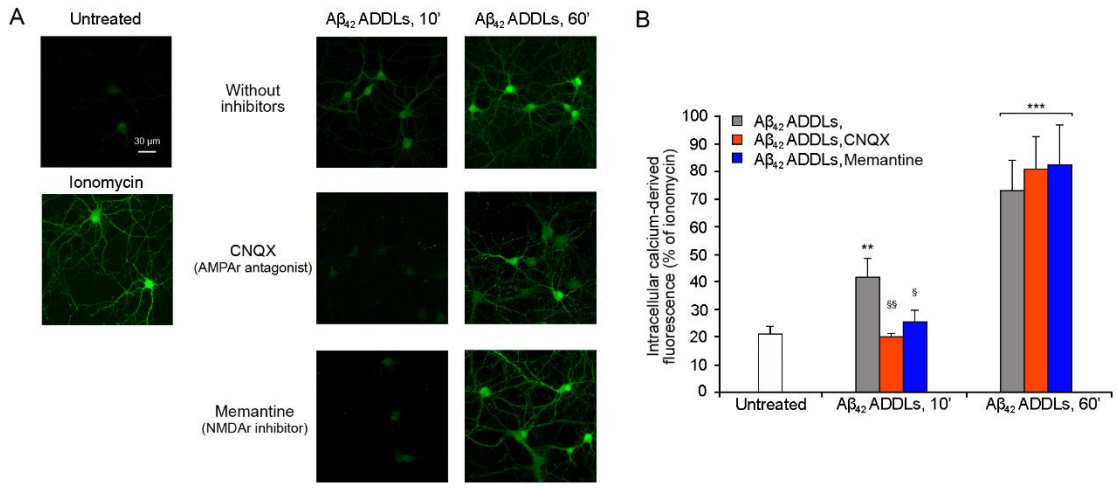

Figure 3.19. (**A**) Representative confocal scanning microscopy images of intracellular free Ca^{2+} level in primary rat cortex neurons treated with 1 µM ionomycin and following the treatment with no inhibitors, 5 µM CNQX and 10 µM memantine, and analysed after 10 and 60 min of treatment with 1 µM (monomer equivalents) $A\beta_{42}$ ADDLs oligomers. (**B**) Semi-quantitative analysis of intracellular free Ca^{2+}-derived fluorescence. Variable numbers of cells (12-22) in three different experiments were analysed for each condition. The single double (**) and triple (***) asterisks refer to p values <0.01 and <0.001, respectively, relative to the untreated. The single (§) and double (§§) symbol refer to p values <0.05 and <0.01, respectively, relative to $A\beta_{42}$ ADDLs oligomers without inhibitors. Error bars: S.E.M.

To confirm these results with a different technique, we pre-treated SH-SY5Y cells with the siRNA against the subunit 2B of the NMDAr. A significant reduction of the NMDAr was observed in the silenced cells (Fig. 3.20A) and significantly lower

intracellular Ca^{2+} levels were observed in cells pre-treated with siRNA after 10 min of treatment with the $A\beta_{42}$ ADDLs oligomers, compared with cells without siRNA treatment (Fig. 3.20B), confirming the results observed with memantine. After 60 min of ADDL treatment, the Ca^{2+} levels increased, but they were still lower than the cells without siRNA (Fig. 3.20B).

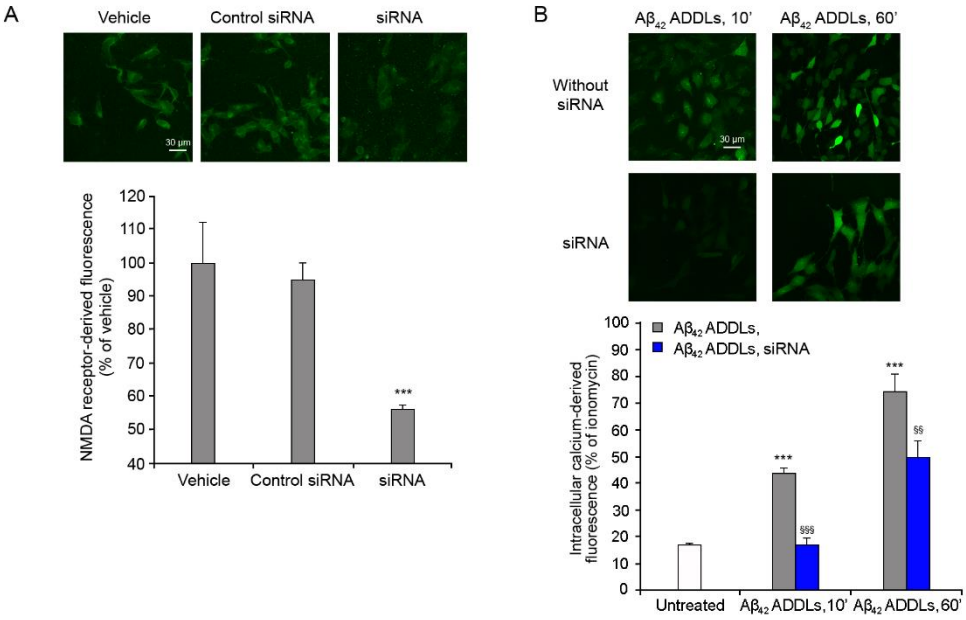

Figure 3.20. (**A**) Representative confocal scanning microscopy images of NMDAr-derived fluorescence (green) in SH-SY5H cells following pre-treatment with vehicle, 25 nM siRNA negative control and 25 nM siRNA, and semi-quantitative analysis. (**B**) Representative confocal scanning microscopy images of intracellular free Ca^{2+} levels in SH-SY5Y cells following pre-treatment with or without 25 nM siRNA and analysed after 10 and 60 min of treatment with 1 µM (monomer equivalents) $A\beta_{42}$ ADDLs oligomers, and semi-quantitative analysis of intracellular free Ca^{2+}-derived fluorescence. Variable numbers of cells (12-22) in three different experiments were analysed for each condition. The triple (***) asterisks refer to p values <0.001 relative to untreated cells. The double (§§) and triple (§§§) symbols refer to p values <0.01 and <0.001, respectively, relative to cells treated with $A\beta_{42}$ ADDLs oligomers.

3.8. Mechanical stimuli propagated through the lipid bilayer are responsible for Aβ$_{42}$ ADDLs oligomer-induced activation of NMDAr

In order to confirm the molecular mechanism of Ca^{2+} influx observed with the type A HypF-N oligomers, the experiments described above, about the SH-SY5Y cellular membranes enrichment with LPC and AA, were repeated before the treatment with Aβ$_{42}$ ADDLs oligomers.

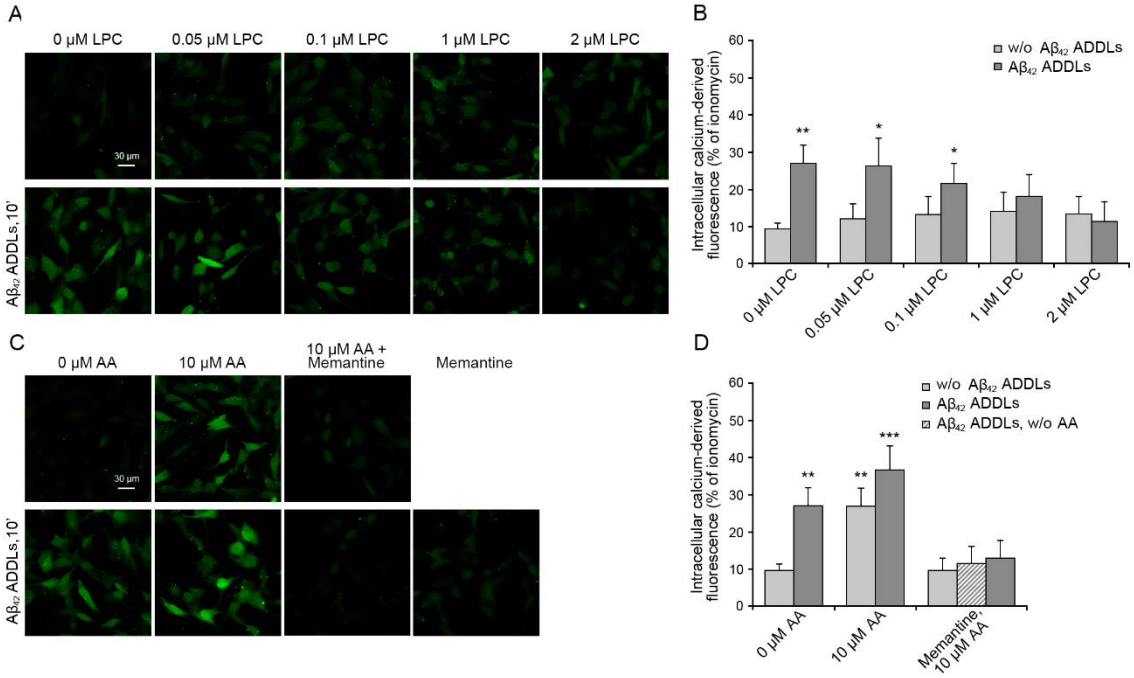

Figure 3.21. (**A**) Representative confocal scanning microscopy images of intracellular free Ca^{2+} in SH-SY5Y cells treated for 10 min with 0, 0.05, 0.1, 1.0 and 2.0 μM LPC with or without Aβ$_{42}$ ADDLs oligomers, and (**B**) semi-quantitative analysis of intracellular free Ca^{2+}-derived fluorescence. (**C**) SH-SY5Y cells treated with 0 or 10 μM AA with or without Aβ$_{42}$ ADDLs oligomers and after pre-treatment with 10 μM Memantine and (**D**) semi-quantitative analysis of intracellular free Ca^{2+}-derived fluorescence. Variable numbers of cells (12-22) in three different experiments were analysed for each condition. The double (**) and triple (***) asterisks refer to p values <0.01 and <0.001, respectively, relative to the untreated.

SH-SY5Y cells were treated with various concentrations of LPC (0-2 μM) for 2 h, and then incubated with 1 μM Aβ$_{42}$ ADDLs for 10 min. The enrichment with 2 μM

LPC caused a complete inhibition of the ADDL-induced Ca^{2+} entry through the NMDAr (Fig. 3.21A,B), in agreement with the results observed before. Moreover, the application of 1 μM $Aβ_{42}$ ADDLs to SH-SY5Y cells pre-treated with 10 μM AA produced a slight higher, but not significant, increase of Ca^{2+} influx, with respect to cells pre-treated with AA alone (Fig. 3.21C,D), again in agreement with observations obtained with HypF-N oligomers and AA-enriched membranes. All these effects are inhibited by memantine, indicating that they all result from an ionic influx involving the NMDAr (Fig. 3.21C, D).

The enrichment with 2 μM LPC and 10 μM AA and the incubation with 1 μM $Aβ_{42}$ ADDLs oligomers for 10 min were repeated in the primary rat cortex neurons. The results confirm the inhibition of the ADDL-induced Ca^{2+} entry in LPC-enriched cells and a slight, but not significant, increase of Ca^{2+} influx in AA-enriched cells with respect to cells pre-treated with AA alone (Fig. 3.22). Memantine treatment again inhibited the Ca^{2+} entry in cells treated with AA and ADDLs, confirming the involvement of the NMDAr (Fig. 3.22).

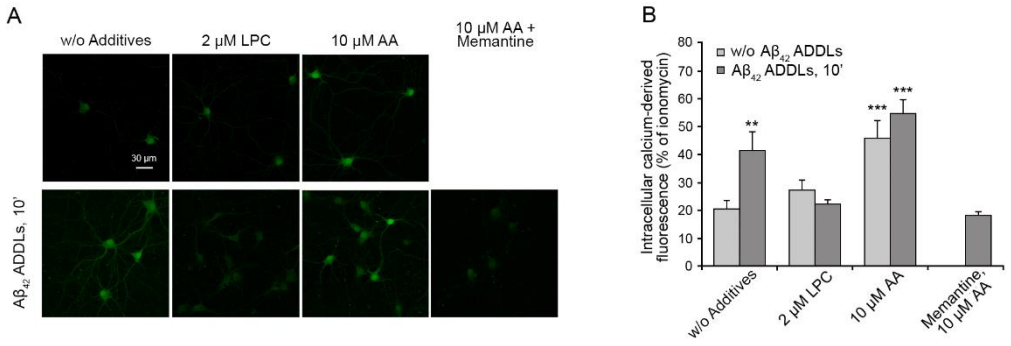

Figure 3.22. (**A**) Representative confocal scanning microscopy images of intracellular free Ca^{2+} in primary rat cortex neurons treated for 2 h with no additives, 2.0 μM LPC, 10 μM AA and 10 μM AA after pre-treatment with 10 μM Memantine, with or without 10 min treatment with 1 μM (monomer equivalent) $Aβ_{42}$ ADDLs oligomers. (**B**) Semi-quantitative analysis of intracellular free Ca^{2+}-derived fluorescence. Variable numbers of cells (12-22) in three different experiments were analysed for each condition. The double (**) and triple (***) asterisks refer to p values <0.01 and <0.001, respectively, relative to the untreated.

3.9. $A\beta_{42}$ ADDLs oligomers change the cellular membrane fluidity

In order to gain a second independent piece of evidence that $A\beta_{42}$ ADDLs activate the NMDAr via mechanical stimuli through the membrane assimilable to a bilayer stretching, we analysed the effects of the oligomers on the rotational diffusion of TMA-DPH, which is known to insert in the polar head group region of the cell membrane due to its charged group (Illinger *et al*., 1995).

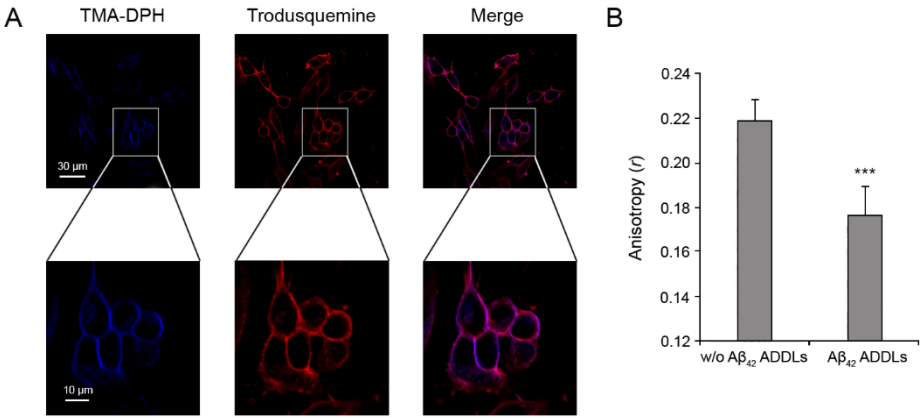

Figure 3.23. (A) Representative confocal scanning microscopy images of SH-SY5Y cells following the treatment for 5 min with 2.0 µM TMA-DPH (blue), for 10 min with 5 µM trodusquemine labelled with Alexa Fluor 594 (red) and the colocalization image (merge). (B) Fluorescence anisotropy (*r*) plot for TMA-DPH obtained in the absence and presence of 1 µM (monomer equivalent) $A\beta_{42}$ ADDLs oligomers. The triple (***) asterisks refer to p values <0.001 relative to the results in the absence of oligomers.

The incorporation of the TMA-DPH in the plasma membrane was observed analysing its colocalization with the trodusquemine, a small molecule which belongs to a family of compound known to bind the membrane (Zasloff *et al*., 2011), labelled with Alexa Fluor 594 (Fig. 3.23A). Both the fluorescence, derived from the TMA-DPH and the Trodusquemine, can be observed on the plasma membrane, and the colocalization can be observed in the merge images (Fig. 3.23A). In the absence and presence of a 10 min treatment with ADDLs, the anisotropy of TMA-DPH was 0.22±0.01 and 0.18±0.01,

respectively (Fig. 3.23B). The lower anisotropy in the presence of the oligomers indicate a higher increase of the rotational freedom of the fluorophore, resulting from a gain of free space between the membrane lipids and fluidity of the whole membrane bilayer.

4. Discussion

A key process in neurodegeneration, particularly in AD, is the disruption of calcium homeostasis in neurons of the neocortex and hippocampus (Lacor *et al*., 2007; Chakroborty *et al*., 2014; Agostini and Fasolato, 2016; Zhang *et al*., 2016; Wang and Reddy, 2017; Tong *et al*., 2018). Aβ oligomers interact with, and destabilize, the cell membrane and its protein components, with a consequent Ca^{2+} influx from the extracellular space to the cytosol of neurons. This influx has been proposed to occur through a destabilization or perforation of the lipid bilayer (Kawahara *et al*., 2000; Demuro *et al*., 2005; Sepùlveda *et al*., 2014; Cascella *et al*., 2017), or activation of iGluRs acting as calcium channels, such as NMDAr (Snyder *et al*., 2005; De Felice *et al*., 2007; Deshpande *et al*., 2009; Alberdi *et al*., 2010; Decker *et al*., 2010; Rönicke *et al*., 2011; Texidò *et al*., 2011; Sinnen *et al*., 2016; Arbel-Ornath *et al*., 2017; Cascella *et al*., 2017) and AMPAr (Tozaki *et al*., 2002; De Felice *et al*., 2007; Zhao *et al*., 2009; Alberdi *et al*., 2010), activation of voltage-dependent Ca^{2+} channels (Ueda *et al*., 1997; Quan *et al*., 2016), activation of transient receptor potential melastatin 2 (TRPM2) (Ostapchenko *et al*., 2015), or activation of transient receptor potential A1 (TRPA1) (Bosson *et al*., 2017).

In this thesis the Ca^{2+} dyshomeostasis induced by the zinc-stabilised $A\beta_{40}$ oligomers and $A\beta_{42}$ oligomeric ADDLs, as well as toxic HypF-N oligomers mimicking those of Aβ, was analysed. All the oligomers were previously found to be toxic to neuronal cells (Lambert *et al*., 1998; Lambert *et al*., 2001; De Felice *et al*., 2007; Campioni *et al*., 2010; Zampagni *et al*., 2011; Tatini *et al*., 2013; Evangelisti *et al*., 2016; Mannini *et al*., 2018). Moreover, ADDLs were also found to be toxic to rat primary hippocampal neurons (De Felice *et al*., 2007; Lacor *et al*., 2007; Wang *et al*., 2010), and HypF-N oligomers were found to affect cholinergic neuronal cells (Zampagni *et al*.,

2011) and rat hippocampal primary neurons (Tatini *et al.*, 2013). Our results show a time-dependent increase of Ca^{2+} in the intracellular space on neuroblastoma cells, microglial cells and primary rat cortex neurons upon exposure of the cells to all three types of oligomers. This increase of Ca^{2+} occurs almost exclusively from the extracellular space in the neuroblastoma cells, as demonstrated using a free Ca^{2+} medium, and from both the extracellular medium and the intracellular stores in the microglial cells. In these cell lines, the toxicity induced by the oligomers is mediated by the influx of Ca^{2+} from the extracellular space, as demonstrated by the absence of cytotoxicity in a free Ca^{2+} medium.

Our further investigation shows that the oligomer-induced influx of Ca^{2+} is mediated by a rapid activation of extrasynaptic NMDAr and, to a lower extent, AMPAr and also by causing, on a slower time scale, a perforation or destabilization of the lipid bilayer of the membrane. This result was also confirmed on cultured rat primary neurons. Indeed, the rise of cytosolic Ca^{2+} ions detected within the first 10 minutes following the exposure of the cells to the oligomers is caused by NMDAr and AMPAr as their specific inhibition with memantine and CNQX, or knockdown with a siRNA against the NMDAr GRIN2B subunit, cause the appearance of a lag phase in the time-dependent rise of intracellular Ca^{2+}, with no significant increase within the first ten minutes. Later, the intracellular Ca^{2+} levels start to increase despite the persistent inactivation of the two receptors and, after 60-120 min, they reach the same levels observed in the absence of any inhibition.

Importantly, the cells that have been most studied in this thesis namely SH-SY5Y, do not have dendrites, axons and synapses and the only AMPAr and NMDAr are extrasynaptic. These results, therefore, reinforce the idea that extrasynaptic NMDAr play a central role in the pathogenesis of AD, not just because they are activated aberrantly in the disease as a result of the excitotoxicity induced by Aβ, but also because of the

interaction of the peptide in aggregated forms with the lipid membranes. Our results also provide an explanation as to why blockage of the receptors is beneficial, but not sufficient, to re-establish calcium homeostasis, as the oligomers also cause a non-specific entry of Ca^{2+} through the destabilized membrane. This concept finds confirmation in the clinical effects that are exerted by memantine as a drug approved by the American Food Drug Agency (FDA), the European Medicine Agency (EMA) and other governmental agencies, which is symptomatic and help improve the cognitive performance of the patients, but is not sufficient to reverse the disease or block its progression. Interestingly, it is recognised that memantine has a high affinity particularly for extrasynaptic NMDAr as opposed to synaptic receptors (Xia *et al*., 2010; Glasgow *et al*., 2017). Early diagnosis of the disease and therapeutic strategies that also interfere with the association of Aβ in oligomeric forms with lipid membranes may add considerable value in the fight against the disease.

None of the Ca^{2+} channels that have been found in a previous interactome study to interact with HypF-N oligomers, namely SCAN, TrpV2, P2X4, FAM38A and LTrpC-7 (Mannini *et al*., 2019), can participate to the observed Ca^{2+} influx induced by either HypF-N, $A\beta_{40}$ and $A\beta_{42}$ oligomers. Similarly, other Ca^{2+} channels previously suggested to be involved on the Aβ-induced alteration of Ca^{2+} homeostasis in some circumstances, such as VGCCs, CRAC, α7nAChR and xCT (Ueda *et al*., 1997; Qin *et al*., 2006; Talantova *et al*., 2013; Quan *et al*., 2016; Feske, 2019), were not found to be involved. Indeed, their specific inhibition in either microglial N13 and neuroblastoma SH-SY5Y cells does not recover the Ca^{2+} dyshomeostasis, either at the early or late times.

It is remarkable to observe that none of the protein subunits forming the AMPAr and NMDAr are present in the HypF-N oligomer interactome studied in N13 cells, despite the presence of these two receptors in this cell line (Mannini *et al*., 2019). Such a lack of interactions further analysed here using the FRET technique between the labelled HypF-

N oligomers and the labelled primary antibody against the NMDAr or AMPAr. Our findings show the colocalization, but the absence of significant FRET between oligomers and receptors, confirming the results observed with the interactome. This finding is not in contrast with the observation that Aβ or HypF-N oligomers colocalize with NMDAr or AMPAr as observed with confocal microscopy or co-immunoprecipitation (De Felice *et al*., 2007; Pellistri *et al*., 2008; Deshpande *et al*., 2009; Zhao *et al*., 2009; Cascella *et al*., 2017). Both species are indeed found to bind to the lipid rafts of the membrane appearing closely associated in these studies. However, within such membrane domains noncovalent interactions between the two species appear to be absent or labile.

How can misfolded protein oligomers activate rapidly extrasynaptic AMPAr and NMDAr in the absence of any interaction between the two species? Specific or generic responses involving other proteins and messengers as mediators might in principle take place. It is indeed increasingly accepted that the Fyn/PrP^C signal transduction is involved in the phosphorylation and downregulation of synaptic NMDAr (Um *et al*., 2012; Zhang *et al*., 2019). However, the extrasynaptic localisation of the two AMPAr and NMDAr in SH-SY5Y cells, the rapidity of their activation (in particular the absence of a lag phase in the time-dependent rise of intracellular Ca^{2+} ions upon addition of the oligomers), and their well-established mechanosensitivity (Paoletti and Ascher, 1994; Casado and Ascher, 1998; Chaban *et al*., 2004; Kloda *et al*., 2007; Singh *et al*., 2012), suggest that the change in membrane tension caused by the oligomers is transmitted energetically to the receptors via the lipid bilayer.

In particular, it was previously observed that NMDAr responses are modulated by changes in osmotic pressure and in hydrostatic pressure (Paoletti and Ascher, 1994). NMDAr currents were potentiated by reductions in external osmolarity and were reduced in hyper-osmotic solutions, for the change of the bilayer tension mediated by this

environment (Paoletti and Ascher, 1994). The mechanical energy transmitted to NMDAr exerted via the lipid bilayer alone is sufficient to modulate the channel activity without interaction with the cytoskeletal proteins (Kloda *et al*., 2007). The effect of stretch and the consequent potentiation of the NMDAr can be also exerted by applying amphipathic molecules, such as AA, which have the shape of an "inverted cone", with a small polar head, and incorporate preferentially within one side of the bilayer modifying its curvature (Paoletti and Ascher, 1994; Casado and Ascher, 1998; Kloda *et al*., 2007). By contrast, lysophospholipids, with their 'cone' shape characterized by a big polar head, would tend to compress integral membrane proteins at the polar region of the phospholipid-protein interface, and they have the ability to inhibit the NMDAr responses (Casado and Ascher, 1998).

In our work, we found that LPC, a lipid that mimics a mechanical compression of the membrane and inhibits the NMDAr without acting as a specific ligand (Casado and Ascher, 1998), is able to neutralise the oligomer-induced activation of the NMDAr, suggesting that this is the case of change in membrane tension energetically transmitted to the receptors via the lipid bilayer. Similarly, the occlusion observed between the effects of the oligomers and that of AA, that by contrast mimics a mechanical stretch and activates the receptors (Paoletti and Ascher, 1994; Casado and Ascher, 1998), also corroborates the hypothesis that the oligomers act with this mechanism. Furthermore, by using the TMA-DPH probe embedded within the polar region of the bilayer in SH-SY5Y cells, we found that the anisotropy of the probe is significantly reduced in the presence of the oligomers, indicating an enhanced increase of free space between the various lipids in the bilayer and membrane fluidity upon interaction with the oligomers, again suggesting a mechanical stretch occurring after the interaction of the oligomers with the bilayer.

In conclusion, zinc-stabilised $A\beta_{40}$ oligomers, $A\beta_{42}$ ADDLs oligomers and type A HypF-N oligomers were found to induce an influx of Ca^{2+} ions across the membrane via an early activation of AMPAr and NMDAr, particularly the latter, and via a later non-specific destabilization of the lipid bilayer of the membrane. The mechanism of action through which Aβ oligomers activate the glutamatergic receptors was found to be based on a change of the mechanical properties of the membrane following the insertion of the oligomers in the lipid bilayer that is transmitted down to the receptors, which are therefore activated due to their mechanosensitivity.

5. References

Acosta C., Anderson H.D., and Anderson C.M. (2017) Astrocyte dysfunction in Alzheimer disease. *J Neurosci Res*, **95**:2430-2447.

Agostini M., and Fasolato C. (2016). When, where and how? Focus on neuronal calcium dysfunctions in Alzheimer's Disease. *Cell Calcium*, **60**:289-298.

Agrawal N., and Skelton A. A. (2017) Binding of 12-crown-4 with Alzheimer's Aβ40 and Aβ42 monomers and its effect on their conformation: insight from molecular dynamics simulations. *Mol Pharm*, **15**:289–299.

Agrawal N., and Skelton A. A. (2019) Structure and Function of Alzheimer's Amyloid βeta Proteins from Monomer to Fibrils: A Mini Review. *Protein J*, **38**:425-434.

Agrawal N., Dasaradhi P. V. N., Mohmmed A., Malhotra P., Bhatnagar R. K., and Mukherjee S. K. (2003) RNA Interference: Biology, Mechanism, and Applications. *Microbiol Mol Biol Rev*, **67**:657–685.

Ahmed M., Davis J., Aucoin D., Sato T., Ahuja S., Aimoto S., Elliott J. I., Van Nostrand W. E., and Smith S. O. (2010) Structural conversion of neurotoxic amyloidbeta1–42 oligomers to fibrils. *Nat Struct Mol Biol*, **17**:561–567.

Alberdi E., Sánchez-Gómez M.V., Cavaliere F., Pérez-Samartín A., Zugaza J.L., Trullas R., Domercq M., and Matute C. (2010) Amyloid beta oligomers induce Ca2+ dysregulation and neuronal death through activation of ionotropic Glu receptors. *Cell Calcium*, **47**:264-272.

Almeida C. G., Takahashi R. H., and Gouras G. K. (2006) Betaamyloid accumulation impairs multivesicular body sorting by inhibiting the ubiquitin-proteasome system. *J Neurosci*, **26**:4277-4288.

Anand P., and Singh B. (2013) A review on cholinesterase inhibitors for Alzheimer's disease. *Arch Pharm Res*, **36**:375-399.

Angelova P. R., Ludtmann M. H., Horrocks M. H., Negoda A., Cremades N., Klenerman D., Dobson C. M., Wood N. W., Pavlov E. V., Gandhi S., and Abramov A. Y. (2016) Ca2þ is a key factor in alpha-synuclein-induced neurotoxicity, *J Cell Sci*, **129**:1792-1801.

Apostolova L. G., Green A. E., Babakchanian S., Hwang K. S., Chou Y. Y., Toga A. W., Thompson P. M. (2012) Hippocampal atrophy and ventricular enlargement in normal aging, mild cognitive impairment (MCI), and Alzheimer disease. *Alzheimer Dis Assoc Disord*, **26**:17–27.

Arbel-Ornath M., Hudry E., Boivin,J. R., Hashimoto T., Takeda S., Kuchibhotla K.V., Hou S., Lattarulo C. R., Belcher A. M., Shakerdge N., Trujillo P. B., Muzikansky A., Betensky R. A., Hyman B. T., and Bacskai B. J.. (2017) Soluble oligomeric amyloid-β induces calcium dyshomeostasis that precedes synapse loss in the living mouse brain. *Mol Neurodegener*, **12**:27.

Arevalo-Rodriguez I., Smailagic N., Roqué I. Figuls M., Ciapponi A., Sanchez-Perez E., Giannakou A., Pedraza O. L., Bonfill Cosp X., and Cullum S. (2015) Mini-Mental State Examination (MMSE) for the detection of Alzheimer's disease and other dementias in people with mild cognitive impairment (MCI). *Cochrane Database Syst Rev*, **2015**:CD010783.

Arimon M., Diez-Perez I., Kogan M. J., Durany N., Giralt E., Sanz F., and Fernandez-Busquets X. (2005) Fine structure study of Abeta1–42 fibrillogenesis with atomic force microscopy. *FASEB J*, **19**:1344–1346.

Arispe N., Diaz J. C., and Simakova O. (2007) Abeta ion channels. Prospects for treating Alzheimer's disease with Abeta channel blockers. *Biochim Biophys Acta*, **1768**:1952–1965.

Arispe N., Rojas E., and Pollard H. B. (1993) Alzheimer disease amyloid beta protein forms calcium channels in bilayer membranes: blockade by tromethamine and aluminum. *Proc Natl Acad Sci U S A*, **90**:567–571.

Arosio P., Knowles T. P., and Linse S. (2015) On the lag phase in amyloid fibril formation. *Phys Chem Chem Phys*, **17**:7606-7618.

Bader R., Bamford R., Zurdo J., Luisi B. F., and Dobson C. M. (2006) Probing the mechanism of amyloidogenesis through a tandem repeat of the pi3-sh3 domain suggests a generic model for protein aggregation and fibril formation. *J Mol Biol*, **356**:189–208.

Baglioni S., Casamenti F., Bucciantini M., Luheshi L. M., Taddei N., Chiti F., Dobson C. M., and Stefani M. (2006) Prefibrillar amyloid aggregates could be generic toxins in higher organisms. *J Neurosci*, **26**:8160-7.

Balchin D., Hayer-Hartl M., and Hartl F. U. (2016) In vivo aspects of protein folding and quality control. *Science*, **353**:aac4354.

Balducci C., Beeg M., Stravalaci M., Bastone A., Sclip A., Biasini E., Tapella L., Colombo L., Manzoni C., Borsello T., Chiesa R., Gobbi M., Salmona M., and Forloni G. (2010) Synthetic amyloid-beta oligomers impair longterm memory independently of cellular prion protein. *Proc Natl Acad Sci U S A*, **107**:2295–2300.

Ball K. A., Phillips A. H., Nerenberg P. S., Fawzi N. L., Wemmer D. E., and Head-Gordon T. (2011) Homogeneous and heterogeneous tertiary structure ensembles of amyloid-β peptides. *Biochemistry*, **50**:7612–7628.

Barghorn S., Nimmrich V., Striebinger A., Krantz C., Keller P., Janson B., Bahr M., Schmidt M., Bitner R. S., Harlan J., Barlow E., Ebert U., and Hillen H. (2005) Globular amyloid beta-peptide oligomer – a homogenous and stable neuropathological protein in Alzheimer's disease. *J Neurochem*, **95**:834–847.

Barry A. E., Klyubin I., Mc Donald J. M., Mably A. J., Farrell M. A., Scott M., Walsh D. M., and Rowan M. J. (2011) Alzheimer's disease brain-derived amyloid-beta-mediated inhibition of LTP in vivo is prevented by immunotargeting cellular prion protein. *J Neurosci*, **31**:7259–7263.

Benilova I., Karran E., and De Strooper B. (2012) The toxic Aβ oligomer and Alzheimer's disease: an emperor in need of clothes. *Nat Neurosci*, **15**:349-357.

Bergmans B. A., and De Strooper B. (2010) γ-secretases: from cell biology to therapeutic strategies. *Lancet Neurol*, **9**:215–226.

Berridge M. J. (1998) Neuronal calcium signaling. *Neuron*, **21**:13–26.

Berridge M. V., Herst P. M., and Tan A. S. (2005) Tetrazolium dyes as tools in cell biology: new insights into their cellular reduction. *Biotechnology Annual Review*, **11**:127-152.

Bitan G., Kirkitadze M. D., Lomakin A., Vollers S. S., Benedek G. B., and Teplow D. B. (2003) Amyloid betaprotein (Abeta) assembly: Abeta 40 and Abeta 42 oligomerize through distinct pathways. *Proc Natl Acad Sci USA*, **100**:330–335.

Bleiholder C., Dupuis N. F., Wyttenbach T., and Bowers M. T. (2011) Ion mobility-mass spectrometry reveals a conformational conversion from random assembly to β-sheet in amyloid fibril formation. *Nat Chem*. **3**:172–177.

Blokesch M. (1), Paschos A., Bauer A., Reissmann S., Drapal N., and Böck A. (2004) Analysis of the transcarbamoylation-dehydration reaction catalyzed by the hydrogenase maturation proteins HypF and HypE. *Eur J Biochem*, **271**:3428-36.

Blokesch M. (2), Rohrmoser M., Rode S., and Böck A. (2004). HypF, a zinccontaining protein involved in NiFe hydrogenase maturation. *J Bacteriol*, **186**:2603–2611.

Bosson A., Paumier A., Boisseau S., Jacquier-Sarlin M., Buisson A., and Albrieux M. (2017). TRPA1 channels promote astrocytic Ca2+ hyperactivity and synaptic dysfunction mediated by oligomeric forms of amyloid-β peptide. *Mol Neurodegener*, **12**:53.

Breydo L., and Uversky V. N. (2015) Structural, morphological, and functional diversity of amyloid oligomers. *FEBS Lett*, **589**:2640–2648.

Brini M., Cali T., Ottolini D., and Carafoli E. (2014) Neuronal calcium signaling: function and dysfunction. *Cell Mol Life Sci*, **71**:2787–2814.

Bucciantini M., Calloni G., Chiti F., Formigli L., Nosi D., Dobson C. M., and Stefani M. (2004) Prefibrillar amyloid protein aggregates share common features of cytotoxicity. *J Biol Chem*, **279**:31374-31382.

Bucciantini M., Giannoni E., Chiti F., Baroni F., Formigli L., Zurdo J., Taddei N., Ramponi G., Dobson C.M., and Stefani M. (2002) Inherent toxicity of aggregates implies a common mechanism for protein misfolding diseases. *Nature*, **416**:507–511.

Caetano F. A., Beraldo F. H., Hajj G. N. M., Guimaraes A. L., Jürgensen S., Wasilewska-Sampaio A. P., Hirata P. H., Souza I., Machado C. F., Wong D. Y., De Felice F. G..,

Ferreira S T., Prado V. F., Rylett R. J., Martins V. R., and Prado M. A. (2011) Amyloidbeta oligomers increase the localization of prion protein at the cell surface. *J Neurochem*, **117**:538–553.

Calella A. M., Farinelli M., Nuvolone M., Mirante O., Moos R., Falsig J., Mansuy I. M, and Aguzzi A. (2010) Prion protein and Abeta-related synaptic toxicity impairment. *EMBO Mol Med*, **2**:306–314.

Calloni G., Zoffoli S., Stefani M., Dobson C. M., and Chiti F. (2005) Investigating the effects of mutations on protein aggregation in the cell. *J Biol Chem*, **280**:10607-13.

Campioni S., Mannini B., Zampagni M., Pensalfini A., Parrini C., Evangelisti E., Relini A., Stefani M., Dobson C. M., Cecchi C., and Chiti F. (2010) A causative link between the structure of aberrant protein oligomers and their toxicity. *Nat Chem Biol*, **6**:140–147.

Campioni S., Mossuto M. F., Torrassa S., Calloni G., de Laureto P. P., Relini A., Fontana A., and Chiti F. (2008) Conformational properties of the aggregation precursor state of HypF-N. *J Mol Biol*, **379**:554-67.

Cantanelli P., Sperduti S., Ciavardelli D., Stuppia L., Gatta V., and Sensi S. L. (2014) Age-dependent modifications of AMPA receptor subunit expression levels and related cognitive effects in 3xTg-AD mice. *Frontiers in Aging Neuroscience*, **6**:200.

Capitini C., Patel J. R., Natalello A., D'Andrea C., Relini A., Jarvis J. A., Birolo L., Peduzzo A., Vendruscolo M., Matteini P., Dobson C. M., De Simone A., and Chiti F. (2018) Structural differences between toxic and nontoxic HypF-N oligomers. *Chem Commun (Camb)*, **54**:8637-8640.

Carmen J., Rothstein J. D., and Kerr D. A. (2009) Tumor necrosis factor-alpha modulates glutamate transport in the CNS and is a critical determinant of outcome from viral encephalomyelitis. *Brain Research*, **1263**:143–154.

Carter S. F., Herholz K., Rosa-Neto P., Pellerin L., Nordberg A., and Zimmer E. R. (2019) Astrocyte Biomarkers in Alzheimer's Disease. *Trends Mol Med*, **25**:77-95.

Carulla N., Zhou M., Arimon M., Gairì M., Giralt E., Robinson C. V., and Dobson C. M. (2009) Experimental characterization of disordered and ordered aggregates populated during the process of amyloid fibril formation. *PNAS*, **106**:7828–7833.

Casado M., and Ascher P. (1998). Opposite modulation of NMDA receptors by lysophospholipids and arachidonic acid: common features with mechanosensitivity. *J Physiol*, **513**:317-330.

Cascella R., Conti S., Mannini B., Li X., Buxbaum J. N., Tiribilli B., Chiti F., and Cecchi C. (2013) Transthyretin suppresses the toxicity of oligomers formed by misfolded proteins in vitro. *Biochim Biophys Acta*, **1832**:2302-14.

Cascella R., Evangelisti E., Bigi A., Becatti M., Fiorillo C., Stefani M., Chiti C., and Cecchi C. (2017) Soluble Oligomers Require a Ganglioside to Trigger Neuronal Calcium Overload. *J Alzheimers Dis*, **60**:923-938.

Caspersen C., Wang N., Yao J., Sosunov A., Chen X., Lustbader J. W., Xu H. W., Stern D., McKhann G., and Yan S. D. (2005) Mitochondrial Abeta: A potential focal point for neuronal metabolic dysfunction in Alzheimer's disease. *FASEB J*, **19**:2040-2041.

Castellani R. J., Rolston R. K., and Smith M. A. (2010) Alzheimer disease. *Dis Mon*, **56**: 484-546.

Cecchi C., Baglioni S., Fiorillo C., Pensalfini A., Liguri G., Nosi D., Rigacci S., Bucciantini M., and Stefani M. (2005) Insights into the molecular basis of the differing susceptibility of varying cell types to the toxicity of amyloid aggregates. *J Cell Sci*, **118**:3459-70.

Chaban V.V., Li J., Ennes H.S., Nie J., Mayer E.A., and McRoberts J.A. (2004) N-methyl-D-aspartate receptors enhance mechanical responses and voltage-dependent Ca2+ channels in rat dorsal root ganglia neurons through protein kinase C. *Neuroscience*, **128**:347-357.

Chakroborty S., and Stutzmann G. E. (2014) Calcium channelopathies and Alzheimer's disease: insight into therapeutic success and failures. *Eur J Pharmacol*, **739**:83-95.

Chernomordik L. V., Vogel S. S., Sokoloff A., Onaran H. O., Leikina E. A., and Zimmerberg J. (1993) Lysolipids reversibly inhibit Ca(2+)-, GTP- and pH-dependent fusion of biological membranes. *FEBS Lett*, **318**:71-76.

Chimon S., Shaibat M. A., Jones C. R., Calero D. C., Aizezi B., and Ishii Y. (2007) Evidence of fibril-like β-sheet structures in a neurotoxic amyloid intermediate ofAlzheimer's β-amyloid. *Nat Struct Mol Biol*, **14**:1157–1164.

Chiti F., and Dobson C. M. (2009) Amyloid formation by globular proteins under native conditions. *Nat Chem Biol*, **5**:15-22.

Chiti F., and Dobson C. M. (2017) Protein misfolding, amyloid formation, and human disease: a summary of progress over the last decade. *Annu Rev Biochem*, **86**:27-68.

Chiti F., Bucciantini M., Capanni C., Taddei N., Dobson C. M., and Stefani M. (2001) Solution conditions can promote formation of either amyloid protofilaments or mature fibrils from the HypF N-terminal domain. *Protein Sci*, **10**:2541-7.

Chromy B. A., Nowak R. J., Lambert M. P., Viola K. L., Chang L., Velasco P. T., Jones B. W., Fernandez S. J., Lacor P. N., Horowitz P., Finch C. E., Krafft G. A., and Klein W. L. (2003) Self-assembly of Abeta(1–42) into globular neurotoxins. *Biochemistry*, **42**:12749–12760.

Clapham D. E. (2007) Calcium signaling. *Cell*, **131**:1047–1058.

Clements J. D., Lester R. A., Tong G., Jahr C. E., and Westbrook G. L. (1992) The time course of glutamate in the synaptic cleft. *Science*, **258**:1498–1501.

Cohen S. I., Linse S., Luheshi L. M., Hellstrand E., White D. A., Rajah L., Otzen D. E., Vendruscolo M., Dobson C. M., and Knowles T. P. (2013) Proliferation of amyloid-β_{42} aggregates occurs through a secondary nucleation mechanism. *Proc Natl Acad Sci USA*, **110**:9758–9763.

Coles M., Bicknell W., Watson A. A., Fairlie D. P., and Craik D. J. (1998) Solution structure of amyloid β-peptide (1–40) in a water–micelle environment. Is the membrane-spanning domain where we think it is? *Biochemistry*, **37**:11064–11077.

Collingridge G. L., Peineau S., Howland J. G., and Wang Y. T. (2010) Longterm depression in the CNS. *Nature Rev Neurosci*, **11**:459–473.

Connor S. A., and Wang Y. T. (2016) A place at the table: LTD as a mediator of memory genesis. *Neuroscientist*, **22**:359–371.

Conway M. E. (2020) Alzheimer's disease: targeting the glutamatergic system. *Biogerontology*, **21**:257-274.

Conway M. E., and Hutson S. M. (2016) BCAA metabolism and NH(3) homeostasis. *Adv Neurobiol*, **13**:99–132.

Cremades N., Cohen S. I., Deas E., Abramov A. Y., Chen A. Y., Orte A., Sandal M., Clarke R. W., Dunne P, Aprile F. A., Bertoncini C. W., Wood N. W., Knowles T. P. J., Dobson C. M, and Klenerman D. (2012) Direct observation of the interconversion of normal and toxic forms of α-synuclein. *Cell*, **149**:1048–1059.

Crescenzi O., Tomaselli S., Guerrini R., Salvadori S., D'Ursi A. M., Temussi P. A., and Picone D. (2002) Solution structure of the Alzheimer amyloid β-peptide (1–42) in an apolar microenvironment: similarity with a virus fusion domain. *Eur J Biochem*, **269**:5642–5648.

Cummings J. L. (2004) Alzheimer's disease. *N Engl J Med*, **351**:56-67.

D'Andrea M. R., Nagele R. G., Wang H. Y., Peterson P. A., and Lee D. H. (2001) Evidence that neurones accumulating amyloid can undergo lysis to form amyloid plaques in Alzheimer's disease. *Histopathology*, **38**:120-134.

De Felice F. G., Velasco P. T., Lambert M. P., Viola K., Fernandez S. J., Ferreira S. T., and Klein W. L. (2007) Abeta oligomers induce neuronal oxidative stress through an N-methyl-D-aspartate receptor-dependent mechanism that is blocked by the Alzheimer drug memantine. *J Biol Chem*, **282**:11590-11601.

De Ture M. A., and Dickson D. W. (2019) The neuropathological diagnosis of Alzheimer's disease. *Mol Neurodegener*, **14**:32.

Decker H., Jürgensen S., Adrover M. F., Brito-Moreira J., Bomfim T. R., Klein W.L., Epstein A. L., De Felice F. G., Jerusalinsky D., and Ferreira S. T. (2010) N-methyl-D-aspartate receptors are required for synaptic targeting of Alzheimer's toxic amyloid-β peptide oligomers. *J Neurochem*, **115**:1520-1529.

DeKosky S. T., and Scheff S. W. (1990) Synapse loss in frontal cortex biopsies in Alzheimer's disease: correlation with cognitive severity. *Ann Neurol,* **27**:457-464.

Demuro A, and Parker I. (2013) Cytotoxicity of intracellular aβ42 amyloid oligomers involves Ca2+ release from the endoplasmic reticulum by stimulated production of inositol trisphosphate. *J Neurosci,* **33**:3824-3833.

Demuro A., Mina E., Kayed R., Milton S. C., Parker I., and Glabe C.G. (2005) Calcium dysregulation and membrane disruption as a ubiquitous neurotoxic mechanism of soluble amyloid oligomers. *J Biol Chem,* **280**:17294-17300.

Demuro A., Parker I., and Stutzmann G. E. (2010) Calcium signaling and amyloid toxicity in Alzheimer disease. *J Biol Chem,* **285**:12463-12468.

Deshpande A., Kawai H., Metherate R., Glabe C. G., and Busciglio J. (2009) A role for synaptic zinc in activity-dependent Abeta oligomer formation and accumulation at excitatory synapses. *J Neurosci,* **29**:4004-4015.

Dill K. A., and Chan H. S. (1997) From Levinthal to pathways to funnels. *Nat Struct Biol,* **4**: 10-19.

Dinner A. R., Sali A., Smith L. J., Dobson C. M., and Karplus M. (2000) Understanding protein folding via free-energy surfaces from theory and experiment. *Trends Biochem Sci,* **25**:331-339.

Diògenes M. J., Dias R. B., Rombo D. M., Miranda H. V., Maiolino F., Guerreiro P., Näsström T., Franquelim H. G., Oliveira L. M. A., Castanho M. A. R. B., Lannfelt L., Bergström J., Ingelsson M., Quintas A., Sebastião A. M., Lopes L. V., and Outeiro T. F. (2012) Extracellular Alpha-Synuclein Oligomers Modulate Synaptic Transmission and Impair LTP Via NMDA-Receptor Activation. *J Neurosci,* **32**:11750 –11762.

Dobson C. M. (2003) Protein folding and misfolding. *Nature*, **426**:884-890.

Dobson C. M., Sali A., and Karplus M. (1998) Protein folding: a perspective from theory and experiment. *Angew Chem Int Ed Eng*, **37**:868-893.

Dohler F., Sepulveda-Falla D., Krasemann S., Altmeppen H., Schluter H., Hildebrand D., Zerr I., Matschke J., and Glatzel M. (2014) High molecular mass assemblies of amyloid-beta oligomers bind prion protein in patients with Alzheimer's disease. *Brain*, **137**:873–886.

Domingues C., da Cruz E. S. O. A. B., and Henriques A. G. (2017) Impact of Cytokines and Chemokines on Alzheimer's Disease Neuropathological Hallmarks. *Curr Alzheimer Res*, **14**:870–882.

Dong D.C., and Winnik M.A. (1984) The Py scale of solvent polarities. *Can J Chem*, **62**:2560–2565.

Douglas P. M., and Dillin A. (2010) Protein homeostasis and aging in neurodegeneration. *J Cell Biol*, **190**:719–729.

Drzazga A., Sowinska A., Krzeminska A., Rytczak P., Koziolkiewicz M., and Gendaszewska-Darmach E. (2017) Lysophosphatidylcholine elicits intracellular calcium signaling in a GPR55-dependent manner. *Biochem Biophys Res Commun*, **489**:242-247.

Dumont A. O., Goursaud S., Desmet N., and Hermans E. (2014) Differential regulation of glutamate transporter subtypes by pro-inflammatory cytokine TNF-alpha in cortical astrocytes from a rat model of amyotrophic lateral sclerosis. *PLoS ONE*, **9**:e97649.

Evangelisti E., Cascella R., Becatti M., Marrazza G., Dobson C.M., Chiti F., Stefani M., and Cecchi C. (2016) Binding affinity of amyloid oligomers to cellular membranes is a generic indicator of cellular dysfunction in protein misfolding diseases. *Sci Rep*, **6**:32721.

Evangelisti E., Cecchi C., Cascella R., Sgromo C., Becatti M., Dobson C. M., Chiti F., and Stefani M. (2012) Membrane lipid composition and its physicochemical properties define cell vulnerability to aberrant protein oligomers. *J Cell Sci*, **125**:2416-27.

Feske S. (2019) CRAC channels and disease - From human CRAC channelopathies and animal models to novel drugs. *Cell Calcium*, **80**:112-116.

Forestier A., Douki T., De Rosa V., Beal D., and Rachidi W. (2015) Combination of Aβ secretion and oxidative stress in an Alzheimer-like cell line leads to the over-expression of the nucleotide excision repair proteins DDB2 and XPC. *Int J Mol Sci*, **16**:17422-17444.

Franks K. M., Stevens C. F., and Sejnowski T. J. (2003) Independent sources of quantal variability at single glutamatergic synapses. *J Neurosci*, **23**:3186–3195.

Freir D. B., Nicoll A. J., Klyubin I., Panico S., Mc Donald J. M., Risse E., Asante E. A., Farrow M. A., Sessions R. B., Saibil H. R., Clarke A. R., Rowan M. J., Walsh D. M., and Collinge J. (2011) Interaction between prion protein and toxic amyloid beta assemblies can be therapeutically targeted at multiple sites. *Nature Comm*, **2**:336.

Friedrich B., and Schwartz E. (1993) Molecular biology of hydrogen utilization in aerobic chemolithotrophs. *Annu Rev Microbiol*, **47**:351-83.

Frost G.R., and Li Y.M. (2017) The role of astrocytes in amyloid production and Alzheimer's disease. *Open Biol*, **7**:170228.

Galzitskaya O. V., Galushko E. I., and Selivanova O. M. (2018) Studies of the process of amyloid formation by Aβ peptide. *Biochemistry (Mosc)*, **83**:S62-S80.

Garai K., and Frieden C. (2013) Quantitative analysis of the time course of Ab oligomerization and subsequent growth steps using tetramethylrhodamine-labeled Ab. *Proc Natl Acad Sci USA*, **110**:3321-3326.

Garzon-Rodriguez W., Sepulveda-Becerra M., Milton S., and Glabe C. G. (1997) Soluble amyloid Abeta-(1–40) exists as a stable dimer at low concentrations. *J Biol Chem*, **272**:21037–21044.

Georganopoulou D. G., Chang L., Nam J. M., Thaxton C. S., Mufson E. J., Klein W. L., Mirkin C. A. (2005) Nanoparticle-based detection in cerebral spinal fluid of a soluble pathogenic biomarker for Alzheimer's disease. *Proc Natl Acad Sci USA*, **102**:2273–2276.

Gilbert J., Shu S., Yang X., Lu Y., Zhu L. Q., and Man H. Y. (2016) Beta-Amyloid triggers aberrant over-scaling of homeostatic synaptic plasticity. *Acta Neuropathol Commun*, **4**:131.

Glabe C. (2001) Intracellular mechanisms of amyloid accumulation and pathogenesis in Alzheimer's disease. *J Mol Neurosci*, **17**:137-145.

Glasgow N. G., Povysheva N. V., Azofeifa A. M., and Johnson J. W. (2017) Memantine and Ketamine Differentially Alter NMDA Receptor Desensitization. *J Neurosci*, **37**:9686-9704.

Glenner G. G., and Wong C. W. (1984) Alzheimer's disease: initial report of the purification and characterization of a novel cerebrovascular amyloid protein. *Biochem Biophys Res Commun*, **120**:885–890.

Goedert M., Spillantini M. G., and Crowther R. A. (2015) A brief history of Tau. *Clin Chem*, **61**:1417-1418.

Gomez-Gonzalo M., Martin-Fernandez M., Martinez-Murillo R., Mederos S., Hernandez-Vivanco A., Jamison S., Fernandez A. P., Serrano J., Calero P., Futch H. S., Corpas R., Sanfeliu C., Perea G., Araque A. (2017) Neuron-astrocyte signaling is preserved in the aging brain. *Glia*, **65**:569–580.

Gong Y., Chang L., Viola K. L., Lacor P. N., Lambert M. P., Finch C. E., Krafft G. A., Klein W. L. (2003) Alzheimer's disease-affected brain: presence of oligomeric A beta ligands (ADDLs) suggests a molecular basis for reversible memory loss. *Proc Natl Acad Sci U S A*, **100**:10417-10422.

Gordon M. L., Kingsley P. B., Goldberg T. E., Koppel J., Christen E., Keehlisen L., Kohn N., and Davies P. (2012) An open-label exploratory study with memantine: correlation between proton magnetic resonance spectroscopy and cognition in patients with mild to moderate Alzheimer's disease. *Dement Geriatr Cogn Disord Extra*, **2**:312-320.

Gosal W. S., Morten L. J., Hewitt E. W., Smith D. A., Thomson N. H., and Radford S. E. (2005) Competing pathways determine fibril morphology in the self-assembly of beta2-microglobulin into amyloid. *J Mol Biol*, **351**:850–864.

Gouras G. K., Olsson T. T., and Hansson O. (2015) β-Amyloid peptides and amyloid plaques in Alzheimer's disease. *Neurotherapeutics*, **12**:3-11.

Gouras G. K., Tampellini D., Takahashi R. H., and Capetillo-Zarate E. (2010) Intraneuronal beta-amyloid accumulation and synapse pathology in Alzheimer's disease. *Acta Neuropathol*, **119**:523-541.

Gouras G. K., Tsai J., Naslund J., Vincent B., Edgar M., Checler F., Greenfield J. P., Haroutunian V., Buxbaum J. D., Xu H., Greengard P., and Relkin N. R. (2000) Intraneuronal Abeta42 accumulation in human brain. *Am J Pathol*, **156**:15-20.

Gyure K. A., Durham R., Stewart W. F., Smialek J. E., and Troncoso J. C. (2001) Intraneuronal abeta-amyloid precedes development of amyloid plaques in Down syndrome. *Arch Pathol Lab Med*, **125**:489-492.

Haass C., and Selkoe D. J. (2007) Soluble protein oligomers in neurodegeneration: lessons from the Alzheimer's amyloid beta-peptide. *Nat Rev Mol Cell Biol*, **8**:101-12.

Hansen K. B., Yi F., Perszyk R. E., Menniti F. S., and Traynelis S. F. (2017) NMDA Receptors in the Central Nervous System. *Methods Mol Biol*, **1677**:1-80.

Hardingham G. E., and Bading H. (2010) Synaptic versus extrasynaptic NMDA receptor signalling: implications for neurodegenerative disorders. *Nat Rev Neurosci*, **11**:682-96.

Hardy J. A., Higgins G. A. (1992) Alzheimer's disease: the amyloid cascade hypothesis. *Science*, **256**:184-185.

Harper J. D. (1), and Lansbury P. T Jr (1997) Models of amyloid seeding in Alzheimer's disease and scrapie: mechanistic truths and physiological consequences of the time-dependent solubility of amyloid proteins. *Annu Rev Biochem*, **66**:385–407.

Harper J. D. (2), Wong S. S., Lieber C. M., and Lansbury P. T.(1997) Observation of metastable Aβ amyloid protofibrils by atomic force microscopy. *Chem Biol*, **4**:119-125.

Harper J. D., Wong S. S., Lieber C. M., and Lansbury P. T. Jr (1999) Assembly of A beta amyloid protofibrils: an in vitro model for a possible early event in Alzheimer's disease. *Biochemistry*, **38**:8972–8980.

Hartl F. U. (1996) Molecular chaperones in cellular protein folding. *Nature*, **381**:571-579.

Hartl F. U. (2017) Protein misfolding diseases. *Annu Rev Biochem*, **86**: 21-26.

Hartl F. U., and Hayer-Hartl M. (2002) Molecular chaperones in the cytosol: from nascent chain to folded protein. *Science*, **295**:1852-1858.

Hartl F. U., and Hayer-Hartl M. (2009) Converging concepts of protein folding in vitro and in vivo. *Nat Struct Mol Biol*, **16**:574-581.

Hartley D. M., Walsh D. M., Ye C. P., Diehl T., Vasquez S., Vassilev P. M., Teplow D. B., and Selkoe D.J. (1999) Protofibrillar intermediates of amyloid β-protein induce acute electrophysiological changes and progressive neurotoxicity in cortical neurons. *J Neurosci,* **19**:8876-8884.

Hascup K. N., and Hascup E. R. (2016) Soluble amyloid-beta42 stimulates glutamate release through activation of the alpha7 nicotinic acetylcholine receptor. *J Alzheimer Dis,* **53**:337–347.

Heneka M. T., Carson M. J., El Khoury J., Landreth G. E., Brosseron F., Feinstein D. L., Jacobs A. H., Wyss-Coray T., Vitorica J., Ransohoff R. M., Herrup K., Frautschy S. A., Finsen B., Brown G. C., Verkhratsky A., Yamanaka K., Koistinaho J., Latz E., Halle A., Petzold G. C., Town T., Morgan D., Shinohara M. L., Perry V. H., Holmes C., Bazan N. G., Brooks D. J., Hunot S., Joseph B., Deigendesch N., Garaschuk O., Boddeke E., Dinarello C. A., Breitner J. C., Cole G. M., Golenbock D. T., and Kummer M. P. (2015) Neuroinflammation in Alzheimer's disease. *Lancet Neurol,* **14**:388–405.

Hilbich C., Kisters-Woike B., Reed J., Masters C. L., and Beyreuther K. (1992) Substitutions of hydrophobic amino acids reduce the amyloidogenicity of Alzheimer's disease beta A4 peptides. *J Mol Biol,* **228**:460–473.

Hipp M. S., Park S. H., and Hartl F. U. (2014) Proteostasis impairment in protein-misfolding and -aggregation diseases. *Trends Cell Biol,* **24**:506–514.

Holtzman D. M., Morris J. C., and Goate A. M. (2011) Alzheimer's disease: the challenge of the second century. *Sci Transl Med,* **3**:77.

Hoshi M., Sato M., Matsumoto S., Noguchi A., Yasutake K., Yoshida N., and Sato K. (2003) Spherical aggregates of β-amyloid (amylospheroid) show high neurotoxicity and activate tau protein kinase I/glycogen synthase kinase-3β. *PNAS,* **100**:6370–6375

Illinger D., Duportail G., Mely Y., Poirel-Morales N., Gerard D., and Kuhry J.G. (1995). A comparison of the fluorescence properties of TMA-DPH as a probe for plasma membrane and for endocytic membrane. *Biochim Biophys Acta*, **1239**:58-66.

Ito E., Oka K., Etcheberrigaray R., Nelson T. J., McPhie D. L., Tofel-Grehl B., Gibson G. E., and Alkon D. L. (1994) Internal Ca2+ mobilization is altered in fibroblasts from patients with Alzheimer disease. *Proc Natl Acad Sci U S A*, **91**:534–538.

Jack C. R. Jr, Bennett D. A., Blennow K., Carrillo M. C., Feldman H. H., Frisoni G. B., Hampel H., Jagust W. J., Johnson K. A., Knopman D. S., Petersen R. C., Scheltens P., Sperling R. A., and Dubois B. (2016) A/T/N: An unbiased descriptive classification scheme for Alzheimer disease biomarkers. *Neurology*, **87**:539-547.

Janek K., Rothemund S., Gast K., Beyermann M., Zipper J., Fabian H., Bienert M., and Krause E. (2001) Study of the conformational transition of Aβ (1–42) using d-amino acid replacement analogues. *Biochemistry*, **40**:5457–5463.

Jansen I. E., Savage J. E., Watanabe K., Bryois J., Williams D. M., Steinberg S., Sealock J., Karlsson I. K., Hagg S., Athanasiu L., Voyle N., Proitsi P., Witoelar A., Stringer S., Aarsland D., Almdahl I. S., Andersen F., Bergh S., Bettella F., Bjornsson S., Brækhus A., Bråthen G., de Leeuw C., Desikan R. S., Djurovic S., Dumitrescu L., Fladby T., Homan T. J., Jonsson P. V., Kiddle S. J., Rongve K. A., Saltvedt I., Sando S. B., Selbæk G., Shoai M., Skene N., Snaedal J., Stordal E., Ulstein I. D., Wang Y., White L. R., Hardy J., Hjerling-Leffler J., Sullivan P. F., van der Flier W. M., Dobson R., Davis L. K., Stefansson H., Stefansson K., Pedersen N. L., Ripke S., Andreassen O. A., and Posthuma D. (2019) Genome-wide meta-analysis identifies new loci and functional pathways influencing Alzheimer's disease risk. *Nat Genet*, **51**:404–413.

Johnson K. A., Fox N. C., Sperling R. A., and Klunk W. E. (2012) Brain Imaging in Alzheimer Disease. *Cold Spring Harb Perspect Med*, **2**:a006213.

Jones B. L., and Smith S. M. (2016) Calcium-Sensing Receptor: A Key Target for Extracellular Calcium Signaling in Neurons. *Front Physiol*, **7**:116.

Kagan B. L., Hirakura Y., Azimov R., Azimova R., and Lin M. C. (2002) The channel hypothesis of Alzheimer's disease: current status. *Peptides*, **23**:1311–1315.

Kalia L. V., and Lang A. E. (2015) Parkinson's disease. *Lancet*, **386**:896-912.

Karch C. M., and Goate A. M. (2015) Alzheimer's disease risk genes and mechanisms of disease pathogenesis. *Biol Psychiatry*, **77**:43–51.

Karplus M (1997) The Levinthal paradox, yesterday and today. *Fold Des*, **2**:569-76.

Kasa P., Rakonczay Z., and Gulya K. (1997) The cholinergic system in Alzheimer's disease. *Prog Neurobiol*, **52**:511-535.

Kawahara M., Kuroda Y., Arispe N., and Rojas E. (2000). Alzheimer's beta-amyloid, human islet amylin, and prion protein fragment evoke intracellular free calcium elevations by a common mechanism in a hypothalamic GnRH neuronal cell line. *J Biol Chem*, **275**:14077-14083.

Kayed R., Head E., Sarsoza F., Saing T., Cotman C. W., Necula M., Margol L., Wu J., Breydo L., Thompson J. L., Rasool S., Gurlo T., Butler P., and Glabe C. G. (2007) Fibril specific, conformation dependent antibodies recognize a generic epitope common to amyloid fibrils and fibrillar oligomers that is absent in prefibrillar oligomers. *Mol Neurodegener*, **2**:18.

Kayed R., Head E., Thompson J. L., McIntire T. M., Milton S. C., Cotman C. W., and Glabe C. G. (2003) Common structure of soluble amyloid oligomers implies common mechanism of pathogenesis. Science, **300**:486–89.

Kayed R., Pensalfini A., Margol L., Sokolov Y., Sarsoza F., Head E., Hall J., and Glabe C. (2009) Annular protofibrils are a structurally and functionally distinct type of amyloid oligomer. *J Biol Chem*, **284**:4230–4237.

Kayed R., Sokolov Y., Edmonds B., McIntire T. M., Milton S. C., Hall J. E., and Glabe C. G. (2004) Permeabilization of lipid bilayers is a common conformation-dependent activity of soluble amyloid oligomers in protein misfolding diseases. *J Biol Chem*, **279**:46363-46366.

Kheterpal I., Lashuel H. A., Hartley D. M., Walz T., Lansbury P. T. Jr, and Wetzel R. (2003) Abeta protofibrils possess a stable core structure resistant to hydrogen exchange. *Biochemistry*, **42**:14092–14098.

Kimberly W. T., Zheng J. B., Guenette S., and Selkoe D. J. (2001) The intracellular domain of the ß-amyloid precursor protein is stabilized by Fe65 and translocates to the nucleus in a notch-like manner. J Biol Chem, **276**:40288-40292.

Kirschner D. A., Inouye H., Duffy L. K., Sinclair A., Lind M., and Selkoe D. J. (1987) Synthetic peptide homologous to beta protein from Alzheimer disease forms amyloid-like fibrils in vitro. *Proc Natl Acad Sci USA*, **84**:6953–6957.

Klein W. L., Stine W. B. Jr, and Teplow D. B. (2004) Small assemblies of unmodified amyloid beta-protein are the proximate neurotoxin in Alzheimer's disease. *Neurobiol Aging*, **25**:569–580.

Kloda A., Lua L., Hall R., Adams D.J., and Martinac B. (2007). Liposome reconstitution and modulation of recombinant N-methyl-D-aspartate receptor channels by membrane stretch. *Proc Natl Acad Sci USA,* **104**:1540-1545.

Klunk W. E., Jacob R. F., and Mason R. P. (1999) Quantifying amyloid by Congo red spectral shift assay. *Methods Enzymol*, **309**:285–305.

Klyubin I., Nicoll A. J., Khalili-Shirazi A., Farmer M., Canning S., Mably A., Linehan J., Brown A., Wakeling M., Brandner S., Walsh D. M., Rowan M. J., and Collinge J. (2014) Peripheral administration of a humanized anti-PrP antibody blocks Alzheimer's disease Abeta synaptotoxicity. *J Neurosci*, **34**:6140–6145.

Knowles T. P. J., Vendruscolo M., and Dobson C. M (2014) The amyloid state and its association with protein misfolding diseases. *Nat Rev Mol Cell Biol*, **15**:384-396.

Knowles T. P. J., Waudby C. A., Devlin G. L., Cohen S. I. A., Aguzzi A., Vendruscolo M., Terentjev E. M., Welland M. E., and Dobson C. M. (2009) An analytical solution to the kinetics of breakable filament assembly. *Science,* **326**:1533-1537.

Knowles T. P., Fitzpatrick A. W., Meehan S., Mott H. R., Vendruscolo M., Dobson C. M., Welland M. E. (2007) Role of intermolecular forces in defining material properties of protein nanofibrils. *Science*, **318**:1900–1903.

Koffie R. M., Meyer-Luehmann M., Hashimoto T., Adams K. W., Mielke M. L., Garcia-Alloza M., Micheva K. D., Smith S. J., Kim M. L., Lee V. M., Hyman B. T., and Spires-Jones T. L. (2009) Oligomeric amyloid beta associates with postsynaptic densities and correlates with excitatory synapse loss near senile plaques. *Proc Natl Acad Sci U S A*, **106**:4012-4017.

Kostylev M. A., Kaufman A. C., Nygaard H. B., Patel P., Haas L. T., Gunther E. C., Vortmeyer A., and Strittmatter S. M. (2015) Prion-Protein-interacting Amyloid-beta Oligomers of High Molecular Weight Are Tightly Correlated with Memory Impairment in Multiple Alzheimer Mouse Models. *J Biol Chem*, **290**:17415–17438.

Krishnan R., and Lindquist S. L. (2005) Structural insights into a yeast prion illuminate nucleation and strain diversity. *Nature*, **435**:765-72.

Krishnan R., Goodman J. L., Mukhopadhyay S., Pacheco C. D., Lemke E. A., Deniz A. A., and Lindquist S. (2012) Conserved features of intermediates in amyloid assembly determine their benign or toxic states. *PNAS*, **109**:11172–11177.

Kunz L., Schroder T. N., Lee H., Montag C., Lachmann B., Sariyska R., Reuter M., Stirnberg R., Stocker T., Messing-Floeter P.C., Fell J., Doeller C.F., and Axmacher N. (2015) Reduced grid-cell-like representations in adults at genetic risk for Alzheimer's disease. *Science*, **350**:430-433.

Kuo Y. M., Emmerling M. R., Vigo-Pelfrey C., Kasunic T. C., Kirkpatrick J. B., Murdoch G. H., Ball M. J., and Roher A. E. (1996) Water-soluble Abeta (N-40, N-42) oligomers in normal and Alzheimer disease brains. *J Biol Chem*, **271**:4077–4081.

Labbadia J., and Morimoto R. I. (2015) The biology of proteostasis in aging and disease. *Annu Rev Biochem*. **84**:435–464.

Lacor P. N., Buniel M. C., Furlow P. W., Clemente A. S., Velasco P. T., Wood M., Viola K. L., and Klein W. L. (2007) Abeta oligomer-induced aberrations in synapse composition, shape, and density provide a molecular basis for loss of connectivity in Alzheimer's disease. *J Neurosci*, **27**:796-807.

Ladiwala A. R., Litt J., Kane R. S., Aucoin D. S., Smith S. O., Ranjan S., Davis J., Van Nostrand W. E., Tessier P. M. (2012) Conformational differences between two amyloid βoligomers of similar size and dissimilar toxicity. *J Biol Chem*, **287**:24765–24773.

LaFerla F. M., Green K. N., and Oddo S. (2007) Intracellular amyloid-beta in Alzheimer's disease. *Nat Rev Neurosci*, **8**:499-509.

Lambert M. P, Viola K. L., Chromy B. A., Chang L., Morgan T. E., Yu J., Venton D. L., Krafft G. A., Finch C. E., and Klein W. L. (2001) Vaccination with soluble Aβ oligomers generates toxicity-neutralizing antibodies. *J Neurochem*, **79**:595–605.

Lambert M. P., Barlow A. K., Chromy B. A., Edwards C., Freed R., Liosatos M., Morgan T. E., Rozovsky I., Trommer B., Viola K. L., Wals P., Zhang C., Finch C. E., Krafft G. A., and Klein W. L. (1998) Diffusible, nonfibrillar ligands derived from Abeta1–42 are potent central nervous system neurotoxins. *Proc Natl Acad Sci USA*, **95**:6448–6453.

Lane C. A., Hardy J., and Schott J. M. (2018) Alzheimer's disease. *Eur J Neurol*, **25**:59–70.

Langui D., Girardot N., El Hachimi K. H., Allinquant B., Blanchard V., Pradier L., and Duyckaerts C. (2004) Subcellular topography of neuronal Abeta peptide in APPxPS1 transgenic mice. *Am J Pathol*, **165**:1465-1477.

Lanznaster D., Mack J. M., Coelho V., Ganzella M., Almeida R. F., Dal-Cim T., Hansel G., Zimmer E. R., Souza D. O., Prediger R. D., and Tasca C. I. (2017) Guanosine prevents anhedonic-like behavior and impairment in hippocampal glutamate transport following amyloid-beta1-40 administration in mice. *Mol Neurobiol*, **54**:5482–5496.

Lashuel H. A., Hartley D. M., Petre B. M., Walz T., and Lansbury P.T. Jr (2002) Amyloid pores from pathogenic mutations. *Nature*, **418**:291.

Lauren J., Gimbel D. A., Nygaard H. B., Gilbert J. W., and Strittmatter S. M. (2009) Cellular prion protein mediates impairment of synaptic plasticity by amyloid-beta oligomers. *Nature*, **457**:1128–1132.

Lee J., Culyba E. K., Powers E. T., and Kelly J. W. (2011) Amyloid-β forms fibrils by nucleated conformational conversion of oligomers. *Nat Chem Biol*, **7**:602–609.

Leissring M. A. (1), Parker I., and LaFerla F. M. (1999) Presenilin-2 mutations modulate amplitude and kinetics of inositol 1, 4,5-trisphosphate-mediated calcium signals. *J Biol Chem*, **274**:32535–32538.

Leissring M. A. (2), Paul B. A., Parker I., Cotman C. W., and LaFerla F. M. (1999) Alzheimer's presenilin-1 mutation potentiates inositol 1,4,5-trisphosphate-mediated calcium signaling in Xenopus oocytes. *J Neurochem*, **72**:1061–1068.

Lesne S. E. (2014) Toxic oligomer species of amyloid-β in Alzheimer's disease, a timing issue. *Swiss Med Wkly*, **144**:w14021.

Lesnè S., Koh M. T., Kotilinek L., Kayed R., Glabe C. G., Yang A., Gallagher M., and Ashe K. H. (2006) A specific amyloid-beta protein assembly in the brain impairs memory. *Nature*, **440**:352–357.

LeVine H. 3rd (1995) Soluble multimeric Alzheimer beta(1–40) pre-amyloid complexes in dilute solution. *Neurobiol Aging*, **16**:755–764.

LeVine H. 3rd (1999) Quantification of beta-sheet amyloid fibril structures with thioflavin T. *Methods Enzymol*, **309**:274–284.

Li J., Kanekiyo T., Shinohara M., Zhang Y., LaDu M. J., Xu H., and Bu G. (2012) Differential regulation of amyloid-β endocytic trafficking and lysosomal degradation by apolipoprotein E isoforms. *J Biol Chem*, **287**:44593-44601.

Li S., Hong S., Shepardson N. E., Walsh D. M., Shankar G. M., and Selkoe D. (2009) Soluble oligomers of amyloid Beta protein facilitate hippocampal long-term depression by disrupting neuronal glutamate uptake. *Neuron*, **62**:788–801.

Li S., Jin M., Koeglsperger T., Shepardson N. E., Shankar G. M., and Selkoe D. J. (2011) Soluble Abeta oligomers inhibit long-term potentiation through a mechanism involving excessive activation of extrasynaptic NR2B-containing NMDA receptors. *Journal of Neuroscience*, **31**:6627–6638.

Liddelow S. A., Guttenplan K. A., Clarke L. E., Bennett F. C., Bohlen C. J., Schirmer L., Bennett M. L., Munch A. E., Chung W. S., Peterson T. C., Wilton D. K., Frouin A., Napier B. A., Panicker N., Kumar M., Buckwalter M. S., Rowitch D. H., Dawson V. L., Dawson T. M., Stevens B., and Barres B. A. (2017) Neurotoxic reactive astrocytes are induced by activated microglia. *Nature*, **541**:481–487.

Linse S. (2017) Monomer-dependent secondary nucleation in amyloid formation. *Biophys Rev*, **9**:329-338.

Liu G., Choi S., and Tsien R. W. (1999) Variability of neurotransmitter concentration and nonsaturation of postsynaptic AMPA receptors at synapses in hippocampal cultures and slices. *Neuron*, **22**:395–409.

Liu J., Liu Z., Zhang Y., and Yin F. (2015) A novel antagonistic role of natural compound icariin on neurotoxicity of amyloid β peptide. *Indian J Med Res*, **142**:190-195.

Lu W., Shi Y., Jackson A. C., Bjorgan K., During M. J., Sprengel R., Seeburg P. H., and Nicoll R. A. (2009) Subunit composition of synaptic AMPA receptors revealed by a single-cell genetic approach. *Neuron*, **62**:254–268.

Lue L. F., Kuo Y. M., Roher A. E., Brachova L., Shen Y., Sue L., Beach T., Kurth J. H., Rydel R. E., and Rogers J. (1999) Soluble amyloid β peptide concentration as a predictor of synaptic change in Alzheimer's disease. *Am J Pathol*, **155**:853-862.

Luttmann E., and Fels G (2006) All-atom molecular dynamics studies of the full-length β-amyloid peptides. *Chem Phys*, **323**:138–147.

Lyons A., Griffin R. J., Costelloe C. E., Clarke R. M., and Lynch M. A. (2007) IL-4 attenuates the neuroinflammation induced by amyloid-beta in vivo and in vitro. *J Neurochem*, **101**:771–781.

Maguire G. (2017) Amyotrophic lateral sclerosis as a protein level, non-genomic disease: Therapy with S2RM exosome released molecules. *World J Stem Cells*, **9**:187-202.

Manczak M., Anekonda T. S., Henson E., Park B. S., Quinn J., and Reddy P. H. (2006) Mitochondria are a direct site of A beta accumulation in Alzheimer's disease neurons: Implications for free radical generation and oxidative damage in disease progression. *Hum Mol Genet*, **15**:1437-1449.

Mannini B., and Chiti F. (2017) Chaperones as suppressors of protein misfolded oligomer toxicity. *Front Mol Neurosci*, **10**:98.

Mannini B., Cascella R., Zampagni M., van Waarde-Verhagen M., Meehan S., Roodveldt C., Campioni S., Boninsegna M., Penco A., Relini A., Kampinga H. H., Dobson C. M., Wilson M. R., Cecchi C., and Chiti F. (2012) Molecular mechanisms used by chaperones to reduce the toxicity of aberrant protein oligomers. *Proc Natl Acad Sci U S A*, **109**:12479-84.

Mannini B., Habchi J., Chia S., Ruggeri F. S., Perni M., Knowles T. P. J., Dobson C. M., and Vendruscolo M. (2018) Stabilization and Characterization of Cytotoxic Aβ40

Oligomers Isolated from an Aggregation Reaction in the Presence of Zinc Ions. *ACS Chem Neurosci*, **9**:2959–2971.

Mannini B., Mulvihill E., Sgromo C., Cascella R., Khodarahmi R., Ramazzotti M., Dobson C. M., Cecchi C., and Chiti F. (2014) Toxicity of protein oligomers is rationalized by a function combining size and surface hydrophobicity. *ACS Chem Biol*, **9**:2309-2317.

Mannini B., Vecchi G., Labrador-Garrido A., Fabre B., Fani G., Franco J. M., Lilley K., Pozo D., Vendruscolo M., Chiti F., Dobson C. M., and Roodveldt C. (2019). Differential interactome and innate immune response activation of two structurally distinct misfolded protein oligomers. *ACS Chem Neurosci*, **10**:3464-3478.

Marcello E., Epis R., Saraceno C., Gardoni F., Borroni B., Cattabeni F., Padovani A., Di Luca M. (2012) SAP97-mediated local trafficking is altered in Alzheimer disease patients' hippocampus. *Neurobiology of Aging*, **33**:422.

Marcon G., Plakoutsi G., Canale C., Relini A., Taddei N., Dobson C. M., Ramponi G., and Chiti F. (2005) Amyloid formation from HypF-N under conditions in which the protein is initially in its native state. *J Mol Biol*, **347**:323-35.

Marcus C., Mena E., and Subramaniam R. M. (2014) Brain PET in the Diagnosis of Alzheimer's Disease. *Clin Nucl Med*, **39**:e413–e426.

Martins I. C., Kuperstein I., Wilkinson H., Maes E., Vanbrabant M., Jonckheere W., Van Gelder P., Hartmann D., D'Hooge R., De Strooper B., Schymkowitz J., and Rousseau F. (2008) Lipids revert inert Aβ amyloid fibrils to neurotoxic protofibrils that affect learning in mice. *EMBO J*, **27**:224–233.

Maruyama T., Kanaji T., Nakade S., Kanno T., and Mikoshiba K. (1997) 2APB, 2-aminoethoxydiphenyl borate, a membrane-penetrable modulator of Ins(1,4,5)P3-induced Ca2+ release. *J Biochem*, **122**:498-505.

Matos M., Augusto E., Machado N. J., dos Santos-Rodrigues A., Cunha R. A., and Agostinho P. (2012) Astrocytic adenosine A2A receptors control the amyloid-beta peptide-induced decrease of glutamate uptake. *J Alzheimer Dis*, **31**:555–567.

Matos M., Augusto E., Oliveira C. R., and Agostinho P. (2008) Amyloidbeta peptide decreases glutamate uptake in cultured astrocytes: Involvement of oxidative stress and mitogen-activated protein kinase cascades. *Neuroscience*, **156**:898–910.

Mattson M.P. (1999) Impairment of membrane transport and signal transduction systems by amyloidogenic proteins. *Methods Enzymol*, **309**:733–768.

McAllister A. K., and Stevens C. F. (2000) Nonsaturation of AMPA and NMDA receptors at hippocampal synapses. *Proc Natl Acad Sci U S A*, **97**:6173–6178.

McLean C. A., Cherny R. A., Fraser F. W., Fuller S. J., Smith M. J., Beyreuther K., Bush A. I., and Masters C. L. (1999) Soluble pool of Aβ amyloid as a determinant of severity of neurodegeneration in Alzheimer's disease. *Ann Neurol*, **46**:860-866.

Megill A., Tran T., Eldred K., Lee N. J., Wong P. C., Hoe H. S., Kirkwood A., Lee H. K. (2015) Defective age-dependent metaplasticity in a mouse model of Alzheimer's disease. *Journal of Neuroscience*, **35**:11346–11357.

Meisl G., Yang X., Hellstrand E., Frohm B., and Kirkegaard J. B., Cohen S. I. A., Dobson C. M., Linse S., and Knowles T. P. J. (2014) Differences in nucleation behaviour underlie the contrasting aggregation kinetics of the Aβ40 and Aβ42 peptides. *PNAS*, **111**:9384–9389.

Mendez M. F. (2017) Early-onset Alzheimer disease. *Neurol Clin*, **35**:263–281.

Miguel-Hidalgo J. J., Alvarez X. A., Cacabelos R., and Quack G. (2002) Neuroprotection by memantine against neurodegeneration induced by beta-amyloid(1-40) *Brain Res*, **958**:210-221.

Miyashita N., Straub J. E., and Thirumalai D. (2009) Structures of β-amyloid peptide 1–40, 1–42, and 1–55—the 672–726 fragment of APP—in a membrane environment with implications for interactions with γ-secretase. *J Am Chem Soc*, **131**:17843–17852.

Morris A. M., Watzky M. A, and Finke R. G. (2009) Protein aggregation kinetics, mechanism, and curve-fitting: a review of the literature. *Biochim Biophys Acta*, **1794**:375-97.

Mosmann T. (1983) Rapid colorimetric assay for cellular growth and survival: application to proliferation and cytotoxicity assays. *J Immunol Methods*, **65**:55-63.

Nelson O., Tu H., Lei T., Bentahir M.., de Strooper B, and Bezprozvanny I. (2007) Familial Alzheimer disease–linked mutations specifically disrupt Ca(2+) leak function of presenilin 1. *Journal of Clinical Investigation*, **117**:1230–1239.

Neumann J. T., Diaz-Sylvester P. L., Fleischer S., and Copello J. A. (2011). CGP-37157 inhibits the sarcoplasmic reticulum Ca^{2+} ATPase and activates ryanodine receptor channels in striated muscle. *Mol Pharmacol*, **79**:141-7.

Nilsson M. R. (2004) Techniques to study amyloid fibril formation in vitro. *Methods*, **34**:151-160.

Nimmrich V., Grimm C., Draguhn A., Barghorn S., Lehmann A., Schoemaker H., Hillen H., Gross G., Ebert U., and Bruehl C. (2008) Amyloid beta oligomers (A beta(1–42)

globulomer) suppress spontaneous synaptic activity by inhibition of P/Q-type calcium currents. *J Neurosci*, **28**:788–797.

Oh E. S., Savonenko A. V., King J. F., Fangmark Tucker S. M., Rudow G. L., Xu G., Borchelt D. R., and Troncoso J. C. (2009) Amyloid precursor protein increases cortical neuron size in transgenic mice. *Neurobiol Aging*, **30**:1238–1244.

Oh S., Hong H. S., Hwang E., Sim H. J., Lee W., Shin S. J., and Mook-Jung I. (2005) Amyloid peptide attenuates the proteasome activity in neuronal cells. *Mech Ageing Dev*, **126**:1292-1299.

Ojha J., Masilamoni G., Dunlap D., Udoff R. A., and Cashikar A. G. (2011) Sequestration of toxic oligomers by HspB1 as a cytoprotective mechanism. *Mol Cell Biol*, **31**:3146-3157.

Olzscha H., Schermann S. M., Woerner A. C., Pinkert S., Hecht M. H., Tartaglia G. G., Vendruscolo M., Hayer-Hartl M., Hartl F. U., Vabulas R. M. (2011) Amyloid-like aggregates sequester numerous metastable proteins with essential cellular functions. *Cell*, **144**:67–78.

Oropesa-Nuñez R., Seghezza S., Dante S., Diaspro A., Cascella R., Cecchi C., Stefani M., Chiti F., Canale C. (2016) Interaction of toxic and non-toxic HypF-N oligomers with lipid bilayers investigated at high resolution with atomic force microscopy. *Oncotarget*, **7**:44991-45004.

Ostapchenko V. G., Chen M., Guzman M. S., Xie Y. F., Lavine N., Fan J., Beraldo F. H., Martyn A. C., Belrose J. C., Mori Y., MacDonald J. F., Prado V. F., Prado M. A., and Jackson M. F. (2015). The transient receptor potential melastatin 2 (TRPM2) channel contributes to β-Amyloid oligomer-related neurotoxicity and memory impairment. *J Neurosci*, **35**:15157-15169.

Padrick S. B., and Miranker A. D. (2002) Islet amyloid: Phase partitioning and secondary nucleation are central to the mechanism of fibrillogenesis. *Biochemistry*, **41**:4694–4703.

Palty R., and Sekler I. (2012). The mitochondrial Na(+)/Ca(2+) exchanger. *Cell Calcium*, **52**:9-15.

Pankratov Y. V, and Krishtal O. A. (2003) Distinct quantal features of AMPA and NMDA synaptic currents in hippocampal neurons: implication of glutamate spillover and receptor saturation. *Biophys J*, **85**:3375–3387.

Panza F., Lozupone M., Seripa D., and Imbimbo B. P. (2019) Amyloid-β immunotherapy for alzheimer disease: Is it now a long shot? *Ann Neurol*, **85**:303-315.

Paoletti P., and Ascher P. (1994). Mechanosensitivity of NMDA receptors in cultured mouse central neurons. *Neuron*, **13**:645-655.

Paravastu A. K., Leapman R. D., Yau W. M., and Tycko R. (2008) Molecular structural basis for polymorphism in Alzheimer's β-amyloid fibrils. *PNAS*, **105**:18349-18354.

Paschos A., Bauer A., Zimmermann A., Zehelein E., and Böck A. (2002) HypF, a carbamoyl phosphate-converting enzyme involved in [NiFe] hydrogenase maturation. *J Biol Chem*, **277**:49945–49951.

Patterson C. (2018) World Alzheimer report 2018. The state of the art of dementia research: New frontiers. (London: Alzheimer's Disease International).

Pchitskaya E., Popugaeva E., and Bezprozvanny I. (2018) Calcium signaling and molecular mechanisms underlying neurodegenerative diseases. *Cell Calcium*, **70**:87-94.

Pellistri F., Bucciantini M., Relini A., Nosi D., Gliozzi A., Robello M., and Stefani M. (2008). Nonspecific interaction of prefibrillar amyloid aggregates with glutamatergic

receptors results in Ca2+ increase in primary neuronal cells. *J Biol Chem*, **283**:29950-29960.

Perl D. P. (2010) Neuropathology of Alzheimer's disease. *Mt Sinai J Med*, **77**:32–42.

Petkova A. T., Leapman R. D., Guo Z., Yau W. M., Mattson M. P., Tycko R. (2005) Self-propagating, molecular-level polymorphism in Alzheimer's beta-amyloid fibrils. *Science*, **307**:262–265.

Petkun S., Shi R., Li Y., Asinas A., Munger C., Zhang L., Waclawek M., Soboh B., Sawers R. G., and Cygler M. (2011) Structure of hydrogenase maturation protein HypF with reaction intermediates shows two active sites. *Structure*, **19**:1773-83.

Piermartiri T. C., Figueiredo C. P., Rial D., Duarte F. S., Bezerra S. C., Mancini G., de Bem A. F., Prediger R. D., and Tasca C. I. (2010) Atorvastatin prevents hippocampal cell death, neuroinflammation and oxidative stress following amyloid-beta (1–40) administration in mice: Evidence for dissociation between cognitive deficits and neuronal damage. *Exp Neurol*, **226**:274–284.

Plakoutsi G., Bemporad F., Calamai M., Taddei N., Dobson C. M., and Chiti F. (2005) Evidence for a mechanism of amyloid formation involving molecular reorganisation within native-like precursor aggregates. *J Mol Biol*, **351**:910–922.

Podlisny M. B., Ostaszewski B. L., Squazzo S. L., Koo E. H., Rydell R. E., Teplow D. B., and Selkoe D. J. (1995) Aggregation of secreted amyloid beta-protein into sodium dodecyl sulfate-stable oligomers in cell culture. *J Biol Chem*, **270**:9564–9570.

Qin S., Colin C., Hinners I., Gervais A., Cheret C., and Mallat M. (2006) System Xc- and apolipoprotein E expressed by microglia have opposite effects on the neurotoxicity of amyloid-beta peptide 1-40. *J Neurosci*, **26**:3345-3356.

Quan Q. K., Li X., Yuan H. F., Wang Y., and Liu W. L. (2016) Ginsenoside Rg1 inhibits high-voltage-activated calcium channel currents in hippocampal neurons of beta-amyloid peptide-exposed rat brain slices. Chin J Integr Med. doi: 10.1007/s11655-015-2301-4.

Quist A., Doudevski I., Lin H, Azimova R., Ng D., Frangione B., Kagan B., Ghiso J., and Lal R. (2005) Amyloid ion channels: a common structural link for protein-misfolding disease. *Proc Natl Acad Sci USA*, **102**:10427–10432.

Raghavachari S., and Lisman J. E. (2004) Properties of quantal transmission at CA1 synapses. *J Neurophysiol*, **92**:2456–2467.

Rambaran R. N., and Serpell L. C. (2008) Amyloid fibrils: abnormal protein assembly. *Prion*, **2**:112–117.

Reissmann S.., Hochleitner E, Wang H., Paschos A., Lottspeich F., Glass R. S., and Böck A. (2003) Taming of a poison: biosynthesis of the NiFe-hydrogenase cyanide ligands. *Science*, **299**:1067-70.

Relini A., Torrassa S., Rolandi R., Gliozzi A., Rosano C., Canale C., Bolognesi M., Plakoutsi G., Bucciantini M., Chiti F., and Stefani M. (2004) Monitoring the process of HypF fibrillization and liposome permeabilization by protofibrils. *J Mol Biol*, **338**:943-57.

Rochet J. C., and Lansbury P. T. Jr (2000) Amyloid fibrillogenesis: themes and variations. *Curr Opin Struct Biol*, **10**:60–68.

Roher A. E., Chaney M. O., Kuo Y. M., Webster S. D., Stine W. B., Haverkamp L. J., Woods A. S., Cotter R. J., Tuohy J. M., Krafft G. A., Bonnell B. S., and Emmerling M. R. (1996) Morphology and toxicity of Abeta-(1–42) dimer derived from neuritic and vascular amyloid deposits of Alzheimer's disease. *J Biol Chem*, **271**:20631–20635.

Rönicke R., Mikhaylova M., Rönicke S., Meinhardt J., Schröder U.H., Fändrich M., Reiser G., Kreutz M. R., Reymann K. G. (2011) Early neuronal dysfunction by amyloid β oligomers depends on activation of NR2B-containing NMDA receptors. *Neurobiol Aging*, **32**:2219-2228.

Rosano C., Zuccotti S., Bucciantini M., Stefani M., Ramponi G., and Bolognesi M. (2002) Crystal structure and anion binding in the prokaryotic hydrogenase maturation factor HypF acylphosphatase-like domain. *J Mol Biol*, **321**:785-796.

Roseman M. A. (1988) Hydrophilicity of polar amino acid side-chains is markedly reduced by flanking peptide bonds. *J Mol Biol*, **200**:513–522.

Ross C. A., and Poirier M. A (2005) Opinion: what is the role of protein aggregation in neurodegeneration? *Nat Rev Mol Cell Biol*, **6**:891–898.

Ryman D. C., Acosta-Baena N., Aisen P. S., Bird T., Danek A., Fox N. C., Goate A., Frommelt P., Ghetti B., Langbaum J. B., Lopera F., Martins R., Masters C. L., Mayeux R. P., McDade E., Moreno S., Reiman E. M., Ringman J. M., Salloway S., Schofield P. R., Sperling R., Tariot P. N., Xiong C., Morris J. C., Bateman R. J. (2014) Dominantly Inherited Alzheimer Network. Symptom onset in autosomal dominant Alzheimer disease: a systematic review and meta-analysis. *Neurology*, **83**:253–260.

Sattler R., and Tymianski M. (2001) Molecular mechanisms of glutamate receptor-mediated excitotoxic neuronal cell death. *Mol Neurobiol*, **1-3**:107-29.

Scheefhals N., and MacGillavry H. D. (2018) Functional organization of postsynaptic glutamate receptors. *Mol Cell Neurosci*, **91**:82-94.

Scheltens P. (2009) Imaging in Alzheimer's disease. *Dialogues Clin Neurosci*, **11**:191–199.

Schiene C., and Fischer G. (2000) Enzymes that catalyse the restructuring of proteins. *Curr Opin Struct Biol*, **10**:40-45.

Schlachetzki J. C., Saliba S. W., and Oliveira A. C. (2013) Studying neurodegenerative diseases in culture models. *Braz J Psychiatry*, **35**:S92-100.

Scimemi A., Meabon J. S., Woltjer R. L., Sullivan J. M., Diamond J. S., and Cook D. G. (2013) Amyloid-beta1-42 slows clearance of synaptically released glutamate by mislocalizing astrocytic GLT-1. *J Neurosci*, **33**:5312–5318.

Selkoe D. J. (1994) Cell biology of the amyloid beta-protein precursor and the mechanism of Alzheimer‘s disease. *Annu Rev Cell Biol*, **10**:373–403.

Selkoe D. J. (2004) Cell biology of protein misfolding: the examples of Alzheimer‘s and Parkinson‘s diseases. *Nat Cell Biol*, **6**:1054.

Selkoe D.J., and Hardy J. (2016) The amyloid hypothesis of Alzheimer's disease at 25 years. *EMBO Mol Med*, **8**:595-608.

Sepúlveda F.J., Fierro H., Fernandez E., Castillo C., Peoples R.W., Opazo C., Aguayo L. G. (2014). Nature of the neurotoxic membrane actions of amyloid-β on hippocampal neurons in Alzheimer's disease. *Neurobiol Aging*, **35**:472-481

Serio T. R., Cashikar A. G., Kowal A. S. Sawicki G. J., Moslehi J. J., Serpell L., Arnsdolf M. F., and Lindquist S. L. (2000) Nucleated conformational conversion and the replication of conformational information by a prion determinant. *Science*, **289**:1317-1321.

Serpell L. C. (2000) Alzheimer's amyloid fibrils: structure and assembly. *Biochim Biophys Acta*, **1502**:16-30.

Serrano-Pozo A. (1), Frosch M. P., Masliah E., Hyman B. T. (2011) Neuropathological alterations in Alzheimer disease. *Cold Spring Harb Perspect Med*, **1**:a006189.

Serrano-Pozo A. (2), Mielke M. L., Gomez-Isla T., Betensky R. A., Growdon J. H., Frosch M. P., Hyman B. T. (2011) Reactive glia not only associates with plaques but also parallels tangles in Alzheimer's disease. *Am J Pathol*, **179**:1373–84.

Singh A. P., Arora S., Bhardwaj A., Srivastava S. K., Kadakia M. P., Wang B., Grizzle W. E., Owen L. B., and Singh S. (2012) CXCL12/CXCR4 protein signaling axis induces sonic hedgehog expression in pancreatic cancer cells via extracellular regulated kinase- and Akt kinase-mediated activation of nuclear factor κB: implications for bidirectional tumor-stromal interactions. *J Biol Chem*, **287**:39115-39124.

Sinnen B. L., Bowen A. B., Gibson E. S., and Kennedy M. J. (2016) Local and Use-Dependent Effects of β-Amyloid Oligomers on NMDA Receptor Function Revealed by Optical Quantal Analysis. *J Neurosci*, **36**:11532-11543.

Snyder E. M., Nong Y., Almeida C. G., Paul S., Moran T., Choi E.Y., Nairn A. C., Salter M. W., Lombroso P. J., Gouras G. K., and Greengard P. (2005) Regulation of NMDA receptor trafficking by amyloid-beta. *Nat Neurosci*, **8**:1051-1058.

Soldi G., Bemporad F., and Chiti F. (2008) The degree of structural protection at the edge beta-strands determines the pathway of amyloid formation in globular proteins. *J Am Chem Soc*, **130**:4295-4302.

Spies P. E., Verbeek M. M., van Groen T., and Claassen J. A. H. R. (2012) Reviewing reasons for the decreased CSF Abeta42 concentration in Alzheimer disease. *Front Biosci (Landmark Ed)*, **17**:2024-2034.

Stancu I. C., Vasconcelos B., Terwel D., and Dewachter I. (2014) Models of β-amyloid induced Tau-pathology: the long and "folded" road to understand the mechanism. *Mol Neurodegener*, **9**:51.

Steele M. L., Robinson S. R. (2012) Reactive astrocytes give neurons less support: implications for Alzheimer's disease. *Neurobiol Aging*, **33**:423 e421–13.

Stefani M. (2010) Biochemical and biophysical features of both oligomer/fibril and cell membrane in amyloid cytotoxicity. *FEBS J*, **277**:4602-4613.

Stefani M., and Dobson C.M. (2003) Protein aggregation and aggregate toxicity: new insights into protein folding, misfolding diseases and biological evolution. *J Mol Med (Berl)*, **81**:678-699.

Stephenson F.A. (2001) Subunit characterization of NMDA receptors. *Curr Drug Targets*, 3:233-239.

Stutzmann G. E., Smith I., Caccamo A., Oddo S., Laferla F. M., and Parker I. (2006) Enhanced ryanodine receptor recruitment contributes to Ca2+ disruptions in young, adult, and aged Alzheimer's disease mice. *J Neurosci*, **26**:5180–5189.

Sulkowski G., Dabrowska-Bouta B., Kwiatkowska-Patzer B., and Struzynska L. (2009) Alterations in glutamate transport and group I metabotropic glutamate receptors in the rat brain during acute phase of experimental autoimmune encephalomyelitis. *Folia Neuropathol*, 47:329–337.

Takashima A., Noguchi K., Sato K., Hoshino T., and Imahori K. (1993) Tau protein kinase I is essential for amyloid betaprotein-induced neurotoxicity. *Proc Natl Acad Sci U S A*, **90**:7789-7793.

Talantova M., Sanz-Blasco S., Zhang X., Xia P., Akhtar M.W., Okamoto S., Dziewczapolski G., Nakamura T., Cao G., Pratt A. E., Kang Y. J., Tu S., Molokanova E., McKercher S. R., Hires S. A., Sason H., Stouffer D. G., Buczynski M. W., Solomon J. P., Michael S., Powers E. T., Kelly J. W., Roberts A., Tong G., Fang-Newmeyer T., Parker J., Holland E. A., Zhang D., Nakanishi N., Chen H. S., Wolosker H., Wang Y., Parsons L. H., Ambasudhan R., Masliah E., Heinemann S. F., Piña-Crespo J. C., and Lipton S. A. (2013). Aβ induces astrocytic glutamate release, extrasynaptic NMDA receptor activation, and synaptic loss. *Proc Natl Acad Sci U S A*. **110**:E2518-2527.

Tatini F., Pugliese A. M., Traini C., Niccoli S., Maraula G., Ed Dami T., Mannini B., Scartabelli T., Pedata F., Casamenti F., and Chiti F. (2013) Amyloid-β oligomer synaptotoxicity is mimicked by oligomers of the model protein HypF-N. *Neurobiol Aging*, **34**:2100-9.

Terry R. D., Masliah E., Salmon D. P., Butters N., DeTeresa R., Hill R., Hansen L. A., and Katzman R. (1991) Physical basis of cognitive alterations in Alzheimer's disease: synapse loss is the major correlate of cognitive impairment. *Ann Neurol*, **30**:572-580.

Texidó L., Martín-Satué M., Alberdi E., Solsona C., and Matute C. (2011) Amyloid β peptide oligomers directly activate NMDA receptors. *Cell Calcium*, **49**:184-90.

Thinakaran G., and Koo E. H. (2008) Amyloid precursor protein trafficking, processing, and function. *J Biol Chem*, **283**:29615–29619.

Tiwari S., Atluri V., Kaushik A., Yndart A., and Nair M. (2019) Alzheimer's disease: pathogenesis, diagnostics, and therapeutics. *Int J Nanomed*, **14**:5541-5554.

Tomaselli S., Esposito V., Vangone P., van Nuland N. A., Bonvin A. M., Guerrini R., Tancredi T., Temussi P. A., and Picone D. (2006) The α-to-β conformational transition of Alzheimer's Aβ-(1–42) peptide in aqueous media is reversible: a step by step

conformational analysis suggests the location of β conformation seeding. *ChemBioChem*, **7**:257–267.

Tong B. C., Wu A. J., Li M., and Cheung K. H. (2018). Calcium signaling in Alzheimer's disease & therapies. *Biochim Biophys Acta Mol Cell Res*, **1865**:1745-1760.

Tong H., Zhang X., Meng X., Xu P., Zou X., and Qu S. (2017) Amyloid beta peptide decreases expression and function of glutamate transporters in nervous system cells. *Int J Biochem Cell Biol*, **85**:75–84.

Torres M., Castillo K., Armisén R., Stutzin A., Soto C., and Hetz C. (2010) Prion protein misfolding affects calcium homeostasis and sensitizes cells to endoplasmic reticulum stress. *PLoS One*, **5**:e15658.

Tozaki H., Matsumoto A., Kanno T., Nagai K., Nagata T., Yamamoto S., and Nishizaki T. (2002) The inhibitory and facilitatory actions of amyloid-beta peptides on nicotinic ACh receptors and AMPA receptors. *Biochem Biophys Res Commun*, **294**:42-45.

Tseng B. P., Green K. N., Chan J. L., Blurton-Jones M., and LaFerla F. M. (2008) Abeta inhibits the proteasome and enhances amyloid and tau accumulation. *Neurobiol Aging*, **29**:1607-1618.

Tweten R. K., Parker M. W., and Johnson A. E. (2001) The cholesterol-dependent cytolysins. *Curr Top Microbiol Immunol*, **257**:15-33.

Ueda K., Shinohara S., Yagami T., Asakura K., and Kawasaki K. (1997) Amyloid beta protein potentiates Ca2+ influx through L-type voltage-sensitive Ca2+ channels: a possible involvement of free radicals. *J Neurochem*, **68**:265–271.

Uhlén M., Fagerberg L., Hallström B. M., Lindskog C., Oksvold P., Mardinoglu A., Sivertsson Å., Kampf C., Sjöstedt E., Asplund A., Olsson I., Edlund K., Lundberg E.,

Navani S., Szigyarto C. A., Odeberg J., Djureinovic D., Takanen J. O., Hober S., Alm T., Edqvist P. H., Berling H., Tegel H., Mulder J., Rockberg J., Nilsson P., Schwenk J. M., Hamsten M., von Feilitzen K., Forsberg M., Persson L., Johansson F., Zwahlen M., von Heijne G., Nielsen J., and Pontén F. (2015) Proteomics. Tissue-based map of the human proteome. *Science*, **347**:1260419.

Ulrich D. (2015) Amyloid-beta impairs synaptic inhibition via GABA(A) receptor endocytosis. *J Neurosci*, **35**:9205–9210.

Um J. W., Nygaard H. B., Heiss J. K., Kostylev M. A., Stagi M., Vortmeyer A., Wisniewski T., Gunther E. C., and Strittmatter S. M. (2012) Alzheimer amyloid-β oligomer bound to postsynaptic prion protein activates Fyn to impair neurons. *Nat Neurosci*, **15**:1227-35.

Uversky V. N. (2009) Intrinsic disorder in proteins associated with neurodegenerative diseases. Protein folding and misfolding: neurodegenerative diseases. *Front Biosci (Landmark Ed)*, **14**:5188-5238.

Uversky V. N., and Fink A. L. (2004) Conformational constraints for amyloid fibrillation: the importance of being unfolded. *Biochim Biophys Acta*, **1698**:131-153.

Vabulas R. M., Raychaudhuri S., Hayer-Hartl M., and Hartl F. U. (2010) Protein folding in the cytoplasm and the heat shock response. *Cold Spring Harb Perspect Biol*, **2**:a004390.

Valerio M., Colosimo A., Conti F., Giuliani A., Grottesi A., Manetti C., and Zbilut J. P. (2005) Early events in protein aggregation: molecular flexibility and hydrophobicity/charge interaction in amyloid peptides as studied by molecular dynamics simulations. *Proteins*, **58**:110–118.

Vendruscolo M., and Dobson C. M. (2005) Towards complete descriptions of the free-energy landscape of proteins. *Philos Transact A Math Phys Eng Sci*, **363**:433-452.

Verma R., Mishra V., Sasmal D., and Raghubir R. (2010) Pharmacological evaluation of glutamate transporter 1 (GLT-1) mediated neuroprotection following cerebral ischemia/reperfusion injury. *Eur J Pharmacol*, **638**:65–71.

Villette V., Poindessous-Jazat F., Bellessort B., Roullot E., Peterschmitt Y., Epelbaum J., Dutar P. (2012) A new neuronal target for beta-amyloid peptide in the rat hippocampus. *Neurobiology of Aging*, **33**:e1121–1114.

Vivekanandan S., Brender J. R., Lee S. Y., and Ramamoorthy A. (2011) A partially folded structure of amyloid-beta (1–40) in an aqueous environment. *Biochem Biophys Res Commun*, **411**:312–316.

Vivoli Vega M., Cascella R., Chen S. W., Fusco G., De Simone A., Dobson C. M., Cecchi C., Chiti F. (2019) The Toxicity of Misfolded Protein Oligomers Is Independent of Their Secondary Structure. *ACS Chem Biol*, **14**:1593-1600.

Volles M. J., Lee S. J., Rochet J. C., Shtilerman M. D., Ding T. T., Kessler J. C., and Lansbury P. T. Jr (2001) Vesicle permeabilization by protofibrillar alpha-synuclein: Implications for the pathogenesis and treatment of Parkinson's disease. *Biochemistry*, **40**:7812-7819.

Vyklicky V., Korinek M., Smejkalova T., Balik A., Krausova B., Kaniakova M., Lichnerova K., Cerny J., Krusek J., Dittert I., Horak M., and Vyklicky L. (2014) Structure, function, and pharmacology of NMDA receptor channels. *Physiol Res*, **63**:S191-203.

Wake H., Moorhouse A. J., Jinno S., Kohsaka S., Nabekura J. (2009) Resting microglia directly monitor the functional state of synapses in vivo and determine the fate of ischemic terminals. *J Neurosci*. **29**:3974–80.

Walsh D. M., Hartley D. M., Kusumoto Y., Fezoui Y., Condron M. M., Lomakin A., Benedek G. B., Selkoe D. J., and Teplow D. B. (1999) Amyloid beta-protein fibrillogenesis: structure and biological activity of protofibrillar intermediates. *J Biol Chem*, **274**:25945–25952.

Walsh D. M., Klyubin I., Fadeeva J. V., Cullen W. K., Anwyl R., Wolfe M. S., Rowan M. J., and Selkoe D. J. (2002) Naturally secreted oligomers of amyloid β protein potently inhibit hippocampal long-term potentiation in vivo. *Nature*, **416**:535-539.

Walsh D. M., Klyubin I., Shankar G. M., Townsend M., Fadeeva J. V., Betts V., Podlisny M. B., Cleary J. P., Ashe K. H., Rowan M. J., and Selkoe D. J. (2005) The role of cell-derived oligomers of Aβ in Alzheimer's disease and avenues for therapeutic intervention. *Biochem Soc Trans*, **33**:1087-1090.

Walsh D. M., Lomakin A., Benedek G. B., Condron M. M., and Teplow D.B. (1997) Amyloid β-protein fibrillogenesis. Detection of a protofibrillar intermediate. *J Biol Chem*, **272**:22364-22372.

Walsh D. M., Tseng B. P., Rydel R. E., Podlisny M. B., and Selkoe D. J. (2000) The oligomerization of amyloid beta-protein begins intracellularly in cells derived from human brain. *Biochemistry*, **39**:10831–10839.

Wang R., and Reddy P.H. (2017) Role of glutamate and NMDA receptors in Alzheimer's disease. *J Alzheimers Dis*, **57**:1041-1048.

Wang X., Perry G., Smith M. A., and Zhu X. (2010) Amyloid-beta-derived diffusible ligands cause impaired axonal transport of mitochondria in neurons. *Neurodegener Dis*, **7**:56-59.

Wasmer C., Lange A., Van Melckebeke H., Siemer A. B., Riek R., and Meier B. H. (2008) Amyloid fibrils of the HET-s (218–289) prion form a βsolenoid with a triangular hydrophobic core. *Science*, **319**:1523-1526.

Weissmann C. (2004) The state of the prion. *Nat Rev Microbiol*, **2**:861–871.

Wenthold R. J., Petralia R. S., Blahos J. II, and Niedzielski A. S. (1996) Evidence for multiple AMPA receptor complexes in hippocampal CA1/CA2 neurons. *J Neurosci*, **16**:1982–1989.

Westermark P., Benson M. D., Buxbaum J. N., Cohen A. S., Frangione B., Ikeda S., Masters C. L., Merlini G., Saraiva M. J., and Sipe J. D. (2005) "Amyloid: toward terminology clarification. Report from the Nomenclature Committee of the International Society of Amyloidosis". *Amyloid*, **12**:1-4.

Whitcomb D. J., Hogg E. L., Regan P., Piers T., Narayan P., Whitehead G., Winters B. L., Kim D. H., Kim E., St George-Hyslop P., Klenerman D., Collingridge G. L., Jo J., and Cho K. (2015) Intracellular oligomeric amyloid-beta rapidly regulates GluA1 subunit of AMPA receptor in the hippocampus. *Scientific Reports*, **5**:1–12.

Williams A. D., Sega M., Chen M., Kheterpal I., Geva M., Berthelier V., Kaleta D. T., Cook K. D., and Wetzel R. (2005) Structural properties of Abeta protofibrils stabilized by a small molecule. *Proc Natl Acad Sci USA*, **102**:7115–7120.

Wirths O., Multhaup G., Czech C., Blanchard V., Moussaoui S., Tremp G., Pradier L., Beyreuther K., and Bayer T. A. (2001) Intraneuronal Abeta accumulation precedes plaque

formation in beta-amyloid precursor protein and presenilin-1 doubletransgenic mice. *Neurosci Lett*, **306**:116-120.

Wolynes P. G., Onuchic J. N., and Thirumalai D. (1995) Navigating the folding routes. *Science*, **267**:1619-1620.

Wu Z., Guo Z., Gearing M., and Chen G. (2014) Tonic inhibition in dentate gyrus impairs long-term potentiation and memory in an Alzheimer's disease model. *Nature Comm*, **5**:4159.

Xia P., Chen H. S., Zhang D., and Lipton S. A. (2010) Memantine preferentially blocks extrasynaptic over synaptic NMDA receptor currents in hippocampal autapses. *J Neurosci*, **30**:11246-11250.

Xiu J., Nordberg A.., Zhang J. T., andGuan Z. Z. (2005) Expression of nicotinic receptors on primary cultures of rat astrocytes and up-regulation of the alpha7, alpha4 and beta2 subunits in response to nanomolar concentrations of the beta-amyloid peptide(1-42). *Neurochem Int*, **47**:281–290.

Xu L. Q., Wu S., Buell A. K., Cohen S. I., Chen L. J., Hu W. H., Cusack S. A., Itzhaki L. S., Zhang H., Knowles T. P. J., Dobson C. M., Welland M. E., Jones G. W., and Perrett S. (2013) Influence of specific HSP70 domains on fibril formation of the yeast prion protein Ure2. *Philos Trans R Soc B*, **368**:20110410.

Xue W. F., Hellewell A. L., Hewitt E. W., and Radford S. E. (2010) Fibril fragmentation in amyloid assembly and cytotoxicity. *Prion*, **4**:20-25.

Yamin, G. (2009) NMDA receptor-dependent signaling pathways that underlie amyloid beta-protein disruption of LTP in the hippocampus. *J Neurosci Res*, **87**:1729–1736.

Yatin S. M., Aksenova M., Aksenov M., Markesbery W. R., Aulick T., and Butterfield D. A. (1998) Temporal relations among amyloid beta-peptide-induced free-radical oxidative stress, neuronal toxicity, and neuronal defensive responses. *J Mol Neurosci*, **11**:183-197.

Ye C. P., Selkoe D. J., and Hartley D. M. (2003) Protofibrils of amyloid beta-protein inhibit specific K+ currents in neocortical cultures. *Neurobiol Dis*, **13**:177-190.

Yoshiike Y., Chui D. H., Akagi T., Tanaka N., and Takashima A. (2003) Specific compositions of amyloid-β peptides as the determinant of toxic β-aggregation. *J Biol Chem*, **278**:23648–23655.

Zampagni M., Cascella R., Casamenti F., Grossi C., Evangelisti E., Wright D., Becatti M., Liguri G., Mannini B., Campioni .S, Chiti F., and Cecchi C. (2011) A comparison of the biochemical modifications caused by toxic and non-toxic protein oligomers in cells. *J Cell Mol Med*, **15**:2106-16.

Zasloff M., Adams A. P., Beckerman B., Campbell A., Han Z., Luijten E., Meza I., Julander J., Mishra A., Qu W., Taylor J. M., Weaver S. C., and Wong G. C. (2011) Squalamine as a broad-spectrum systemic antiviral agent with therapeutic potential. *Proc Natl Acad Sci U S A*, **108**:15978-83.

Zhang Y., Li P., Feng J., and Wu M. (2016). Dysfunction of NMDA receptors in Alzheimer's disease. *Neurol Sci*, **37**:1039-1047.

Zhang Y., Zhao Y., Zhang L., Yu W., Wang Y, and Chang W. (2019) Cellular prion protein as a receptor of toxic amyloid-β42 oligomers is important for Alzheimer's disease. *Front Cell Neurosci*, **13**:339.

Zhao W. Q., Santini F., Breese R., Ross D., Zhang X. D., Stone D. J., Ferrer M., Townsend M., Wolfe A. L., Seager M. A., Kinney G. G., Shughrue P. J., and Ray W. J. (2009) Inhibition of calcineurin-mediated endocytosis and alpha-amino-3-hydroxy-5-methyl-4-isoxazolepropionic acid (AMPA) receptors prevents amyloid beta oligomer-induced synaptic disruption. *J Biol Chem*, **285**:7619-7632.

Zhu L., Zhong M., Elder G. A., Sano M., Holtzman D. M., Gandy S., Cardozo C., Haroutunian V., Robakis N. K., and Cai D. (2015) Phospholipid dysregulation contributes to ApoE4-associated cognitive deficits in Alzheimer's disease pathogenesis. *Proc Natl Acad Sci USA*, **112**:11965-11970.